TESE DE DOUTORAMENTO

An Optimized Prediction of Solar Resource by a Numerical Weather Prediction Model and a Photovoltaic Technology Evaluation for a semi-desert climate zone.

Asdo. .....

Ian Mateo Sosa Tinoco

Doutorado en Enerxías Renovables e Sustentabilidade Enerxética

FACULTADE DE FÍSICA

SANTIAGO DE COMPOSTELA

AÑO 2015

USC
UNIVERSIDADE
DE SANTIAGO
DE COMPOSTELA

ÁNGELES LÓPEZ AGÜERA, PROFESORA TITULAR DEL ÁREA DE FÍSICA ATÓMICA MOLECULAR Y NUCLEAR DE LA UNIVERSIDAD SANTIAGO DE COMPOSTELA

AUTORIZA a Don Ian Mateo Sosa Tinoco a presentar la tesis titulada "AN OPTIMIZED PREDICTION OF SOLAR RESOURCE BY A NUMERICAL WEATHER PREDICTION MODEL IN A PHOTOVOLTAIC TECHNOLOGY EVALUATION FOR A SEMI-DESERT CLIMATE ZONE", para optar por el grado de Doctor, la cual ha sido realizada bajo mi dirección en el departamento de Física de Partículas en el marco del programa Doctoral de Energías Renovables y Sostenibilidad Energética.

Y para que así conste, se expide en Santiago de Compostela en Septiembre de 2015.

Fdo. Dra. Ángeles López Agüera

IAN MATEO SOSA T.

Fdo. Don Ian Mateo Sosa Tinoco

USC
UNIVERSIDADE
DE SANTIAGO
DE COMPOSTELA

A mi flaquita y mi familia

USC
UNIVERSIDADE
DE SANTIAGO
DE COMPOSTELA

AGRADECIMIENTOS

Primeramente quiero agradecer a mi Flaquita por estos años de paciencia, compañía e inspiración. La cual puso parte de sus proyectos personales en espera por un proyecto en equipo que culmina con este documento.

A mi directora de tesis Qki (Ángeles López Agüera), por la paciencia y convicción en el proyecto, el cual cambio con los años adecuándose a mis inquietudes profesionales y a las necesidades del grupo de investigación, siempre le estaré agradecido.

A mis compañeros de grupo (SEAG) y amigos con los cuales aprendí muchísimas cosas en estos cuatro años, realizamos proyectos, viajes, comidas, pero sobre todo abrieron sus puertas y corazones. Gracias por todo el apoyo que me dieron (Iago, Vanessa, Juan, Emerita, Gagik, Manuel, Joao, Daniel, Esteban y Akbar).

A Carlos y todos los chicos de Física No Lineal, gracias por los consejos, apoyo y colaboración, espero seguir colaborando con ustedes, así como al Dr Miguez-Macho, por los consejos dados durante la realización del artículo.

Al CONACYT por el apoyo sin fallo alguno de la beca que me fue otorgada hace 4 años. Sin esta institución esta tesis no hubiera sido posible.

A las distintas instituciones que me suministraron los datos meteorológicos necesarios para la validación de resultados:

- Patronato para la Investigación y Experimentación Agrícola del Estado de Sonora A.C.
- Instituto Nacional de Investigaciones Forestales, Agrícolas y Pecuarias
- A la Coordinación General del Servicio Meteorológico Nacional (CGSMN) de la Comisión Nacional del Agua (CONAGUA).

Al Centro de Supercomputación de Galicia (CESGA), por todas las facilidades dadas, sin este soporte la ejecución del modelo meteorológico no hubiera sido posible.

A Ferroatlántica en especial al grupo Silicio Ferrosolar, por la disposición de los paneles solares y la colaboración en el proyecto INTERCONECTA.

USC
UNIVERSIDADE
DE SANTIAGO
DE COMPOSTELA

DERIVED PUBLICATIONS

I. I. Sosa-Tinoco, J. Peralta-Jaramillo, C. Otero-Casal, A. López-Agüera, G. Miguez-Macho, and I. Rodríguez-Cabo, "VALIDATION OF A GLOBAL HORIZONTAL IRRADIATION ASSESSMENT FROM A NUMERICAL WEATHER PREDICTION MODEL IN THE SOUTH OF SONORA-MEXICO.," *J. Renew. Energy*, pp. 1–14, 2015.. Impact Factor 3.476 (IN REVIEW)

II. I.Sosa-Tinoco, C. Otero-Casal, J. Peralta-Jaramillo, A. López-Agüera, G. Miguez-Macho, and I. Rodríguez-Cabo, "OPTMIZATION OF A GLOBAL HORIZONTAL IRRADIATION MAP PRODUCED BY A NUMERICAL WEATHER PREDICTION MODEL IN A SEMI-DESERT CLIMATE" (In Development.)

Other publications related with the thesis

I. A. López-Agüera, J. Domingues-Azevedo, I. Rodríguez-Cabo, D. Rey-Rey, V. Gándara-Villadoniga, E. Vieites-Montes, J. Peralta, I. Sosa, J. Guerra, and M. Alguacil, "Ecoaldeas or Self-Sustainable Communities and renewable energy solutions (SSC). First approach Ecuador and Mexico," in RENEWABLE ENERGY & POWER QUALITY JOURNAL, 2012, pp. 487–494.

II. J. Peralta, C. Otero, Á. López, I. Sosa, D. Emérita, and B. Alfredo, "Identificación y Evaluación del Potencial de Recursos Renovables en el Ecuador y su Viabilidad de Desarrollo Local," in *Tercer Congreso Argentino de Ingeniería Mecánica III CAIM 2012*, 2012, pp. 1–12.

III. J. Peralta, Á. Lopez, A. Barriga, I. Sosa, and E. Delgado, "Análisis estadístico de la información meteorológica para la explotación de energías renovables en el Ecuador," in *Primer Congreso Internacional y Expo Cientifica Investigacion Sostenible: Energías Renovables y Eficiencia Energética*, 2013, pp. 1–9.

USC
UNIVERSIDADE
DE SANTIAGO
DE COMPOSTELA

RESUMEN

El proyecto se enmarca en el área de recursos energéticos renovables. La presente investigación se centra en un doble objetivo: Por un lado, la elaboración de una metodología para el desarrollo de atlas de recurso energético solar mediante el uso de Modelos Numéricos de Predicción Meteorológica (MNPM) y por otro el estudio de la respuesta de diferentes tecnologías de módulos fotovoltaicos en función de las condiciones climáticas, en particular irradiación y temperatura. El estudio se ha focalizado en una región climática semiárida específica: el sur del estado de Sonora en México.

En el Capítulo 1 se hace un recorrido sobre el estado actual y los avances en el sector energético y en especial en las energías renovables primeramente de México, después del estado de Sonora y por último de la región sur del estado. México, como país productor de petróleo siempre se ha caracterizado por tener una política energética basada en productos fósiles como fuente. De hecho, México siempre ha sido un país energéticamente independiente, incluso excedentario, eso sí, con producción variable. De hecho, en los 70's el país paso por un boom de producción que se detuvo a partir de 1980, manteniéndose hasta principios del nuevo milenio. A partir de ahí, hubo un pequeño aumento y una posterior disminución en el consumo de petróleo y un ligero aumento en el consumo de gas natural. Hasta el año 2013, la producción energética del país siempre sobrepasaba el consumo nacional, pero a partir de ahí el índice de independencia energética se redujo, manteniendo una tendencia a la baja para los próximos años, no solo por la disminución de la producción de derivados del petróleo sino además por el aumento de la demanda energética en los últimos años. Esto supone sin duda una situación de desventaja energética para el país al requerir de la importación de energía. En esta coyuntura, el gobierno mexicano en los últimos 3 años ha creado instrumentos legales para promover el uso de energías renovables a diferentes escalas. Dichos instrumentos planean incrementar el uso de la capacidad instalada en renovables hasta 17.5 GW para el 2020 como meta mínima.

Una de las aplicaciones articuladas por el gobierno mexicano, a través de la Secretaria de Energía fue la creación de un portal donde se recopilan diferentes estudios realizados, sobre la evaluación de los recursos energéticos renovables de la nación, por distintas instituciones públicas. Los resultados de estos estudios dan valores orientativos que identifican zonas de posible explotación del recurso. Desgraciadamente, las metodologías empleadas para obtener los datos a disposición no son claras y las resoluciones tanto espaciales como temporales son deficientes. En estas condiciones, la información

disponible no es suficiente para un dimensionado responsable de plantas de explotación del recurso energético. En el trabajo se describen en detalle los estudios a disposición, sus características y sus carencias.

A nivel cualitativo, y como tendencia general, todos los estudios prevén una alta capacidad de recurso solar en el país, así como una alta capacidad eólica en ciertas regiones como el istmo de Tehuantepec, Baja California y Tamaulipas y media-baja en el resto de regiones. Además, se considera la existencia de un alto nivel de recurso geotérmico de alta entalpia en la mayoría de los estados, y una notable capacidad de producción de energía oceánica. Como dato de interés, los proyectos de extracción de energías renovables ya en funcionamiento solo representan el 8.4% de la capacidad total de producción.

El trabajo que se presenta, se centra de modo específico en la región de Sonora, en particular en la zona sur de la región, por lo cual sus características interesan de modo particular. El sur de Sonora es una región semiárida que comprende un territorio que abarca 14 municipios y aglutina el 38% de la población del estado. Los niveles de marginalidad social son altos en dos municipalidades, existiendo alguna otra con niveles medio-alto de marginalidad. El estado de Sonora se caracteriza por ser un estado seco, aunque el sur dispone de un conjunto de presas hidráulicas que fomentan la existencia de agricultura extensiva en la región. A pesar de ello, existen problemas en la distribución del agua asociados a perdidas en los canales de distribución y a la fuerte estacionalidad en el reabastecimiento de las presas. Este reabastecimiento proviene de los ríos que vienen de las montañas y por tanto su caudal, al depender de las épocas de lluvias resulta altamente variable. De hecho, existen años con largos periodos de sequía, lo cual conlleva una sobre explotación de los mantos acuíferos, lo que constituye otro problema regional.

En términos energéticos el sur de Sonora se abastece de grandes centrales hidroeléctricas y de turbogas. Existen además algunos proyectos de huertas solares en la región así como registros del uso de paneles fotovoltaicos, generadores eólicos y bombas de agua eólicas en lugares remotos de la región. Los problemas sociales, de agua y la falta de competencia energética hacen del sur de Sonora una región ideal para instalaciones de energías renovables, como el abastecimiento energético eólico o solar, que vendría facilitado por la existencia de mapas adecuados de recurso energético, de los que no se dispone en la actualidad.

El Capítulo 2 comienza con una recopilación de los modelos de irradiación solar más utilizados y referenciados en la literatura, sus características y su capacidad de predicción y su nivel de validación. Una vez evaluados, se seleccionó como más adecuado para la zona en estudio un Modelo Numérico de Predicción Meteorológica, de amplia utilización en la predicción de variables climatológicas y eventos meteorológicos e incluso en estudios de cambio climático a pesar de su pobre resolución espacial. Para el trabajo que se presenta se seleccionó un modelo numérico de mesoescala, el WRF (Weather Research Forecast por sus siglas en inglés) altamente replicable, usado habitualmente para investigación y meteorología y sobretodo, fácilmente configurable para cualquier

característica climatológica del planeta. En base a este modelo, se elaboró una metodología para generar una base de datos de irradiación global horizontal de la región del sur de Sonora. Una de las innovaciones aportadas, es la propuesta de definición de un año de irradiación media tipo, el cual permite seleccionar los días más representativos de una base de datos de 30 años, que conlleva un importante ahorro en los tiempos de ejecución de los procesos de simulación. La base de datos se obtuvo a partir del modelo numérico global ERA-Interim, desarrollado por el Centro Europeo de Previsiones Meteorológicas a Plazo Medio. Un año tipo de irradiación media es aquel en el cual cada día es seleccionado en modo que su irradiación sea la más cercana a la media del mismo día en la base histórica de 30 años disponible. Para esto, se calcula la media de cada día en los 30 años, se compara cada día con esta media y el día que tenga la menor diferencia con la media se selecciona como el día tipo y así hasta completar los 365 días del año tipo. Esta metodología constituye una base de datos global que puede ser usada para cualquier lugar del planeta sin la necesidad de bases de datos locales.

En estas condiciones se elaboran los mapas de recurso solar en la región. Los resultados obtenidos se validan con una serie de 32 estaciones agro-meteorológicas con un rango histórico de datos de 3 a 8 años y frecuencia horaria. Estas estaciones fueron seleccionadas por su calidad de entre las más de mil existentes en la zona, tras la aplicación de filtros estrictos de calidad. Los resultados obtenidos con WRF se comparan con los resultados de un MNPM global abierto (ERA-Interim, con parametrización de cúmulos) en condiciones idénticas y en la región en estudio. Los resultados se evalúan mediante dos estimadores estadísticos, MBE y rRMSE. Como principales resultados, cabe destacar que a nivel anual, ERA-Interim presenta valores solo ligeramente mejores que WRF. De hecho, ERA-Interim muestra mejores prestaciones en los meses de verano, mientras que el modelo WRF muestra mejores valores en invierno. En cuanto a las medidas de correlación (R^2) entre los datos obtenidos por los modelos frente a las observaciones experimentales, ésta es más que aceptable en ambos modelos (ERA-Interim 0.93; WRF 0.88).

Como resumen, la precisión obtenida con el modelo WRF es buena y la resolución alta en comparación a resultados de investigaciones previas. Además, aunque el estudio realizado ha sido optimizado para la región del Sur de Sonora, los resultados obtenidos pueden ser extrapolados a cualquier otra región de características climáticas similares. Por último, el uso del año de irradiación media tipo propuesta optimiza los tiempos de simulación.

En el Capítulo 3, para mejorar la respuesta del modelo WRF, se realizó un estudio de sensibilidad de parametrizaciones de cúmulos. La necesidad de este estudio, surge de los resultados del capítulo anterior, donde se observó cómo los peores resultados del modelo WRF aparecen asociados a meses con fenómenos climatológicos adversos en periodos de nubosidad muy variable como los monzones. En el estudio, se comparan siete parametrizaciones de los efectos convectivos que afectan indirectamente la irradiación solar y directamente la formación de hidrometeoros en la parametrización de microfísica del modelo WRF. Las parametrizaciones seleccionadas para la comparación son: Kain Fritsch(KF), Betts Miller Janjic (BM), Grell Freitas (GF), Old Simplified Arakawa

Schubert (OSAS), Grell 3 (G3), Tiedtke (Ts) y por ultimo New Simplified Arakawa Schubert (NSAS). Además se agregaron los resultados del modelo ERA-Interim para comparación. Dado que se habían detectado diferencias de comportamiento entre verano e invierno, ambos periodos fueron estudiados separadamente. Como representativo del verano, se seleccionó el mes de Julio que es el que presentaba mayores errores en el capítulo anterior. Los mejores resultados en este caso los presenta la parametrización NSAS, seguida de la OSAS. El resto de las parametrizaciones exhiben errores más altos que ERA-Interim. En el caso del invierno, el mes seleccionado para simular fue diciembre. Los resultados muestran mayor similitud entre todos los casos y una mayor exactitud en tres casos KF, G3 y NSAS con casi el mismo error estimado. En estas condiciones, se puede afirmar que globalmente la parametrización de cúmulos New Simple Arakawa-Schubert resultó la más adecuada.

Tratando de profundizar sobre los resultados obtenidos, se realizaron estudios de predicción de precipitación con las parametrizaciones KF y NSAS ya que estas muestran comportamientos extremos en verano y resultan semejantes en invierno. Las predicciones se compararon con las observaciones experimentales. Como variables de estudio se utilizaron aquellas que estiman los hidrometeoros (hielo, gotas de lluvia, nubes, granizo y nieve) producidos por la parametrización de microfísica, los cuales afectan directamente la densidad óptica de la atmosfera y afectan la salida de irradiación solar en la superficie del modelo en cada caso. Se observa cómo, en verano, el modelo simulado con KF, presenta menor densidad de humedad en la atmosfera promedio que el caso simulado con NSAS. Es decir, en el caso simulado con KF existe una menor permanencia de humedad en la atmosfera, lo cual aumenta la irradiación solar recibida en la superficie. De ahí la sobreestimación respecto a las observaciones de las estaciones meteorológicas. Por último, se realizó una tercera prueba para determinar la respuesta del modelo en una estación del año intermedia (primavera), tanto para NSAS como para KF. En este caso, también se analizó la previsión de hidrometeoros y se comprobó cómo es la convectividad producida por el monzón norteamericano la que afecta los resultados de las simulaciones.

Como resumen, los resultados obtenidos por el modelo WRF con la parametrización NSAS fueron los cercanos a las observaciones, con errores estadísticos menores del 6%, en cualquier periodo del año. Esto permite proponer esta configuración para la elaboración de una base de datos de irradiación global horizontal en las condiciones establecidas en el estudio. Además, el resultado obtenido en este ejercicio supera los resultados previamente obtenidos en la literatura, lo cual supone un nuevo punto de partida para el uso de este tipo de modelos numéricos de predicción meteorológica.

Hasta este momento, se ha trabajado en la evaluación de recurso solar con la mayor precisión y una buena resolución tanto espacial como temporal. Sin embargo hay otro parámetro a tener en cuenta a la hora de la explotación de la energía solar fotovoltaica: La elección de la tecnología apropiada, en función de su respuesta, su vida útil y, por supuesto, su precio.

En el Capítulo 4 se presenta un estudio comparativo experimental sobre la respuesta de diferentes tecnologías de paneles fotovoltaicos en función de las características climáticas de la zona de aplicación con el objetivo de seleccionar la tecnología fotovoltaica apropiada. De esta manera, un mapa de recursos podría ir acompañado de un tipo óptimo de generador fotovoltaico por regiones. Para ello, se ha puesto en funcionamiento un sencillo dispositivo experimental en el que se han incorporado paneles de silicio monocristalino, de silicio policristalino y de capa delgada, todos ellos de diferentes marcas comerciales. En el caso de paneles de silicio policristalino se evalúan dos tecnologías de producción: el método Czochralski, que consideramos tecnología estándar y el método metalúrgico de calidad solar o UMG. En el caso de paneles de capa delgada, se ha trabajado con paneles de los denominados CIS (Cobre, Indio y Selenio).

De una manera comparable al estudio de recurso energético solar estudiado en los capítulos anteriores, este capítulo comienza con una breve descripción de los diferentes tipos de tecnologías de paneles fotovoltaicos. En modo general, los datos de que se dispone se centran en la eficiencia de los sistemas en condiciones standard y de los parámetros óptimos de funcionamiento en esas condiciones. Existen sin embargo otras características más específicas, como el comportamiento en condiciones extremas que rara vez son tenidas en cuenta. Como ejemplo, lugares de muy altos o muy bajos niveles de irradiación y/o temperaturas extremas. Sin embargo, es bien sabido que los módulos fotovoltaicos muestran, en particular su potencia, una fuerte correlación tanto con la irradiación como con la temperatura de funcionamiento. Como no existen estudios sistemáticos de estos parámetros, se ha puesto en funcionamiento un sencillo dispositivo experimental, que permita estudios experimentales comparativos de funcionamiento de cuatro tipos de paneles solares, atendiendo exclusivamente a su respuesta en condiciones climatológicas extremas. Todos los datos han sido obtenidos en sol real y en condiciones normales de operación.

Para cada una de las tecnologías se han realizado medidas de las curvas I-V características en un amplio rango de niveles de irradiación y temperatura ambiental, así como medidas termográficas de control. A partir de los datos experimentales, se ha podido calcular los parámetros de dependencia de las variables significativas (corriente, voltaje y potencia) tanto con la irradiación como con la temperatura mediante ajuste de las curvas características. En todos los casos, la dependencia observada es lineal.

Los resultados obtenidos muestran como la tecnología policristalina presenta una menor dependencia con la variación de temperatura, en particular la estándar. Por tanto, en el caso de instalaciones en condiciones extremas de temperatura, sería ésta la tecnología más apropiada. Este es el caso de la región del Sur de Sonora, caracterizada por altas temperaturas, pero también lo sería para regiones polares con temperaturas particularmente bajas. Le sigue la tecnología monocristalina con dependencia media-baja siendo la CIS aquella que muestra el peor comportamiento.

En cuanto a la dependencia con la irradiación, el razonamiento es un poco más complicado. Dependencias menores, son óptimas para niveles bajos, mientras altas dependencias serán las más adecuadas para zonas de altos niveles de irradiación. En este caso, la tecnología CIS de capa delgada es la que mejor se comporta para zonas de altos niveles de irradiación, seguida de la tecnología policristalina UMG. Por el contrario, la tecnología monocristalina constituirá la mejor solución para zonas poco irradiadas, seguida de la tecnología policristalina estándar.

Si bien dados los altos niveles de irradiación propias de la región semidesértica del sur de Sonora lo módulos fotovoltaicos de película delgada (CIS), serían el candidato idóneo, las altas temperaturas donde los CIS han mostrado los peores resultados, hacen difícil la decisión. De hecho, la tecnología policristalina UMG, presenta el mejor compromiso y puede por tanto ser considerado como el candidato más adecuado.

Como conclusión, los estudios presentados analizan el recurso solar a un nivel de detalle nunca llevado en la región, constituyendo un punto de partida en la predicción del recurso solar por medio de modelos numéricos meteorológicos ya que presenta resultados jamás alcanzados en la literatura. Una de las principales innovaciones del trabajo radican en el detallado estudio de las condiciones de nubosidad propias de la época de lluvia de la región mediante optimización de las parametrizaciones de cúmulos, siendo la denominada New Simple Arakawa Schubert la que proporciona el mejor compromiso. En el apartado de identificación de la tecnología fotovoltaica apropiada, se han evaluado cuatro tecnologías resolviéndose que es la policristalina UMG la que muestra las mejores prestaciones lo que permitirá mejorar las futuras tomas de decisiones en cuanto a las aplicaciones de sistemas fotovoltaicos en la región de estudio.

Como recomendaciones futuras, será de especial interés profundizar en el estudio de las parametrizaciones utilizadas en por el modelo WRF, en particular en las correspondientes a la radiación de onda corta ya que también pueden afectar la predicción de los niveles de irradiación solar horizontal. De particular interés, resultaría también extraer los valores de las diferentes componentes (difusa y directa) de irradiación solar, cara a evaluar la capacidad de producción de los diversos tipos de instalaciones solares, en particular fotovoltaicas y termosolares. Uno de las dificultades asociadas a este último estudio es la ausencia en muchos casos de estaciones meteorológicas locales que permitan validar las salidas del modelo con estas componentes y que cuenten con un histórico aceptable de datos con medidas de irradiación difusa.

Con respecto a la selección de tecnología apropiada, la continuación del trabajo pasa incorporar otras tecnologías al estudio (tecnología de silicio amorfo de capa delgada o paneles solares multicapa). En la misma dirección es de interés el estudio de la influencia de la resistividad en la respuesta de los módulos solares. Por último, un detallado estudio de tiempo de vida útil de las diferentes tecnologías, o en su defecto estudios de envejecimiento en condiciones extremas permitiría añadir una variable de crucial interés en la toma de decisiones sobre tecnología fotovoltaica apropiada.

ABSTRACT

The project is framed in the field of renewable energy resources. This research focuses on two objectives: firstly, the development of a methodology for the development of solar energy resource maps using Numerical weather prediction models (NWP) and secondly the study of the response of different PV module technologies depending on weather conditions, particularly irradiation and temperature. The study has focused on a specific semi-arid climatic region: the southern state of Sonora in Mexico.

In Chapter 1 a tour of the current status and developments in the energy sector, especially in renewable energy primarily from Mexico, after the state of Sonora and finally the southern region of the state is made. Mexico, as an oil-producing country has always been characterized by having an energy policy based on fossil products as a source. In fact, Mexico has always been an energy independent country, even surplus, albeit with varying production. In fact, in the 70s the country went through a production boom that stopped since 1980, continuing until the beginning of the new millennium. From there, there was a small increase and subsequent decline in oil consumption and a slight increase in the consumption of natural gas. Until 2013, the country's energy production always exceeded domestic consumption, but from there the rate of energy independence was reduced while maintaining a downward trend for the coming years, not only by decreasing the production of oil derivatives but also because of the increased energy demand in recent years. This is undoubtedly a situation of energy disadvantage for the country that requires imported energy. At this juncture, the Mexican government in the past three years has created legal instruments to promote renewable energy use at different scales. These instruments are planning to increase the use of renewable installed to 17.5 GW in 2020 as a minimum target of power capacity.

One application articulated by the Mexican government, through the Ministry of Energy was to create a web portal where various studies on the assessment of the renewable energy resources of the nation by various public institutions are collected. The results of these studies provide guidelines, which identify areas of potential exploitation of the resource. Unfortunately, the methodologies used to obtain the data available are not clear and both spatial and temporal resolutions are poor. Under these conditions, the available information is not sufficient for a plant responsible exploitation of energy resources dimensioning. On the Chapter further details of the studies available, their characteristics and their shortcomings are shown.

At qualitative level, and as a general trend, all studies provide a high capacity of solar resource in the country, as well as high wind capacity in certain regions such as the Isthmus of Tehuantepec, Baja California and Tamaulipas and low-mid capacity in the rest of the regions. In addition, is considered the existence of a high level of high enthalpy geothermal resource in most states, and a remarkable production capacity of ocean energy. As a matter of interest, extraction renewable energy projects are already operational and represent only 8.4% of the total production capacity.

The work presented focuses specifically on the Sonora state, particularly in the southern part of the region, so their characteristics interested in a particular way. Southern Sonora is a semiarid region comprising an area covering 14 municipalities and encompasses 38% of the state's population. Social marginalization levels are high in two municipalities, and some other with medium-high levels of marginality. The state of Sonora is characterized by having a dry climate, but the south has a set of hydraulic dams that promote the existence of extensive agriculture in the region. However, there are problems associated with the distribution losses in the distribution channels and strong seasonality in the refilling water dams. This replenishment comes from rivers coming from the mountains and therefore its flow rely on the rainy season that is highly variable. In fact, there are years with long periods of drought, which leads to over-exploitation of aquifers, which is another regional problem.

In energy terms southern Sonora is supplied by large hydro and gas turbine power plants. There are also some projects of solar farms in the region as well as records of the use of photovoltaic panels, wind generators and wind water pumps in remote parts of the region. Social problems, lack of water and energy competition in southern Sonora make an ideal region for renewable energy facilities such as wind or solar energy, which would facilitated by the existence of adequate energy resource maps, of which is not available today.

Chapter 2 begins with a collection of solar radiation models used and referenced in the literature, its characteristics and its predictability and the level of validation. Once evaluated, it was selected the most suitable for the study area, the numerical weather prediction (WRF), widely used in predicting climate variables and meteorological events and even in studies of climate change despite its poor spatial resolution. In this research the WRF model was selected due to the characteristics of the model. The different parameterizations allow to use the model in different climates and to have results according to the research. However in this research we developed a MRY in order to easily generate (with only one input, GHI in this case) and to analyze a complete region (not a single station or a single cell).The database was obtained from the overall ERA-Interim numerical model developed by the European Centre for Medium-Range Weather Forecasts. A year on average irradiation type is one in which every day is selected so that its irradiation is closest to the middle of the day in the historic core of 30 years available. For this, the average of each day in the 30 years is calculated, it is compared daily with the media and the day that has the slightest difference to the average is selected as the type day

and so on to complete 365 days of such year. This methodology uses a global database that can be used to anywhere in the world without the need for local databases.

Once the typical days are selected the solar resource maps are produced in the region. The results are validated with a series of 32 agro-meteorological stations with historical data range 3-8 years, and hourly. These stations were selected for their quality among the thousand existing in the area, after application of strict quality filters. The results obtained with WRF compared to the results of a global NWP (ERA-Interim) under the same conditions and in the region under study. The results are evaluated by two statistical estimators' rRMSE and MBE. As main results, it is noteworthy that on an annual basis, ERA-Interim has only slightly better than WRF values. In fact, ERA-Interim shows better performance in the summer months, while the WRF model shows better values in winter. Regarding correlation (R^2) between the data obtained by the models against experimental observations, it is more than acceptable in both models (ERA-Interim 0.93; 0.88 WRF).

In summary, the precision obtained with the WRF model is good and has both spatial and temporal high resolution compared to previous research results. Furthermore, although the study has been optimized for the region of Southern Sonora, the results can be extrapolated to any other region of similar climatic features.

In Chapter 3, to improve the response of the WRF model, a study of sensitivity cumulus parameterization was performed. The need for this study comes from the results of the previous chapter, where it was observed that the worst WRF model results appear associated with adverse weather events months in periods of high humidity and monsoons. In the study seven cumulus parametrization are compared, which establish convective effects that indirectly affect the solar irradiation and directly the formation of hydrometeors in microphysics parameterization. The settings selected for comparison are: Kain Fritsch (KF), Betts Miller Janjic (BM), Grell Freitas (GF), Old Simplified Arakawa Schubert (OSAS), Grell 3 (G3), Tiedtke (Ts) and finally New Simplified Arakawa Schubert (NSAS). In addition the results of the ERA-Interim added model for comparison. Since behavioral differences between summer and winter had been seen in Chapter 2, both periods were studied separately. As representative of the summer, the month of July had the higher error that presented in the previous chapter. The best results, in this case, are presented by the NSAS parameterization, followed by OSAS. The rest of the parameterizations exhibit higher errors than ERA-Interim. In the case of winter, the selected month was December. The results show greater similarity between all cases and greater accuracy in three cases KF, G3 and NSAS estimated almost the same error. Under these conditions, we can say that overall cumulus parameterization New Simple Arakawa-Schubert was the most appropriate.

Trying to elaborate on the results obtained, precipitation prediction studies were conducted with KF and NSAS settings as they show extreme behaviors in summer and are similar in winter. The predictions were compared with experimental observations. Moreover as study

variables hydrometeors (ice, raindrops, clouds, hail and snow) produced directly by the microphysics parametrization but indirectly feeded by the CP. The hydrometeors directly affect the optical density of the atmosphere and affect the output of solar radiation used in model surface in each case. It shows how, in summer, the KF case, has lower density of moisture in the atmosphere mean that the NSAS case. That is, the KF case output shows less retention of moisture in the atmosphere, which increases the solar radiation received at the surface. Hence the overestimation on observations of weather stations. Finally, a third test was performed to determine the response of the model in an intermediate year season (spring), for both NSAS to KF. In this case the forecast hydrometeors was also analyzed and found how the convective produced by the American monsoon affects the results of the simulations.

In summary, the results obtained by the WRF model with parameterization NSAS were close to the observations, with less statistical error of 6%, at any time of year. This allows this setting to propose the development of a database of global horizontal irradiation in the conditions of the study. In addition, the result obtained in this exercise presents better results in comparison with the results previously obtained in the literature, which is a new departure for the use of this type of numerical weather prediction models.

So far in this research, has been developing the evaluation of solar resources with greater precision and a good resolution both spatial and temporal. However there is another parameter to consider when operating the photovoltaic solar energy: the choice of appropriate technology, depending on its response, its lifetime expectancy and, of course, its price.

In Chapter 4 an experimental comparative study on the response of different technologies of photovoltaic panels depending on the climatic characteristics of the region of application in order to select the appropriate photovoltaic technology is presented. Thus, a resource map could be matched by an optimal type of photovoltaic technology by region. For this purpose, it has been set up an experimental device that uses 4 different PV modules (monocrystalline silicon, polycrystalline silicon, thin-layer), each from different brands. Two panels of polysilicon different production technology (the Czochralski process, we consider standard technology and upgraded metallurgical grade method of solar or UMG) are evaluated. In the case of thin-film panels, the technology chosen was CIS (copper indium selenide).

In a comparable way to the previous chapters studied, this chapter begins with a brief description of the different types of technologies of photovoltaic panels. In general, data that has focus on the efficiency of systems in standard conditions and optimum operating parameters under such conditions. However, there are other more specific characteristics, such as behavior under extreme conditions that are rarely considered. As an example, places with very high or very low levels of radiation and/or extreme temperatures. However, it is well known that photovoltaic modules display, particularly its power, a

strong correlation with both irradiation and operating temperature. Since there are no systematic studies of these parameters, it has set up a simple experimental device that allows experimental benchmarking performance of four types of solar panels, based exclusively on their response in extreme weather conditions. All data is based on actual sun and under normal operating conditions.

For each of technologies measures IV characteristics curves were performed in a wide range of levels and environmental temperature and irradiation. From experimental data, it was possible to calculate the parameters of dependence significant variables (current, voltage and power) both as irradiation with temperature by adjusting the characteristic curves. In all cases, the observed dependence is linear.

The results show as the polycrystalline technology has a lower dependence on temperature variation, in particular standard. Therefore, in the case of installations in extreme temperature conditions, UMG would be the most appropriate technology. This is the case in the region of Southern Sonora, characterized by high temperatures, but so would be to polar regions with particularly low temperatures. In this case the one with the worst response was the CIS technology.

As for the dependence on irradiation, the reasoning is a bit more complicated. Minor dependencies are optimal for low irradiation levels, while high dependencies will be most suitable for areas with high levels of radiation. In this case, the CIS thin-film technology is the best in conduct to areas of high levels of radiation, followed by UMG polycrystalline technology. By contrast, the monocrystalline technology constitutes the best solution for sparsely irradiated regions, followed by standard polycrystalline technology.

Although given the high irradiation level characteristic of the semi-desert region of southern Sonora, thin film photovoltaic modules (CIS) would be the ideal candidate if only irradiation was accounted, however the high temperatures of the region, make the decision difficult. In fact, the UMG polycrystalline technology presents the best compromise and can therefore be considered as the most suitable candidate.

In conclusion, the studies presented analyze the solar resource at a level of detail never led in the region, providing a starting point for predicting the solar resource by meteorological numerical models as it has ever achieved results in the literature. One of the main innovations of the work lie in the detailed study of the conditions typical of the rainy season in the region by optimizing the convective parameterization, being the New Simple Arakawa Schubert which provides the best compromise. In the chapter on proper identification of photovoltaic technology, four technologies have been evaluated resolved that the polycrystalline UMG is showing the best performance which will improve future decision-making regarding the application of photovoltaic systems in the study region.

As future recommendations will be of particular interest to deepen the study of the parameterization on the WRF model, in particular those relating to the short-wave

radiation and that may also affect the prediction of levels of horizontal irradiation. Of particular interest, it would also be to evaluate the irradiance values of the different components (diffuse and direct) to assess the production capacity of various types of solar installations, in particular photovoltaic and solar thermal. One of the difficulties associated with this latest study is the absence in many cases of local weather stations to validate the model outputs with these components and that have an acceptable historical data with measurements of diffuse radiation.

With regard to the selection of appropriate technology, further work passes to the study incorporate other technologies (amorphous silicon technology or multilayer thin film solar panels). In the same direction it is of interest to study the influence of the resistivity response of the solar modules. Finally, a detailed study of lifetime of different technologies, or otherwise aging studies in extreme conditions would add a variable of crucial interest in making appropriate decisions on photovoltaic technology.

INDEX

FIGURES LIST

TABLES LIST

NOMENCLATURE

ASHRAE model:
ASM: All Sky Models
BMJ: Betts-Miller-Janjic
CESGA: Supercomputer Center of Galicia (Centro de Supercomputación de Galicia).
CFE: Comisión Federal de Electricidad
CICESE: Centro de Investigación Científica y de Educación Superior de Ensenada
CONAGUA: Comisión Nacional del Agua
CONAPO. Consejo Nacional de Población
CONUEE: Comisión Nacional para el Uso Eficiente de la Energía
CP: Cumulus Parameterization
CSM: Clear Sky Models
DNI: Direct Normal Irradiance
ECMWF: European Centre for Medium-Range Weather Forecasts.
EII: Energy independence index.
ERA-Interim: It's the latest global atmospheric reanalysis produced by the ECMWF.
G3: Grell-3
GF: Grell-Freitas
GFS: Global Forecast System
GHI: Global Horizontal Irradiation per day.
IIE: Instituto de Investigaciones Eléctrica
INEGI: Instituto Nacional de Estadística y Geografía
INERE: National Inventory of Renewable Energies
INIFAP: National Institute of Forestry, Agricultural and Livestock Research (Instituto Nacional de Investigaciones Forestales, Agricolas y Pecuarias).
KF: Kain-Fritsch
MBE: Mean bias error.
METEOSAT: Meteorological Satellite
MRY: Mean radiation year methodology
NARR: North American Regional Reanalysis
NREL: National Renewable Energy Laboratory
NSAS: New Simplified Arakawa-Schubert
NWP: Numerical weather prediction model
OSAS: Old Simplified Arakawa-Schubert
PB: Physics-Based Models
PIEAES: Board for Agricultural Research and Experimentation of Sonora
PV: Photovoltaic solar energy
RAINC: Convective Rain Output of the Model WRF
RAINNC: Non Convective Rain Output of the Model WRF
RE: Renewable Energies.

rRMSE: Relative root mean square error.
SAGARPA: Secretaria de Agricultura, Ganadería, Desarrollo Rural, Pesca y Alimentación
SEAG: Sustainable Energy Applications Group
SEDESOL: Secretaria de Desarrollo Social
SENER: Energy Secretary of Mexico
SMN: National Meteorological Service (Servicio Meteorológico Nacional)
$SSDR_{d:}$ Surface solar downwards radiation by day output from ERA-Interim
SUNY: State University of New York
TMY: Typical Meteorological Year
Ts: Tiedtke scheme
UNAM: Universidad Nacional Autónoma de México
WRF: Weather Research and Forecasting Model.

USC
UNIVERSIDADE
DE SANTIAGO
DE COMPOSTELA

CHAPTER 1 . RENEWABLE ENERGIES IN MEXICO

The aim of the present chapter tries to show the advances of the Renewable Energies (RE) in Mexico, in order to understand the importance of this research. In particular the status of the renewable energy use in the south of Sonora region and the possibilities of large scale energy production projects and also small scale use for sustainable communities. In this chapter is also detailed the government support, in recent years, to the renewable energy industry. The main objective of this chapter is to understand the context of country and to justify the research explained in Chapters 2, 3 and 4.

1.1 Energy in Mexico

According to the International Energy Agency the energy production balance in Mexico from 1972 to 1982 changed exponentially mainly driven by the oil production and industrialization of the country, however from 1983 the energy production seems really stable with small changes from 2000 to 2006 due to an oil overproduction in that period [1], as shown in Fig. 1. Since the beginning of the 90s in the Mexican energy system increased the use of natural gas due to their lower emissions and higher efficiency generation in combined cycle plants. However, this boom in demand for gas has brought negative consequences, such as to contribute to the imbalance in the trade balance with the outside due to increasing gas imports to meet demand, and have generated significant energy dependence.

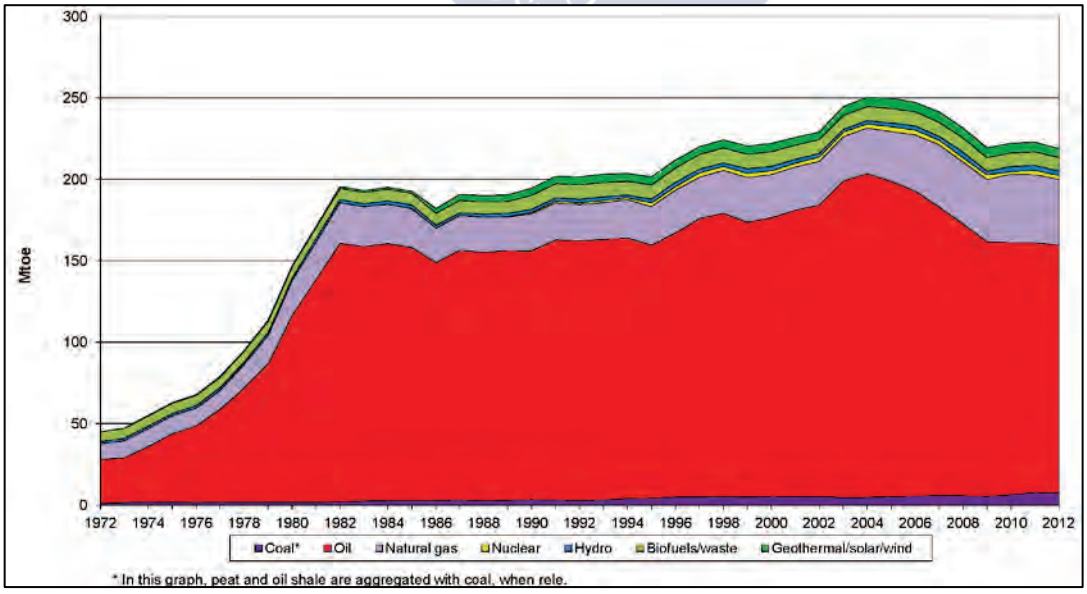

Fig. 1 Energy balance of Mexico (1972-2012) [1]

Another important aspect in Mexico is the energy independence: during the period of 2003-2013 the production of energy has always been above the consumption, as shown in Fig. 2. Both aspects were decisive and have driven Mexico toward a change in the energy balance towards the renewable energy production in this last 2 years.

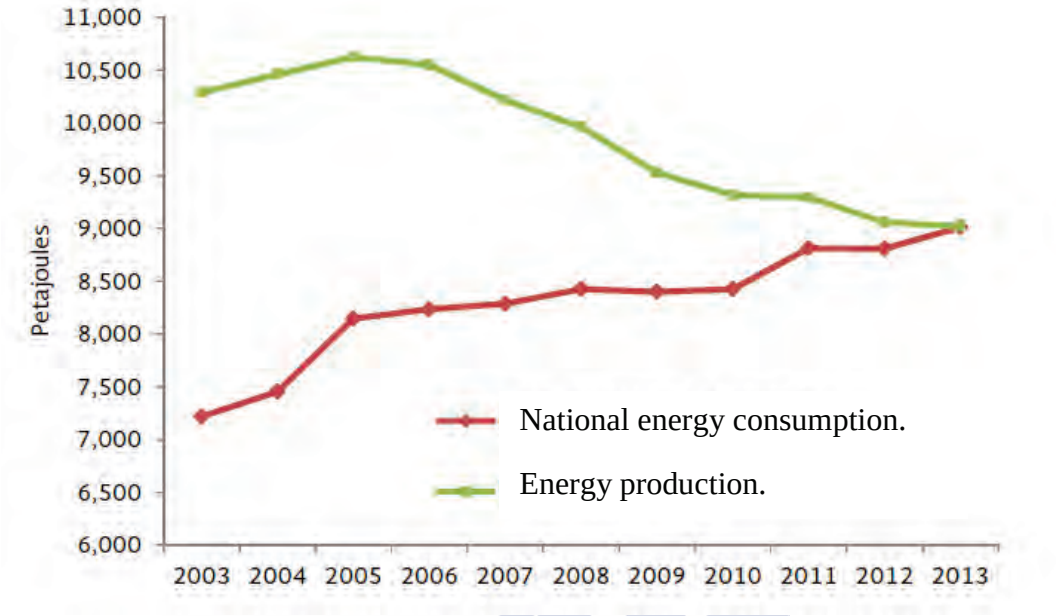

Fig. 2 Energy production vs consumption. (In green energy production, in red consumption).[2]

Furthermore the energy independence index (EII) has always been mainly above 1.0, but in 2013 the EII got to 1.0 with a tendency of getting even lower (Fig. 3). This is the product of the increase of energy consumption throughout time. However, in recent years, there have been certain efforts from the federal government to encourage the use of renewable energies and change energy balance and increase the energy production.

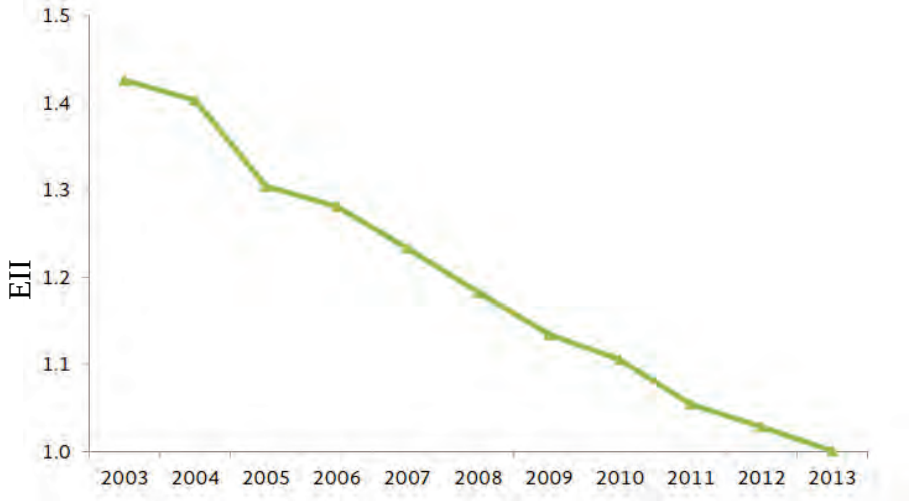

Fig. 3 Energy Independence Index of Mexico [2]

Lately, three main legal instruments were established in order to promote RE in Mexico. One is the recent Energy Reform approved by the Congress of the Union[3]. The second instrument is the General Law for Climate Change adopted in May 2012 which sets the goal of 35% of energy generated in the country should come from renewable sources by 2024[4]. Although the degree of contribution for each technology has not been defined, renewable energy sources installed capacity is planned to increase to 1, 2, 12 and 1.5 GW for biomass, geothermal, wind and solar energy, respectively by 2020. Finally, the Law for the Use of Renewable Energy and Finance of the Energy Transition recently modified and approved. This Law establishes, among other issues, the legal aspects and conditions for the use of renewable energy and clean technologies as well as reducing the employment and dependency of fossil fuels[5]. Additionally, the Law creates a Fund for the transition to clean and RE and technologies. The Fund will create a Technical Committee for the administration, and the assignment and distribution of resources in order to promote the goals of the strategy. The Committee might also decide on the use of the Fund for channeling credit and other financing support to foster the energy transition, energy saving, clean technologies and RE. These three legal instruments are expected to create a better framework to support renewable energy in general and also a future environmental conscious economy in the country.

The current situation of RE generation in Mexico could be called as a fertile land, according to the Energy Secretary of Mexico (SENER) only the 8.4% of primary energy produced comes from renewable sources [2]. In Fig. 4 the total electricity generation is detailed, and it is easily noticeable that renewables still are a small fraction of the total generation.

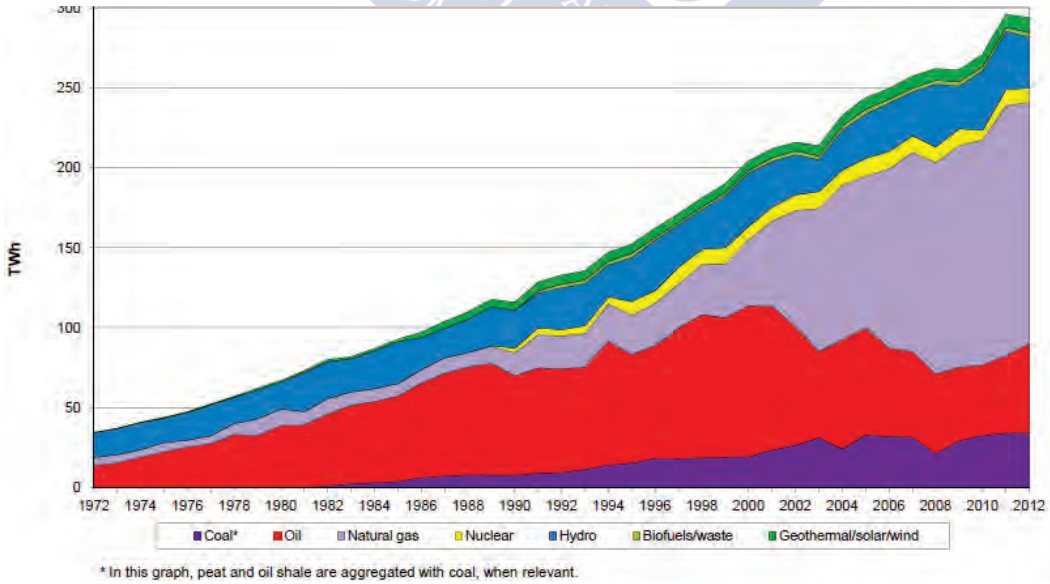

Fig. 4 Electricity generation by type of fuel/source [1]

As reported by SENER, the consumption of energy from renewable energies in the residential sector is low; around 0.55% of the energy used on houses is solar energy. If we consider the wood as a renewable energy, than 34.39% of consumption is also used on homes. On commercial buildings only solar energy is accounted as renewable energy used. The total solar energy used is 2.06%[2]. Table 1 shows the total energy use in the residential and commercial sector.

Table 1Energy consumption in residential and commercial sector. (Petajoules) [2]

	2012	2013	Percentage change 2013/2012	Percentage structure 2013
Residential	*758.02*	*742.74*	*-2.02*	*100*
Solar	3.66	4.07	11.18	0.55
Wood	256.74	255.42	-0.51	34.39
Total Petroleum derivate	275.58	258.31	-6.27	34.78
Liquid gas	274.38	256.96	-6.35	34.60
Kerosene	1.21	1.35	12.01	0.18
Dry gas	32.06	33.80	5.44	4.55
Electricity	189.98	191.14	0.61	25.73
Commercial	*132.51*	*133.0*	*0.50*	*100*
Solar	2.47	2.74	11.18	2.06
Total Petroleum derivate	69.36	69.43	0.10	52.18
Liquate gas	65.12	65.03	-0.14	48.88
Kerosene	4.24	4.40	3.67	3.30
Dry gas	10.29	11.10	7.90	8.34
Electricity	50.40	49.78	-1.23	37.42

However, in the industrial sector the use of renewable energies is less extended, only 0.02% of solar energy is used and also 3.84% of biomass (bagasse) [2]. In Table 2 a further analysis of the industrial sector consumption is explained, in green the renewable energy fraction is highlighted.

Table 2 Industry sector energy consumption (Petajoules) [2]

	2012	2013	Percentage change 2013/2012	Percentage structure 2013
Total	*1,522.30*	*1,612.31*	*5.91*	*100*
Solar	0.30	0.33	11.18	0.02
Bagasse	40.99	61.99	51.22	3.84
Coal	97.37	127.26	30.70	7.89
Coke	64.34	65.13	1.23	4.04
Petroleum coke	100.02	97.66	-2.36	6.06
Total Petroleum derivate	139.56	135.79	-2.70	8.42
Liquid gas	41.01	45.05	9.85	2.79
Gasoline	0.41	0.85	107.59	0.05
Diesel	64.99	64.53	-0.71	4.00
Fuel oil	33.15	25.36	-23.49	1.57
Dry gas	551.60	593.18	7.54	36.79
Electricity	528.13	530.97	0.54	32.93

Moreover the total primary energy supply of electricity in Mexico also has a fraction of sustainable energies. Around 5.93% of the total primary energy supply in 2013 came from renewables (geoenergy, biogas, biomass, solar and wind). The proportion of renewable energies from the fraction of primary supply energy is shown in Fig. 5. The highest portion of renewable energy supply in Mexico comes from biomass (~72%), the second highest is geoenergy (~25%) and the rest are wind and solar (< 2%).

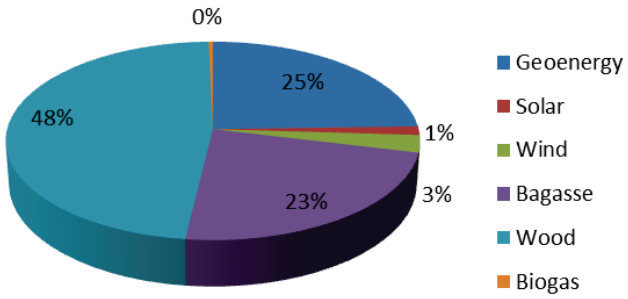

Fig. 5 Renewable energies share in Mexico 2013 [6]

In Table 3 a summary of the total primary energy in Mexico is presented. The Table shows the distribution of energy used for energy transformation, to final use in the country. Most of the renewable energies used in Mexico are used by the energy suppliers for transformation, and only a small fraction is used directly in the different sectors (residential, commercial, public and industrial).

Table 3 Primary energy balance Mexico (Petajoules) [2]

	Coal	Oil	Condensates	Natural gas	Nuclear	Hydro	Geoenergy	Solar	Wind	Bagasse	Wood	Biogas	Total energy
National Production	316.27	5798.74	101.2	2045.61	122.6	100.66	131.33	7.52	15.07	123.83	255.42	1.97	9020.21
From other sources	0	0	0	772.38	0	0	0	0	0	0	0	0	772.38
Imports	216.97	0	0	0	0	0	0	0	0	0	0	0	216.97
Inventory variation	17.88	-18.26	-0.08	-12.77	0	0	0	0	0	0	0	0	-13.23
Total supply	551.12	5780.48	101.11	2805.22	122.6	100.66	131.33	7.52	15.07	123.83	255.42	1.97	9996.33
Exports	-0.14	-2736.95	-8.95	0	0	0	0	0	0	0	0	0	-2746.03
Non used energy	0	-0.82	0	-52.64	0	0	0	0	0	-1.36	0	0	-54.83
Gross domestic supply	550.98	3042.71	92.16	2752.57	122.6	100.66	131.33	7.52	15.07	122.47	255.42	1.97	7195.47
Total transformation	-423.72	-2825.89	-92.16	-1892.16	-122.6	-100.66	-131.33	-0.38	-15.07	-60.3	0	-1.97	-5666.24
Coking ovens	-83.77	0	0	0	0	0	0	0	0	0	0	0	-83.77
Refineries and chamfering	0	-2825.89	-7.24	0	0	0	0	0	0	0	0	0	-2833.13
Gas and bottling plants	0	0	-84.93	-1892.16	0	0	0	0	0	0	0	0	-1977.09
Power stations	-338.41	0	0	0	-122.6	-98.81	-131.33	-0.05	-0.68	0	0	0	-691.87
PIE Power plants	0	0	0	0	0	0	0	0	-5.85	0	0	0	-5.85
Self-generation power plants	-1.54	0	0	0	0	-1.85	0	-0.33	-8.54	-60.3	0	-1.97	-74.53
Power consumption by sector	0	0	0	-301.95	0	0	0	0	0	0	0	0	-301.95
Inter-product transfer	0	0	0	-288.72	0	0	0	0	0	0	0	0	-288.72
Recirculation	0	0	0	-269.74	0	0	0	0	0	0	0	0	-269.74
Statistic differences	0	-184.92	0	0	0	0	0	0	0	0	0	0	-184.92
Losses	0	-31.9	0	0	0	0	0	0	0	0	0	0	-31.9
Final consumption	127.26	0	0	0	0	0	0	7.14	0	62.17	255.42	0	452
Final non-energy consumption	0	0	0	0	0	0	0	0	0	0.18	0	0	0.18
Other economic branches	0	0	0	0	0	0	0	0	0	0.18	0	0	0.18
Final energy consumption	127.26	0	0	0	0	0	0	7.14	0	61.99	255.42	0	451.81
Residential, Commercial and Pub.	0	0	0	0	0	0	0	6.81	0	0	255.42	0	262.23
Industrial	127.26	0	0	0	0	0	0	0.33	0	61.99	0	0	189.58

1.2 Photovoltaic solar energy and solar thermal

Mexico has a great opportunity while using solar energy; its solar irradiation, in some areas, is one of the highest in the world and there could be an excellent market niche[7], [8]. The annual mean solar irradiation in the territory is around 5kWh/m^2. In Fig. 6 the global horizontal irradiance worldwide is presented and shows the excellent situation on a macroscale context of Mexico.

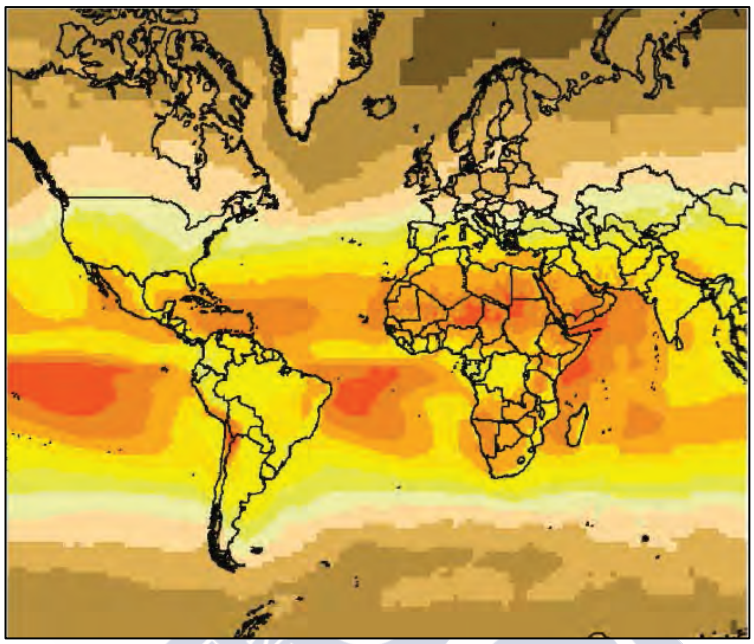

Fig. 6 Global Horizontal Irradiance Worldwide. [9]

In this precise moment the country is experiencing a PV boom due to the aperture of the market and the subsidies that the government is giving. Thanks to this situation the electric energy produced by distributed PV panels is cheaper than the provided by the electric company [10]. In Fig. 7 the accumulated photovoltaic growth is shown, from 1992 until 2010 the growth has a shallow tendency, however from 2013 is becoming exponential.

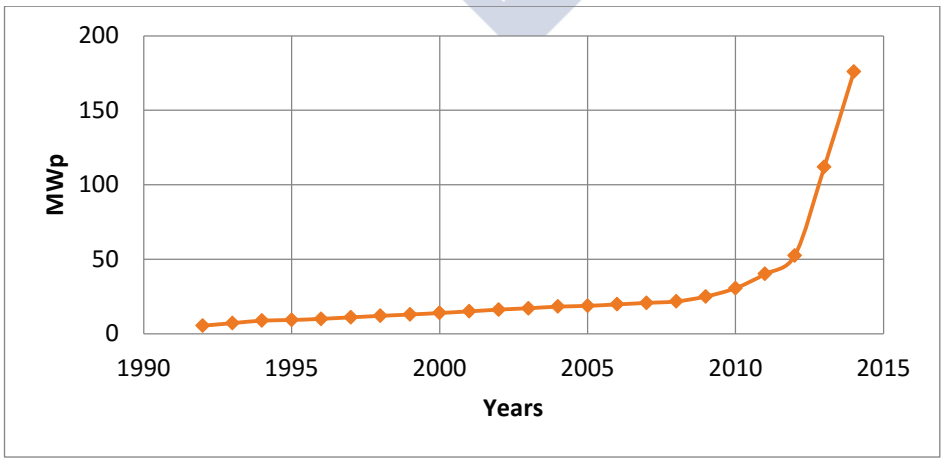

Fig. 7 Photovoltaic energy capacity growth in Mexico. [11]

For these reasons, since 2013, several companies are investing in large scale photovoltaic plants; the Energy Regulatory Commission has given permission for almost 5GW of PV power plants [12], [13], however only 195MW are currently installed [14], [15]. For example the Spanish company OPDE has at least 10 PV projects in development at the country; in Fig. 8 a map of Mexico is presented with the projects of OPDE.

Fig. 8 OPDE PV projects in Mexico 2015 (some projects are overlapped due to the zoom) [16]

Alternatively Mexico has only one power plant that uses high concentration solar thermal technology, at the northern state of Sonora. Agua Prieta II is a power plant that has an overall capacity of 478 MW (464 MW combined cycle, 14 MW solar input), and is one of a kind worldwide due to the hybrid capabilities of its design[17]. In Fig. 9 a picture of the power plant is shown, at the left side several rows of parabolic concentrators, on the right the combined cycle plant.

Fig. 9 Agua Prieta II Hybrid Power Plant. [18]

Additionally, in the same state as the past example, there is a research facility, managed by the University of Sonora and UNAM; that tests a high concentrated solar furnace and functions as a heliostat testing facility [19], [20], in Fig. 10 the facility used for tests is shown.

Fig. 10 Heliostat test field at Hermosillo, Mexico. [21]

As previously stated, the country has a high potential of solar energy, it's starting to develop in the solar supply industry and there are several maps and tables of solar radiation of Mexico published by different authors, however few measured data have been available for the preparation of these maps [22].

Recently there have been efforts to carry out the assessment of the solar resource in Mexico. In 2010 a national inventory of solar and wind energy was published by the "Instituto de Investigaciones Electrica" (IIE) on its website (Fig. 11). The main problem with this map is that the information about scientific methods of this project was not given publicly and it makes really difficult to evaluate the quality of the data [22].

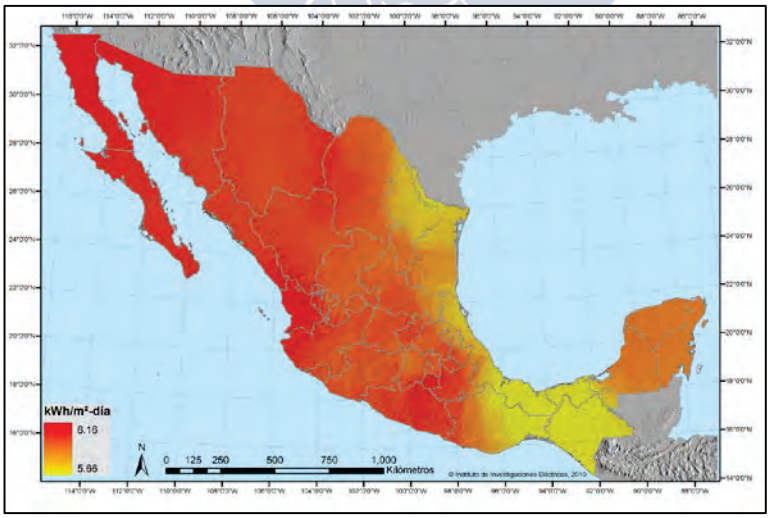

Fig. 11 Solar map of Mexico (GHI) [23]

Also, since 2013 the National Inventory of Renewable Energies (INERE) has been publishing maps of different providers/institutions with the objective of displaying the potentialities of

the country toward establishing the use of renewable energies. INERE has published a solar map developed by CFE with a resolution of 10 km by 10km elaborated from satellite images (Fig. 12). The advantage of this map versus the done in 2010 by IIE is that it gives the irradiation components of direct and diffuse irradiation. However, there was not given confidence intervals of the results, resembling most of the maps given by the Mexican government.

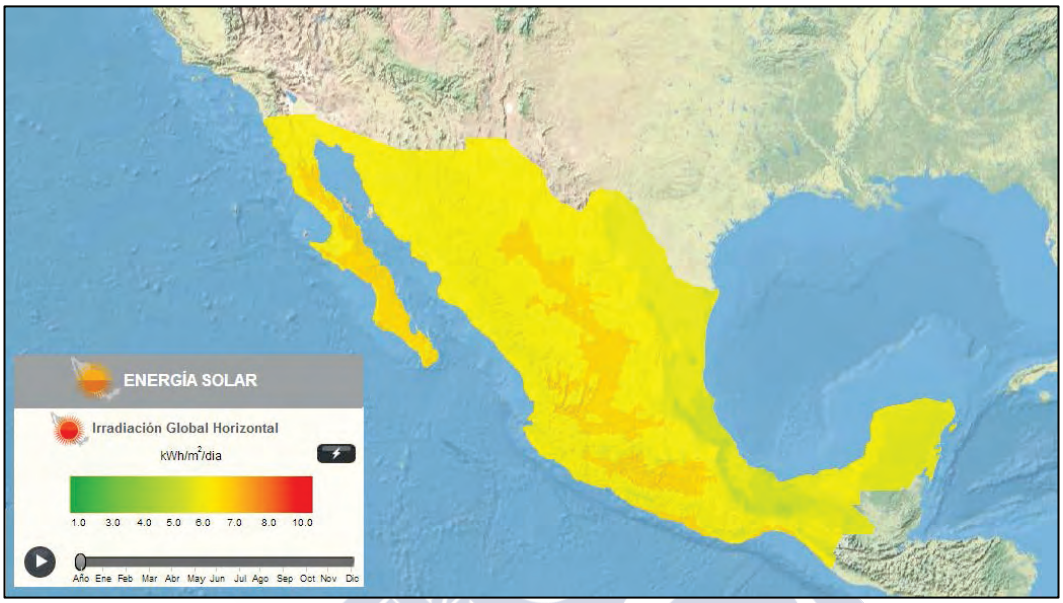

Fig. 12 Annual Global Horizontal Irradiation of Mexico.[24]

1.3 Wind energy

Besides the solar energy potential, there are regions in the country which has been investigated in detail by different national and international institutions due to the high potential of wind energy. Two clear cases are the Tehuantepec isthmus and Baja California Norte [25]–[29]. Even though this both cases are well studied, it is necessary to perform further research in the rest of the country in order to use this resource instead of nonrenewable alternatives. In Fig. 13 a wind map of Oaxaca State is shown, the high potentiality of the Tehuantepec isthmus is noticeable on the western part of the state. Several sites of wind power class from 5 to 7 are pointed out. This result makes this region highly attractive for wind power investment.

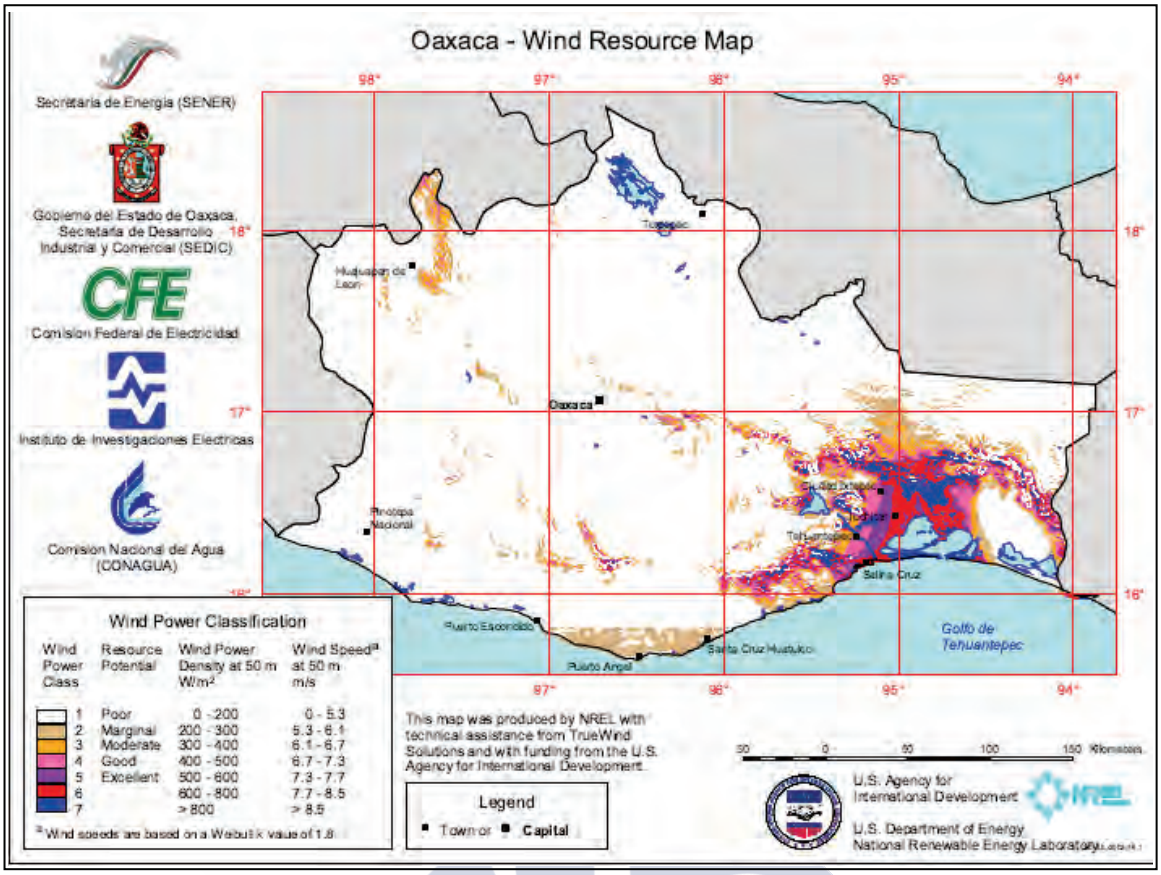

Fig. 13 Oaxaca wind resource map. [29]

The study was carried out in collaboration with the National Renewable Energy Laboratory (NREL) of USA and several Mexican agencies in 2003. The benefits of this research were the seed of the project for the two largest wind farms in Mexico. Most of the wind energy produced in Mexico comes from this region. Another assessment developed by NREL was done for the State of Baja California Norte's border region (Fig. 14); the methodology followed was the same as the Oaxaca assessment done in 2003[30].

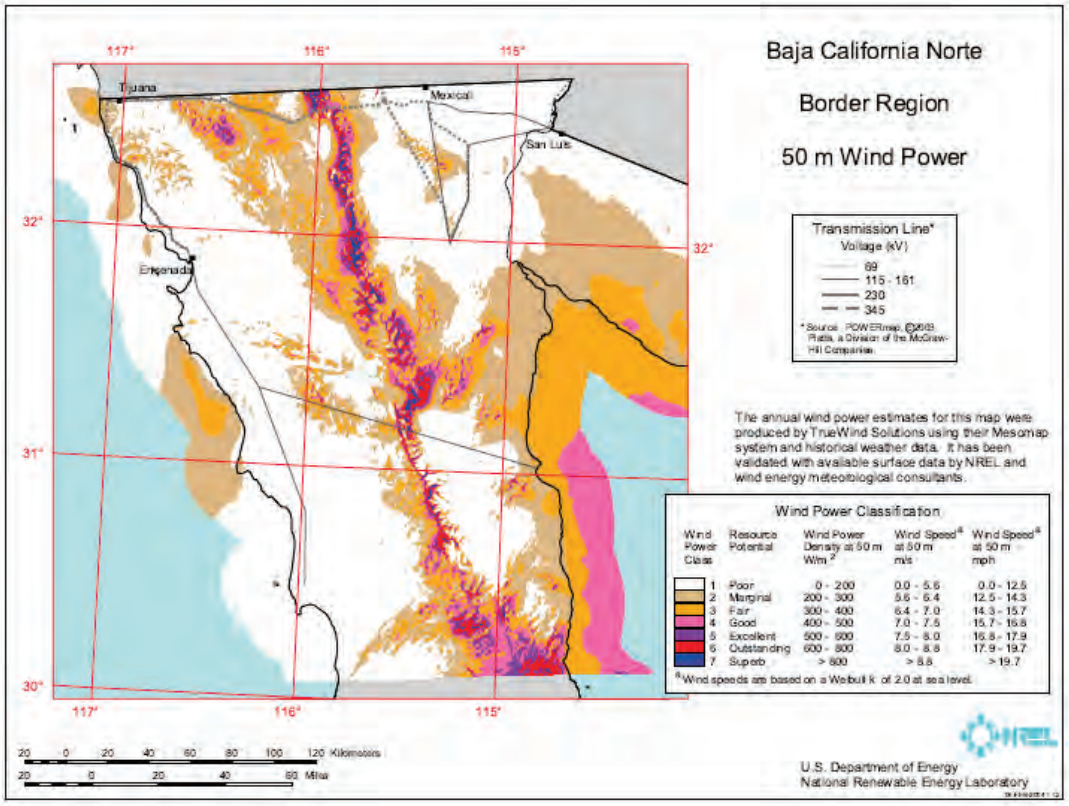

Fig. 14 Baja California Norte border region 50m wind power assessment. [30]

In 2010 a wind assessment map (Fig. 15) was also developed by the IIE for the SENER, as previously stated the map has the same lack of confidence intervals as the solar map. The map identifies the regions that could have high potential to project a wind farm. According to this map the power capacity of the country is about 71,000 MW.

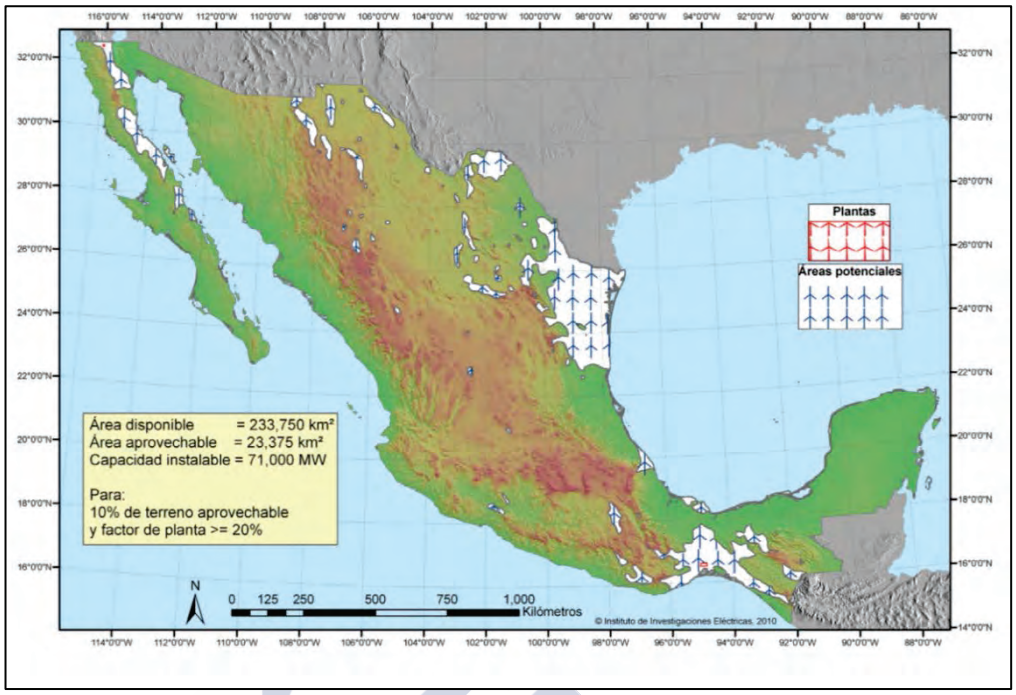

Fig. 15 Wind energy potential area map of Mexico. [23]

The wind atlas developed by Vestas in 2013 (Fig. 16) presents the results of an analysis obtained by numerical models of the atmosphere which was designed to provide an overview of the wind resources and other relevant conditions in a specific region of interest[31]. Wind data used in this report were obtained from 13 years of mesoscale simulations with 3 kilometers of horizontal resolution. The wind atlas has maps of annual and monthly average wind speed and power density. All maps were delivered in 50m, 80m and 120m heights above the ground[24].

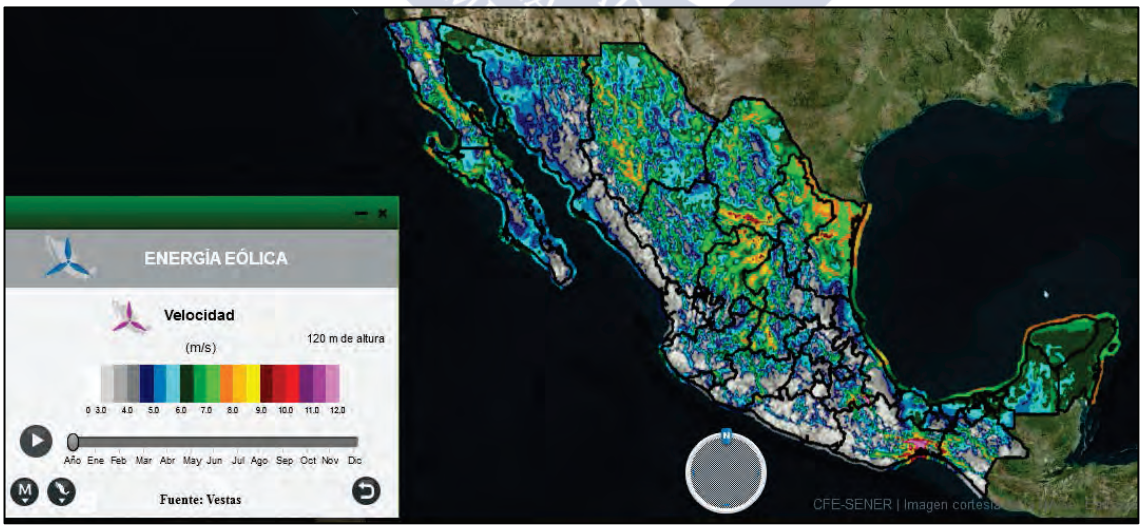

Fig. 16 Wind speed map at 120m height of Vestas. [24]

In the current government administration, a more detailed researched was developed at different heights (30, 50, 80 and 120 meters) and a lesser horizontal resolution map (7x7 km)

of the country. For all calculations, 10 years of data from the North American Regional Reanalysis (NARR) were used, combined with observation data and numerical modeling, in order to obtain a set of databases in high resolution of some variables of interest (in this case, wind)[32]. The methodology is based on the proposal by Mikhail and Justus to correct the wind at different heights[33].

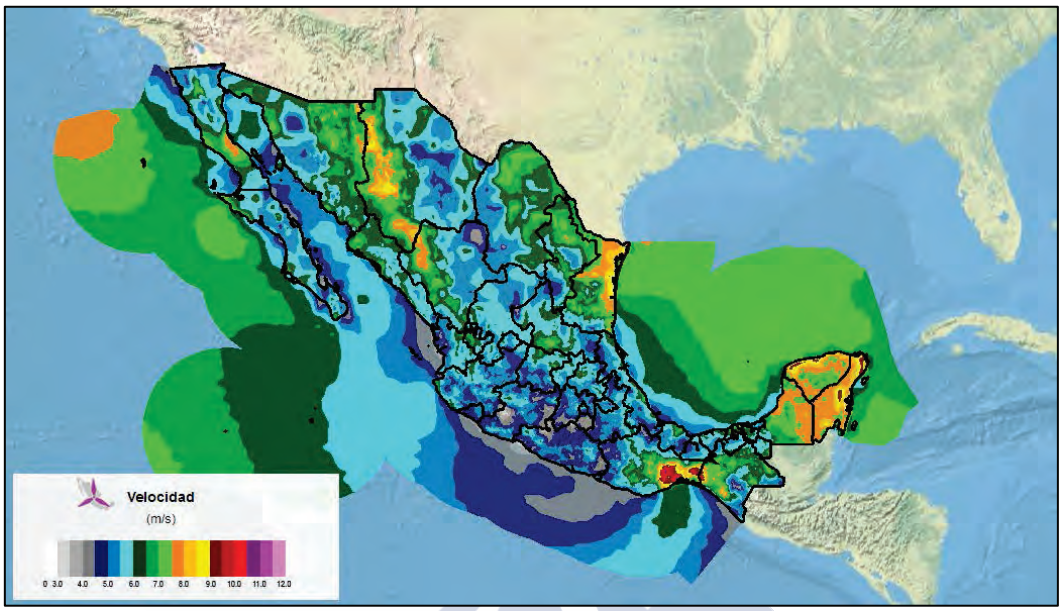

Fig. 17 Annual wind speed map of Mexico by CFE at 120m. [32]

In Mexico the wind energy is becoming really important and several companies have installed wind farms mostly in the state of Oaxaca due to several studies that shows the promising situation. The wind potential in the site is comparable to sites as productive as Galicia and Denmark[34]. In Fig. 18 a map of the wind power stations and its location is shown. The high density of power plants in Oaxaca is noticeable in the map.

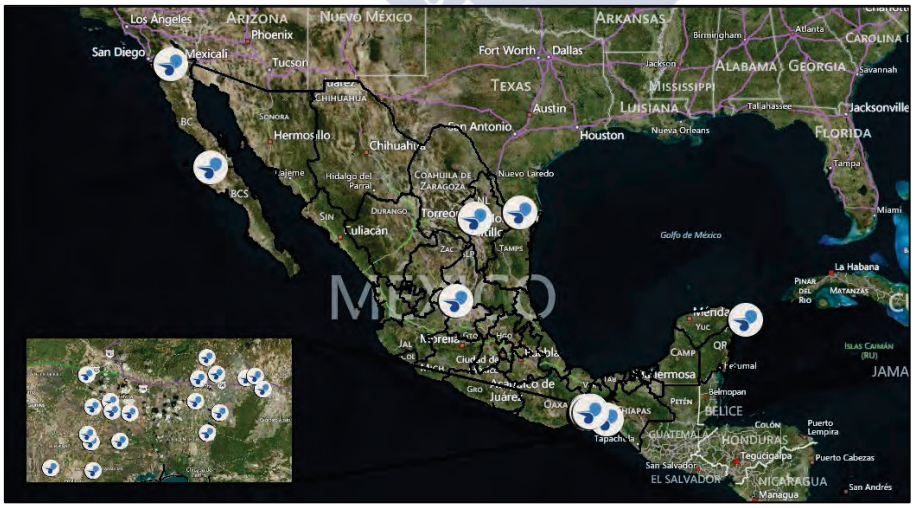

Fig. 18 Wind power stations in Mexico. [24]

1.4 Biofuels and biomass

There are other renewable resources that are being used in Mexico. With regard to bioenergy potential it has been estimated at 3035 PJ/year and 4550 PJ/year, representing between 54% and 81% of the Internal Energy Offer national Gross in 2006 [35]. The estimated potential indicates that 40 percent comes from wood fuel, 26 percent of biofuels and 0.6 percent of municipal by-products. However, it is thought that the country has a potential of 73 million tons of agricultural and forest residues that may be exploitable and municipal solid waste from 10 major cities can be harnessed to generate electricity from its thermal processing[36]. The use of organic residues of feedstock on anaerobic digesters is a common activity for local power generation. For example, during the period of 2008-2012, the federal government through SAGARPA supported the construction of 327 digesters and the acquisition of 137 electrical generators from biogas[37]. Currently a large amount of companies and farms use anaerobial digesters in order to reduce the energy consumption, at the same time reducing greenhouse effect gases[35]. The CFE also develop a series of maps of biomass assessment in the country for the SENER website INERE[24]. An example of this series of maps is shown below (Fig. 19). This map takes into account only biomass that could be used sustainably for energy purposes, among which is considered the residual biomass, biomass produced for energy purposes and biomass that can be used for energy purposes without affecting the environment, obtaining 6 large groups of biomass; residual agricultural and forestry industrial waste, urban waste, waste livestock, specialty crops and forests.

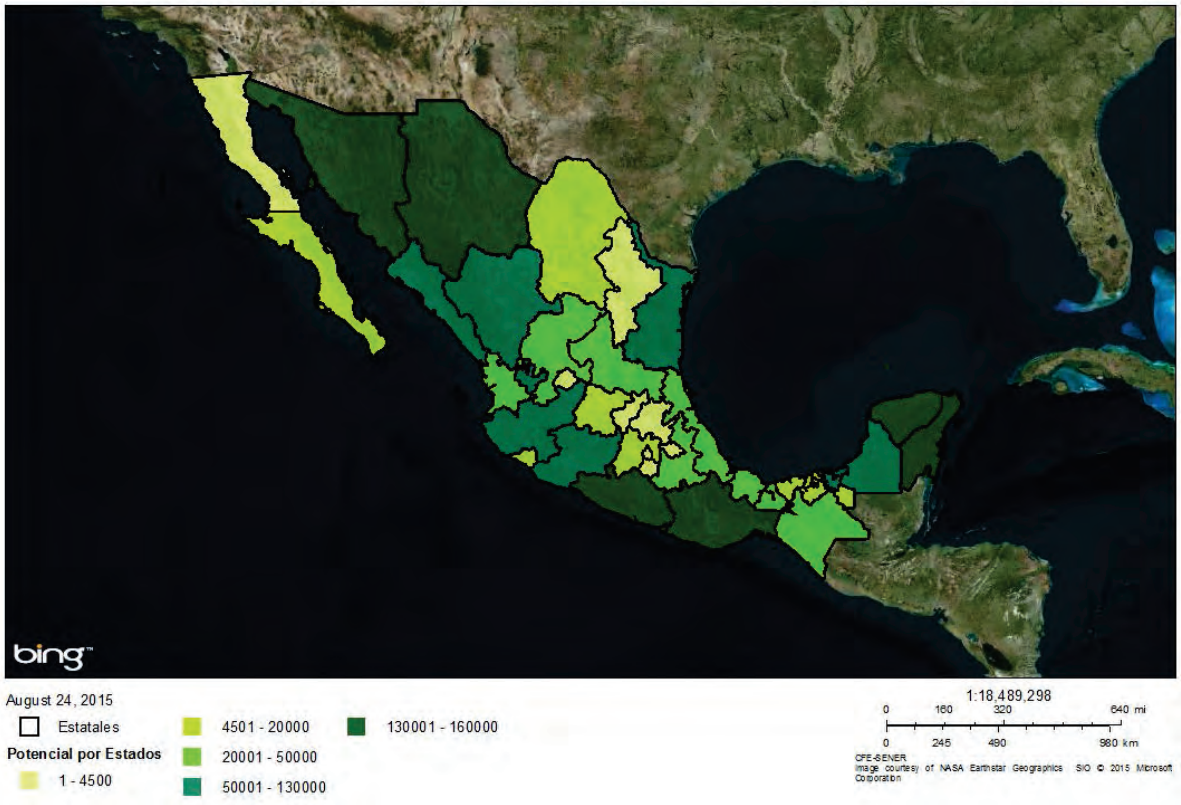

Fig. 19 Forest potential map of Mexico (TJ/a) .[24]

1.5 Marine energy

It is possible to generate electricity by using energy from the ocean in five forms of exploitation: tidal power, wave power, ocean currents, ocean thermal and salinity gradient. The global theoretical potential for energy supply which is estimated could bring around 82,950 TWh annually, highlighting the ocean thermal with 53%, wave 36%, tidal 9%, and the use of salt gradient 2%.

The marine energy is a technology option that the country could have high potential since Mexico has the second place on littoral extension in America. However, there is few research done by UNAM and other universities, and according to different authors the technology is not mature enough to be used in a large scale fashion [38].

The Annual Report 2014 of "The Executive Committee of Ocean Energy Systems" states that the marine energy development in Mexico is driven mainly by private companies working on different stages of the development of marine energy prototype devices. During the Workshop "Towards Marine Renewable Energy, Achievements, Challenges and Networks", organized by CICESE (Centro de Investigación Científica y de Educación Superior de Ensenada) in October 2014, the company Energy Forever presented a wave power plant project, which consists of the design, construction and commercialization of a buoy system that converts wave power to electricity. In fact, they have already started the corresponding procedures to deploy the first prototype at the Sauzal Port of Ensenada, Baja California, in association with the CFE [39].

In Fig. 20 a map of the tidal range illustrate possible sites for exploitation of tidal energy in Mexico; the most promising region appears to be in the Baja California Gulf between Sonora and Baja California at the northwestern part of the country.

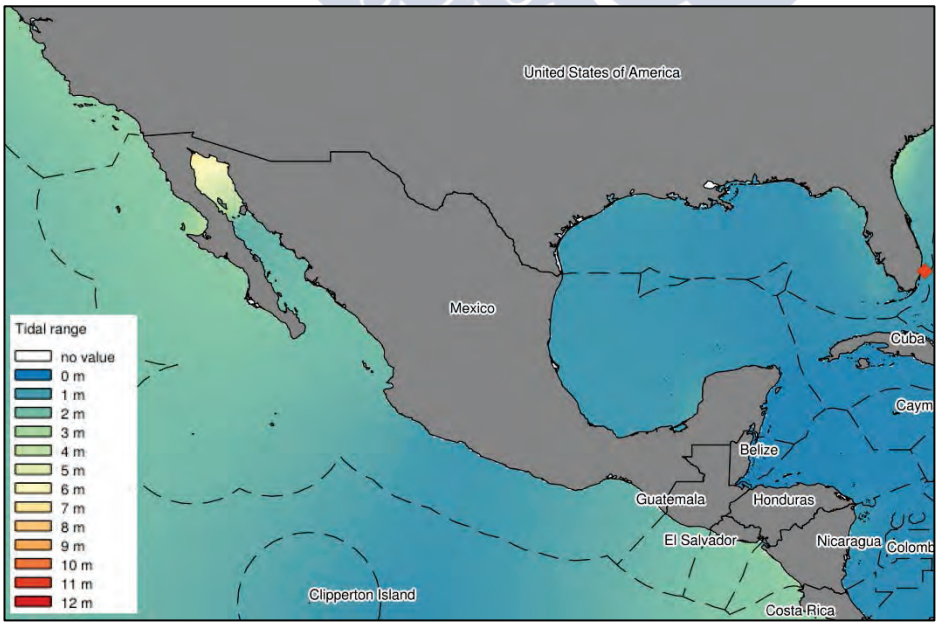

Fig. 20 Tidal range map of Mexico [39]

If we analyze the map of wave energy potential (Fig. 21), Mexico seems to have enough wave potential to use it as a possibility for renewable energy in the future, however there should be more research to understand the potential with higher resolution maps and to carefully choose sites that are not environmentally protected.

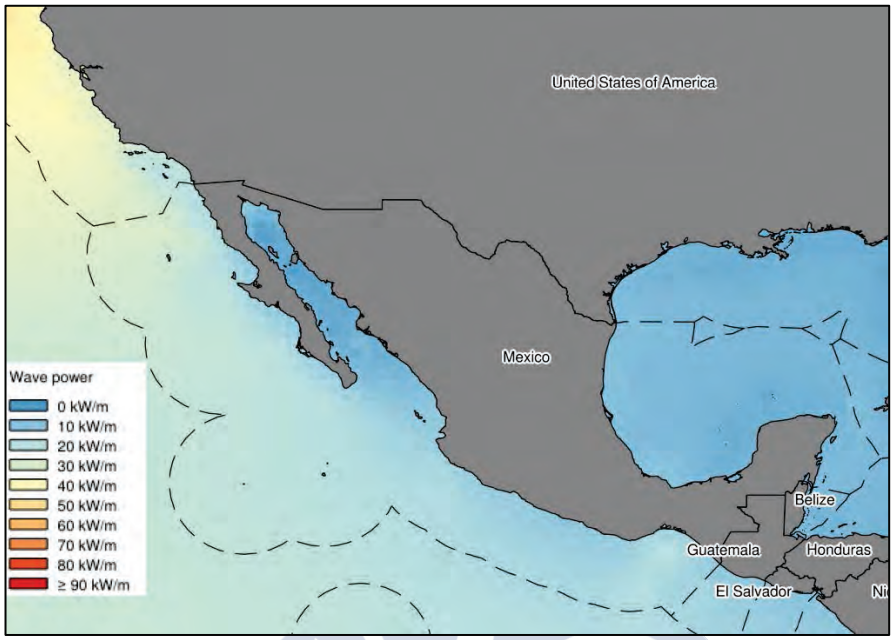

Fig. 21 Wave power potential map of Mexico.

1.6 Small hydro energy

Small hydro energy is another option that also should be contemplated, according CONUEE; this energy is only exploited about 2.5% in the country. Small hydro is further subdivided into mini hydro, usually defined as 100 to 1,000 kW, and micro hydro which is 5 to 100 kW.

The installed capacity is 80MW in operation, most of them private[40]. This type of technology is an option for rural communities suffering from shortages of electricity and that have a continuous river flow. The country also has a large amount of rivers all over its territory. The rivers and streams of Mexico constitute a hydrographic network of 633,000 kilometers. Through the channels of the 50 major rivers (Fig. 22) flows 87% of the superficial draining of the country and its basins cover 65% of the continental land area [41].

Fig. 22 Main rivers in Mexico.[41]

1.7 Geothermal energy

Geothermal energy is a renewable source that has been used worldwide to generate electricity since 1911, in Mexico since 1959 when it began to operate the first geothermal unit in the country, with 3.5 MW of capacity in the geothermal field of Pathé, Hidalgo, currently out of operation[42]. Since the country has extensive experience in geothermal generation, through the CFE, currently operates 38 units with a total installed capacity of 958 MW, it is clear that further development of geothermal energy could be achievable.

Since 1983 the CFE, in order to identify and evaluate geothermal resources, has been conducting the census of over 1300 thermal spots in Mexico, for which it has collected samples of all thermal springs that are inventoried and thereby determining analytical chemical parameters such as sodium, potassium, calcium, magnesium, chlorides, sulfates, silica, etc., necessary to determine the origin and waters classification and to calculate water-rock equilibrium temperatures, as indicative of the temperatures in the subsoil[15]. From this census, the map of geothermal potential was produced (Fig. 23). In the same figure the location of the several geothermal power plants is shown.

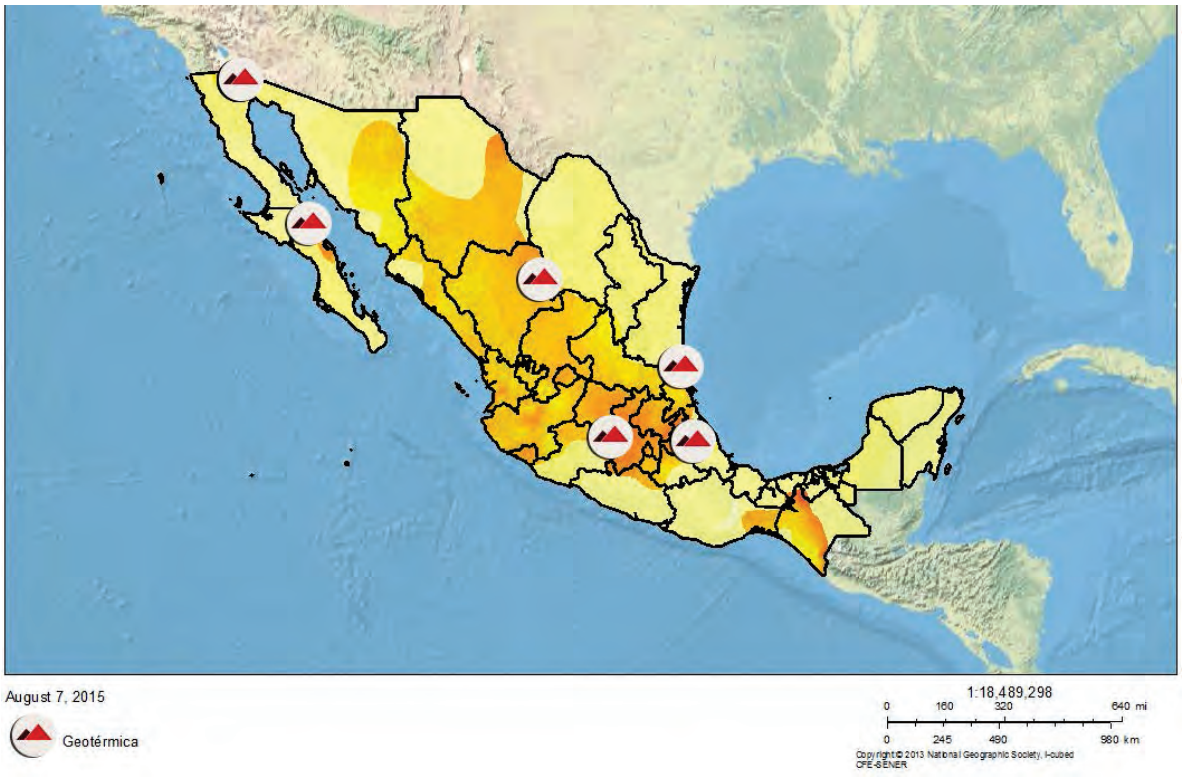

Fig. 23 High enthalpy geothermal energy potential map of Mexico with actual geothermal power stations. [24]

In Table 4 a list of geothermal energy plants is shown, the list shows a higher number of plants in Baja California State, since a part of the energy produced are exported to California granting additional revenue to these power plants.

Table 4 List of geothermal energy plants in México. [24]

State	Municipality	Name	Supplier	Power Units	Effective Capacity (MW)	Generation (GWH)
Baja California	Mexicali	Cerro Prieto I	CFE	5	30	302.22
Baja California	Mexicali	Cerro Prieto II	CFE	2	220	1420
Baja California	Mexicali	Cerro Prieto III	CFE	2	220	1420
Baja California	Mexicali	Cerro Prieto IV	CFE	4	100	815.05
Baja California Sur	Mulegé	Las Tres Vírgenes	CFE	2	10	51.07
Michoacán	Cd. Hidalgo	Los Azufres	CFE	14	191.6	1540.85

Puebla	Chignautla	Los Humeros	CFE	9	51.8	450.47
Tamaulipas	Altamira	Generadora Petrocel	Private	1	16.38	66.22
Coahuila	Torreón	Met-Mex Peñole	Private	1	7	37.84

Another type of the geothermal energy that is poorly exploited in Mexico is the low-enthalpy geothermal energy.

1.8 South of the State of Sonora region

Though the country has many regions contained in 31 states, with different resources, climate and necessities in this research we are going to focus in the south of Sonora. However, in this subchapter we are going to explain some aspects of the necessities, resources and climate of the State of Sonora, because for some aspects there is not clear differentiation between the north and south region. Moreover the results of the research are focused only for the south of Sonora region.

1.8.1 Geography and politic division

Sonora is one of the 31 states in which Mexico is divided; the state is situated at the northwest of the country. The state is bordered to the north by Arizona, to the east by Chihuahua, to the northwest by Baja California, to the south by Sinaloa and to the west by the sea of Cortez. The state has 72 municipalities, 55% of the population is concentrated in Hermosillo, Nogales and Cajeme.

Sonora's terrain, shown in Fig. 24, is varied and includes mountain ranges, broad plateaus, high valleys, and coastal plains. Much of Sonora is mountainous, with less than half the state higher than 1000m above sea level. The eastern part of Sonora is dominated by the Sierra Madre Occidental, with peaks exceeding 2600m, which trends north to south continuing to Sinaloa. The elevation of Hermosillo is around 200m. A coastal plain characterizes the western part of the state. There is a large desert in the northern Sonora.

Fig. 24 Sonora orography map. [43]

1.8.2 Population

The total population is 2,662,480 inhabitants according to the last census[43]. The population growth has been concentrated mostly on the coastline due to the agriculture and fishing. However the growth in the municipalities of the Sierra region (east) has been decreasing due to the less economic advantages and the difficulty of access. Regardless of the population growth in the whole State of Sonora (Fig. 25) is still the third least densely populated (14.8 inhabitants/km^2) state in the country.

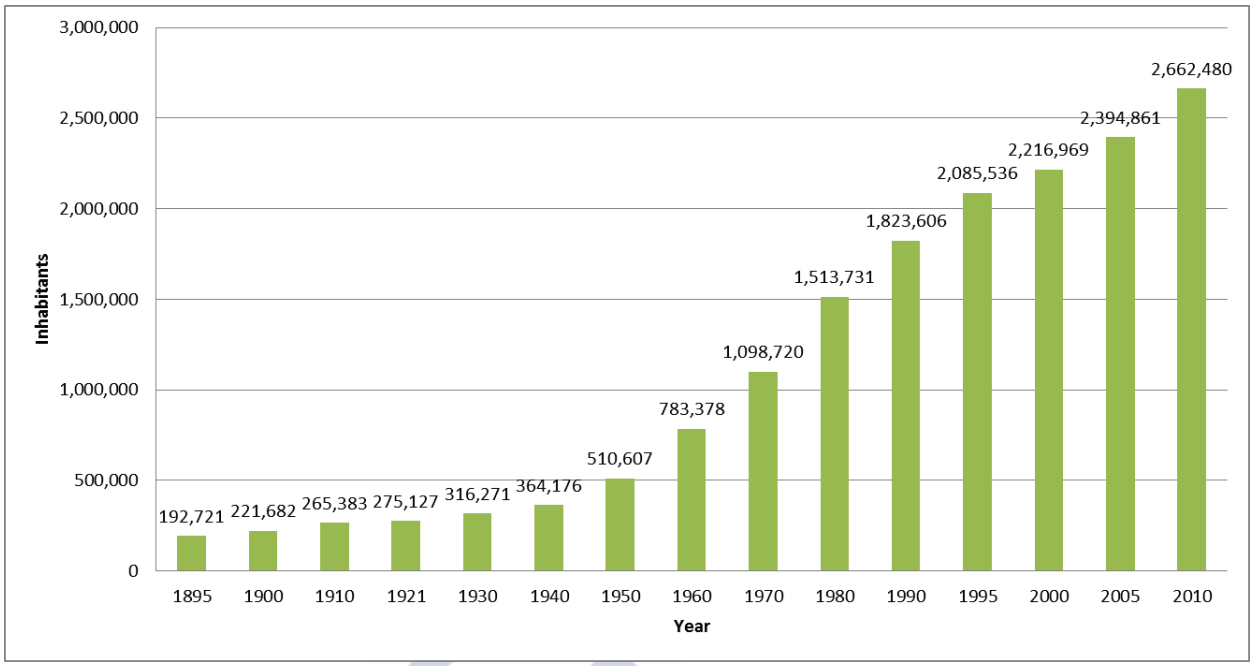

Fig. 25 Population growth in the State of Sonora.[43]

Fig. 26 is a political map of Sonora that shows the three most populated municipalities. The capital of Sonora and largest city is Hermosillo, with a population of 715,061[43]. Likewise is appreciated that the largest municipalities are in the coastline and the majority of them are the most populated with the exception of Nogales.

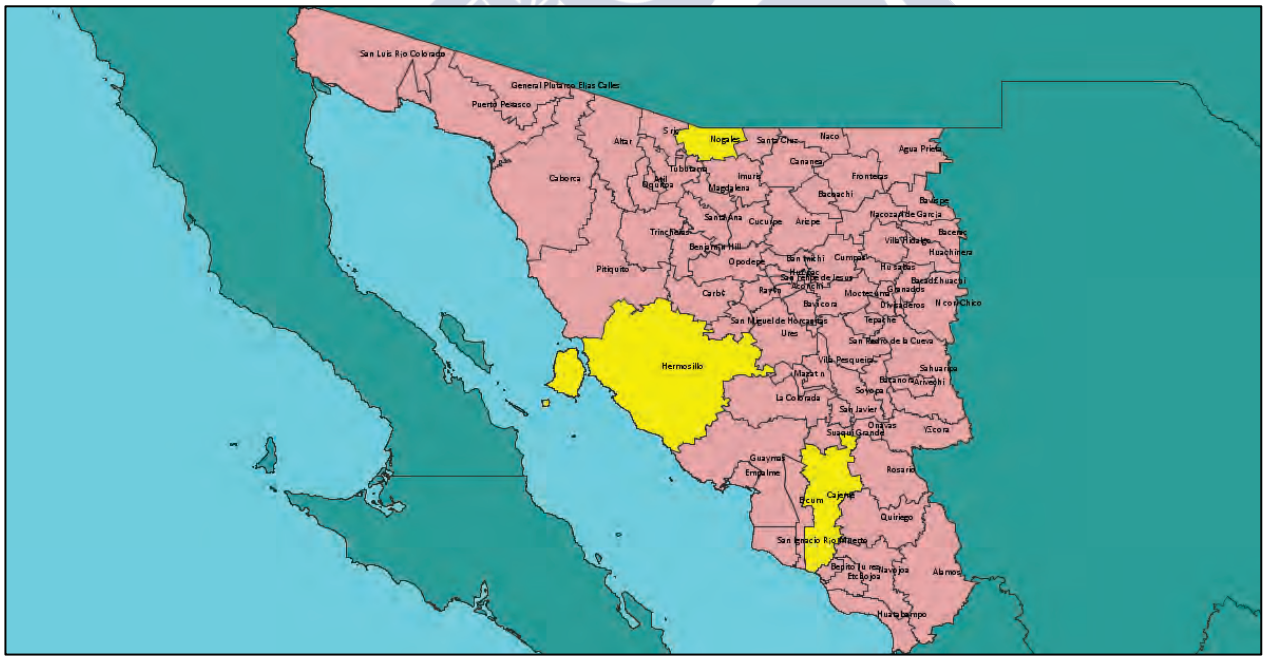

Fig. 26 Municipalities of Sonora (in yellow the three most populated).

Furthermore, is important to mention that the state has 8 indigenous groups that maintain much of their way of life in the territory. Sonora has 60,310 inhabitants that talk an

indigenous language; they represent only 3% of the population. However, more than 100,000 indigenous are registered by the last census. Additionally, ten of the thirteen municipalities that have indigenous groups are from the south of Sonora region.

This research takes in consideration 13 municipalities of the south shown in Fig. 27. The south of Sonora region has three main climates: very dry, dry and semi-dry, according to the climate classification of the National Institute of Statistics and Geography from Mexico[44].

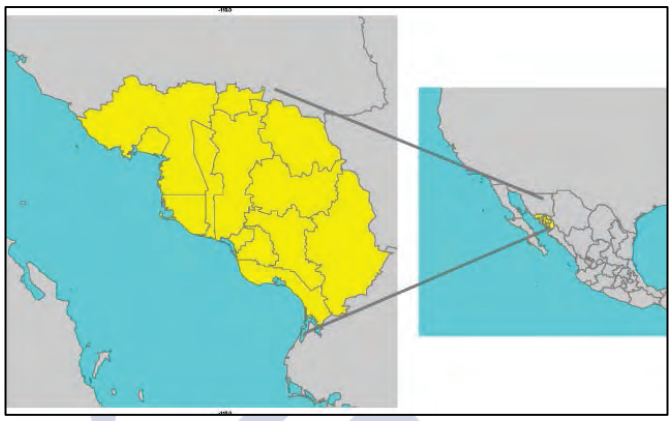

Fig. 27 State of Sonora location (in yellow municipalities of the south region).

The southern region of the State of Sonora extends from the municipalities of Huatabampo and Alamos in the south of the state to the municipalities of Guaymas, Cajeme and Quiriego passing the municipalities of Empalme, San Ignacio Rio Muerto, Bácum, Benito Juárez, Navojoa, Etchojoa and Rosario. This region has 38% of the state's population [45].

Although, Sonora is considered by CONAPO as a state with low marginalization, is planned to study the southern state of Sonora, because it represents the region with the highest number of municipalities with mid to high marginalization [46]. Two of these municipalities, Quiriego and Alamos, are classified as highly marginalized and as a priority area by SEDESOL[47]. In Fig. 28 a representation of the municipalities of the south of Sonora and the index of marginalization is shown. In red/orange the municipalities with highest marginalization index are presented.

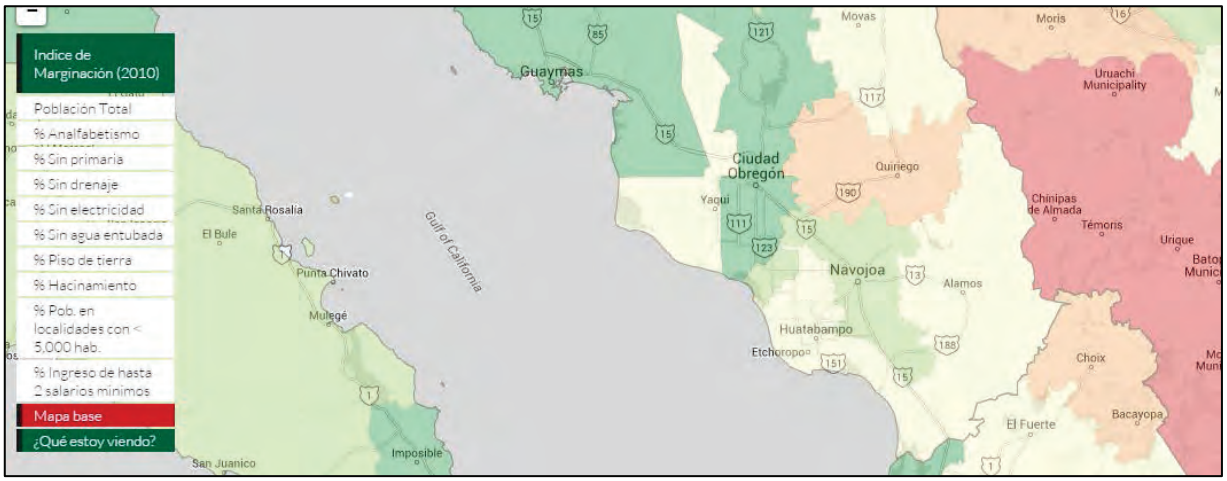

Fig. 28 Marginalization index in the south of Sonora municipalities.

1.8.3 Economic activities

According to the INEGI the unemployment in Sonora is about 5.56 % of the economically active population. Sonora has a PIB that generally is higher of the rest of the country and has strong bonds with Arizona State (USA)[48], [49]. Most of the industry is related with the agriculture, fishing, and food processing, however many industrial plants, called “maquiladoras”, were installed along the border with USA giving influence and modernization to the border municipalities[43].

Another traditionally element in the Sonora economy is the mining. Sonora is the number one producer of gold, graphite, molybdenum and wollastonite. Also Sonora has the largest carbon reserves in the country; also Sonora is the third producer worldwide of copper[43].

Another important activity is tourism. Mostly of the tourism in Sonora is related to the beaches; and two of the most visited destinations are San Carlos and Puerto Peñasco. Nonetheless, sustainable rural tourism is also been promoted by the Secretary of Tourism of the State of Sonora[50].

1.8.4 Water

The water is a critical aspect of production in any functioning economy. It has to be developed, treated, transported and distributed sufficiently and affordable to users. Moreover, using and treatment of water, releases byproducts that have implications on the environment. Water supply also conveys the use of energy. The water for Sonora, due to its climate, becomes a major importance as a resource.

Sonora has had water scarcity all over the State; however water is scarcer in the northern municipalities than in the south. The southern region also suffers from draughts that in past years almost dry out the water storages during several years [51].

The water is also important for cooling in standard energy generation processes. However for solar photovoltaic power or wind power the amount of water needed is almost forgettable[52], [53].

1.8.5 Energy

Electricity generation in Sonora is carried out in the follows: 38% thermal, 56% combined cycle, 5% hydro, the rest is through turbo gas plants and internal combustion engines (Fig. 29). This balance gives a high margin to use renewable energies in the state.

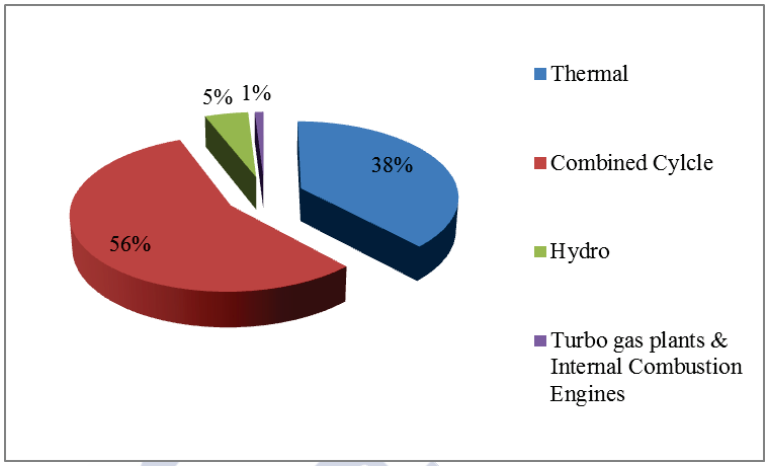

Fig. 29 Energy production in Sonora state.[15]

From this graphic, it seems that there is no use of renewable energy in the state's energy balance, however there is a PV plant of 1MW of power in the Municipality of Miguel Aleman of a private company for self-consumption(Fig. 30), that annually contributes about 0.66GWh [13].

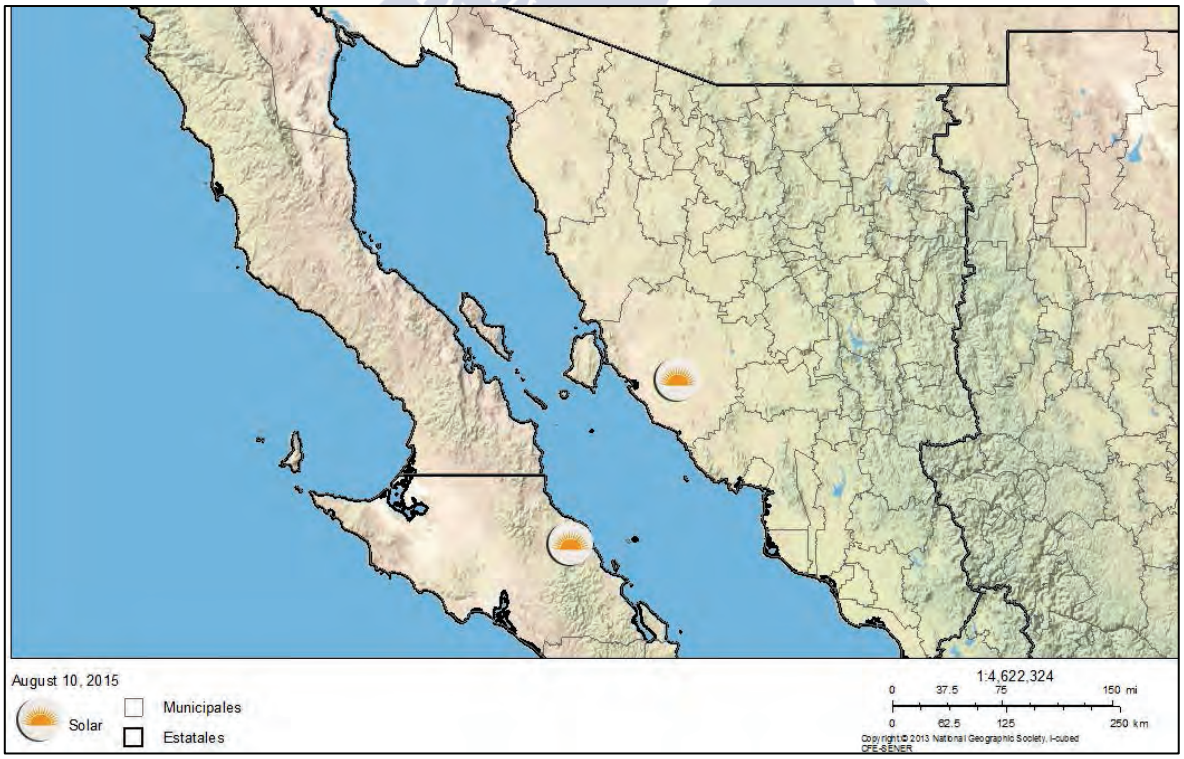

Fig. 30 Location of PV plant in Sonora [24]

Also the use of wood for heating and cooking is an extended custom on the Sierra municipalities, however there is not accountability of the amount of energy used by this way, but there is some data about the deforestation due to this custom[54]–[56]. According to Carton et. al., 28% of the evergreen woodland in the center of Sonora decreased from 1973 to 1992.

In 2003 a wind power assessment of the north-west border of Mexico (Fig. 31) was elaborated by NREL. This map shows estimations at 50m and most of the northern municipalities of Sonora resulted in a poor to fair wind potential[30]. According to NREL the results had been validated by surface data, however there were not many records of wind data nationally in that region[57].

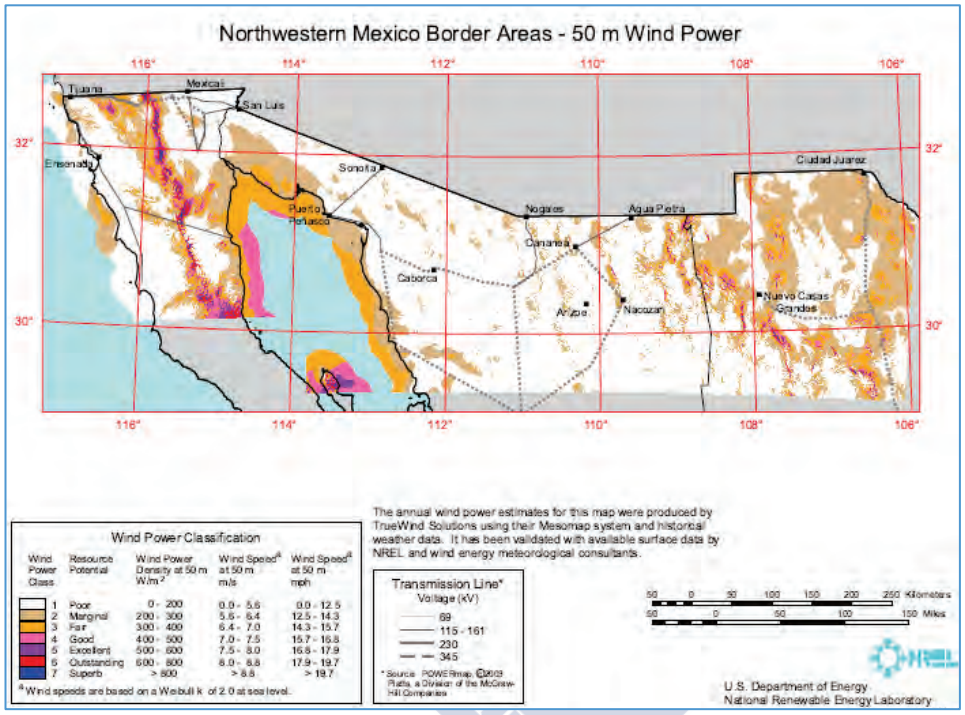

Fig. 31 Wind power assessment of north western Mexico border areas at 50m

The state of Sonora also has some evidences that wind energy could be used at least on small scale. According to the government agency CONUEE, on some rural communities of Sonora the use of wind pumps is disseminated on places where there is no grid electricity[25]. In the port of Guaymas there is a small scale wind turbine (6kWp) that generates enough electricity for the luminaries of the roadway. Also, in Puerto Peñasco touristic city, the “Energía Sonora AC” civil association installed a 2 MWp wind turbine in January of 2015, according to its webpage[58]. Apart of these small examples of wind energy use, it seems necessary to assess with a higher precision the wind power potential of the south of Sonora, as well as to consider the offshore wind energy.

1.9 Conclusions

Even though, the renewable energy sector looks promising in Mexico, in particular de geothermal, wind and solar energy, most of the studies of resource have been done without any validation and/or using inaccurate methods(linear interpolation of weather stations) to determine the resource in whole country. Another aspect of Mexico that difficult good results in energy assessment is the area of the country; Mexico is so large, that even there are places without human contact and the assessment result really challenging due to the weather station density and the complexity of the topography and climatology. Doing a micro-region, resource assessment results in a better understanding of the energy possibilities and giving better tools for development.

While the solar resource in Sonora was believed to be significant based on limited past data, understanding the spatial and temporal variability requires significantly more data and analysis in order to optimize planning and placement of solar energy power plants.

The wind assessment of the State of Sonora made by Vestas gave fewer wind power possibilities for the south region than to the north; however in the assessment made by CFE the wind power possibilities are better closer to the sierra in the south region. Moreover the methodology followed by these two recent studies is not clear, and validation for this kind of resource is necessary on a micro-scale level.

From this remark, we conclude, that is necessary to focus on a region that has enough data to have a convincing result and to have an energy resource analysis method that gave less uncertainty in comparison to past methods. For this reason the south of Sonora seems like a suitable region to do this research because the region apparently has many resources but also has needs that could be cover by renewable energies.

USC
UNIVERSIDADE
DE SANTIAGO
DE COMPOSTELA

CHAPTER 2 GLOBAL HORIZONTAL IRRADIANCE ASSESSMENT METHODOLOGY FROM A NUMERICAL WEATHER PREDICTION MODEL IN A SEMI-DESERT REGION

2.1. Introduction

During the last 7 years the Sustainable Energy Applications Group (SEAG) in collaboration with the Non Lineal Physics Group at the Santiago Compostela University and different associate researchers around the world, several actions have been done in order to create a procedure protocol based in the parametric study of different micro-regions around the world, so as to the establishment of a self-sustainable communities network [59]–[62].

The procedure protocol comprehends the identification and evaluation of local energy resources. The solar energy is one of the key resources to be evaluated in each region. The current state of development of solar energy technologies is increasing the need for more detailed radiation information. A solar map lets us determine the solar energy potential for the region in study. As previously stated in Chapter 1, Mexico has different solar studies previously developed, however none of these have a certainty of validation probably due to the dimensions of the country.

In this Chapter we developed a methodology to use a Numerical Weather Prediction model to generate a year of data used to produce a solar map for semi-desert region on the north-west of Mexico validated with agro-climatic stations. Section 2.2 is about a contextualization on Solar Radiation Models, and also states the reasons of selecting WRF model for this research. In section 2.3

2.2. Solar radiation models

There are many methodologies to develop a solar map and/or forecast (inference from in situ data, satellite observations and models)[61], [63]–[69]. In this work the GHI was estimated by a numerical weather forecast model and from the solar data given of the ERA-Interim reanalysis[70]. The use of similar approaches has been assessed by some authors[69], [71]–[73]; yet, variations in the output depend upon the location due to variable weather conditions and partially cloudy days.

The solar modeling could be divided in two different group types, clear sky solar radiation and under all sky conditions.

2.2.1 Clear sky solar radiation models

The atmosphere is a continuously variable filter operating on the solar radiation. The atmospheric filter modifies not only the intensity but also the spectral distribution. In this subchapter we denote of clear sky as the absence of clouds, which are made up of water vapor droplets, frozen ice crystal or a mixture of both. The use of clear sky helps to simplify the model equations considerably because radiation modelling in the presence of clouds can be challenging. Clear sky radiation models could also be subdivided in three types of models: physics-based models, empirical models and parametrization models [74].

2.2.1.1 Physics-based (PB) models

PB models regularly start with the sunlight reaching the top of the atmosphere; these are based on the interaction of matter and radiation. The extraterrestrial radiation is a function of the day of the year since the elliptical orbit of Earth brings it closer than the mean Earth-Sun distance in the Northern Hemisphere winter and father away from the mean distance in the Northern Hemisphere summer. The irradiance depends on the inverse square law (I/r^2) where r is the distance from a point source (the sun) to the endpoint (atmosphere). This results in 3% greater extraterrestrial irradiance results in January than the irradiance at the mean Earth-Sun distance and 3% less than extraterrestrial irradiance in July[75].

2.2.1.2 Empirical models

These are based on correlation or functions derived through linear regression or curve fitting analysis. This approach assumes that measured solar radiation data can be described as a function of some other independently measured variable. The independent variables that are mostly used are: temperature, relative humidity, day length, cloud cover, sunshine duration between others.

Examples of these types of models are: Meinel and Meinel (1976) developed a model that only needs the extraterrestrial irradiance, the Earth-Sun distance and the air mass at sea level [76], in 1970 the model of Laue included the altitude in to the expression[77]. One of the most popular models was developed by Linke and is based on the optical thickness of the atmosphere[78].

2.2.1.3 Parametrization models

The main elements of the atmosphere are gas molecules, which have several dimensions on the order of wavelength light in the extraterrestrial irradiance spectral distribution. Some parts of the solar spectrum are absorbed by, reflected or scattered from the molecules. Rayleigh showed that the sky is blue due to the average size of the molecules is shorter than the wavelength of photons, which correspond to the blue region of the human color perception range, are scattered out of the sunlight. Predominantly atmospheric gases, water vapor, ozone and aerosols filter and attenuate the sunlight as it passes through the atmosphere. These constituents of the atmosphere could be considered to have a transmittance that can be parameterized in the terms of the air mass and concentration.

The Bird model for clear sky total hemispherical irradiance takes in consideration these transmittances and used them in order to determine the DNI and Diffuse Irradiance. With both components is easy to calculate the GHI. This model use different for each of the constituents of the atmosphere, Rayleigh scattering transmittance [79], [80], aerosol transmittance [81], ozone and water vapor attenuation [82].

Another parametrization model used by the Heliostat-3 European Meteosat project is the simplified SOLIS model[83]. This complex model needs atmospheric water vapor column and aerosol input parameters. It is a spectral physical model based on radiative transfer model calculations.

Moreover, REST2 model is a high performance model to predict sky broadband irradiance, illuminance and photo-synthetically active radiation from atmospheric data[84]. The model is based on a two band scheme. The solar irradiance is separated into two spectral regions on from 290 to 700nm and the second region from 700nm to 4000 nm, almost half each of the total energy. According to Myers, the first region is affected mainly by aerosols and Rayleigh scattering, the second region by water vapor and gaseous absorption[74]. Something important to mention, is that this model doesn't take in consideration about 1.5 to 2 % of solar irradiance beyond 4000nm. However this small underestimation could be added into the ending result of the calculation. The parameters needed for the model are listed next: site coordinates, station pressure, precipitable water, angstrom turbidity coefficient, angstrom wavelength exponent, aerosol single-scattering albedo, total column ozone amount, total column nitrogen dioxide amount and ground albedo. The REST2 model address additional gases (nitrogen dioxide) and has different functions for transmittances in each of regions than the Bird model.

There are some research [85]–[88] that discuss results of this type of solar models for different sites and most of them put the model of REST2 in a more than fair position. However, REST2 model since is so complex needs a long amount of inputs, that in some cases make it unfeasible to use.

2.2.2 Solar radiation models under all sky conditions

According to Myers (2013), "modeling solar radiation under all sky conditions is considerably more difficult and uncertain than modeling clear sky solar radiation" [89]. The physics of cloud transmittance and the enormously extensive diversity of spatial distributions of clouds are the main contributors to these difficulties.

The solar radiation models under all sky condition are also divided in 4 types: simple correlation models, clouds modeling, empirical all sky radiation models, all sky solar radiation from weather satellites and numerical weather forecast models.

2.2.2.1 Simple correlation models

This type of models are based on physically induced correlation between solar radiation values and meteorological variables, air temperature, atmospheric constituents, observed cloud cover and also hours of sunshine.

The agricultural research groups has long studied the relationship between temperature and solar radiation to develop models for evapotranspiration of water to determine irrigation needs[74]. One model that uses this correlation is the one developed by Hargreaves and Samani [90]. This model compares the accumulated daily solar radiation with the difference between the maximum and minimum daily temperatures. Other authors also included the atmospheric pressure in the expression.

One of the most famous correlation models is the one developed by Angstrom. This model correlates the monthly accumulated sunshine with the monthly solar radiation, by using an empirical constant (α) and the average monthly clear sky total irradiance[91]. Later, Prescott modified this model by changing the average monthly clear sky total irradiance with the extraterrestrial monthly average solar irradiance, easing the computing of this model[92]. The main issue with these models is that α is a site dependent coefficient. Besides, in order to generate the coefficient for a site is necessary to measure the GHI and sunshine duration.

Another widely used solar model is ASHRAE solar model[93], for hourly radiation, is based on a set of tables given for many locations around the planet. The model needs as an impute the declination angle, latitude, longitude and the standard time, one of the main problems with this model is the necessity of the constant tables that are not calculated for all the places in the world.

2.2.2.2 Cloud modeling

There are many different types of clouds. The different types of clouds vary in terms of their effectiveness at reflecting incoming sunlight and their ability to trap outgoing infrared radiation. Effective climate modeling and prediction needs to go beyond determining merely whether there will be more or fewer clouds; the types and locations of clouds matter a lot. Clouds are the second largest influence on solar radiation after the day-night cycle. The modeling of clouds could be very complicated due to their diverse characteristics (three-dimensionality, structures, dimensions, movement, and distribution). Is really important to properly model because clouds are the greatest unknown in all of physical climate modeling; they radically alter the distribution of radiant energy and latent heating in ways that have proven really hard to capture in climate models[94].

Due to the complexity of the clouds, the solar radiation model designers had to develop empirical engineering approaches to modeling how clouds have an impact on the transfer of solar radiation through the atmosphere. Examples of this models or schemes are: Manabe scheme developed in 1964 [95], Arakawa-Schubert parameterization in 1974[96], Tiedke scheme in 1989 for large scale models[97], Betts-Miller scheme in 1986 [98], Kain-Fritsch parameterization for NWP models in 1993[99] and improved in 2004[100], between others.

2.2.2.3 Empirical all sky radiation models

An empirical all sky radiation model consists on a parameterization or correlation of measured solar radiation and cloud observations. There are some examples of this approach, however this type of models require input data related to solar measurements in the first place, like direct to global or beam to diffuse ratios, sunshine duration, Linke turbidity factor, clearness index between others. One example is the Kasten-Czeplak model[101] that analyzed radiation correlations with cloud coverage and type. Ehnberg and Bollen also developed a model that relates the global solar radiation, solar elevation angle and cloud cover[102].

2.2.2.4 All sky solar radiation from weather satellites

These kinds of models use satellite images and empirical data to obtain solar radiation values. Deriving solar radiation data from weather satellite images have been developed and applied worldwide by two available models. These models are Heliostat-2[75], [83], [103], developed in the European Community, based on the METEOSAT series of satellites and later Perez et al. developed the SUNY (State University of New York) satellite model based on the U.S. GOES series of satellite images[104]. This kind of models are being used regularly to develop solar maps in many places for preliminary assessments[22], [105]–[113]. One of this examples is the latest solar atlas of Mexico produced by SENER[24] already mentioned in Chapter 1.

2.2.2.5 Numerical Weather Prediction models

Recently, the use of NWPs to simulate the globe's climate has considerably grown. Numerical weather prediction uses mathematical models of the atmosphere and oceans to predict the weather based on current or past weather conditions. Though first attempted in the 1920s, it was not until the arrival of computer simulation in the 1950s that numerical weather forecasts produced realistic results. A number of global and regional forecast models are run in different countries worldwide, using current weather observations relayed from radiosondes, weather satellites or other NWPs outputs as inputs to the models[114].

The ECMWF model is a spectral primitive equation model with a semi-lagrangian, semi-implicit time scheme and a comprehensive treatment of physical processes. It is coupled interactively to an ocean wave model. Its spatial resolution is 25 km and there are 91 vertical levels. Initial data for the forecasts are prepared using a four-dimensional variational assimilation scheme, which uses a large range of conventional and satellite observations over a 12-hour time window[115].

Another global scale NWP model available is the Global Forecast System (GFS). The GFS model is a coupled model, composed of four separate models (an atmosphere model, an ocean model, a land/soil model, and a sea ice model), which work together to provide the weather conditions of the world[116]. The entire globe is covered by the GFS at a base horizontal resolution of 28 kilometers between grid points, which is used by the operational forecasters who predict weather out to 16 days in the future. Several of atmospheric and land-soil

variables are available through this dataset, from temperatures, winds, and precipitation to soil moisture and atmospheric ozone concentration[117].

The WRF (Weather Research and Forecasting), is a NWP mesoscale model of new generation, initially designed for use in forecasting and atmosphere study. It is probably the most intensively used around the world and extensively assessed NWP model. The WRF model can be used at the level of research in different fields such as atmospheric, weather forecasting, climate change and energy among others. Besides the latest updates it presents significant improvements in relation to physical settings as part microphysics, cumulus parameterization, the atmospheric boundary layer, the surface layer soil model and radiation[118], [119].

2.2.3 Solar model selection

In this research the selection of the model is based on choosing from the models that has the highest accuracy to a specific area, with a high resolution output. Moreover, an all sky model is also preferable in order to have a real sense of the atmosphere in the region and to have a full year accounted. In Table 5 a summary of the models mention before is shown and the parameters of selection are presented as well. Among the huge number of possibilities, choosing the right model is complicated. The decision should take into account not only the sensitivity of the method but the availability of the information that the model needs to define the initial conditions. For that reason, usually the lack of adequate historical is regularly the main constraint to deciding the model used. The second condition to consider is the climate region to run the model selected since accuracies achieved are very different.

Table 5 Decision matrix of Solar models

Model	Type of model	Parameters used	Accuracy
Meinel and Meinel	CSM	Extraterrestrial irradiance, Air mass	MBE: 1.7-30.7%, RMSE: 3.3-38.9%, MAE: 2.5-32.4% (validated with several solarimetric stations on arid conditions). [120]
Bird	CSM	Extraterrestrial irradiance, Rayleigh scattering transmittance, Aerosol transmittance, Ozone and Water vapor attenuation.	MBE: ±10%, RMSE<20% (Prediction in Romania, Clear sky condition).[88]
Simplified SOLIS	CSM	Atmospheric water vapor column and Aerosol transmittance	MBE: 1.6-4.5%, RMSE: 2.6-7.2%, MAE: 2.1-5.0% (validated with several solarimetric stations on arid conditions). [120] MBE: ±10%, RMSE<20% (Prediction in Romania, Clear sky condition).[88]
REST2	CSM	Coordinates, Station pressure, Precipitable water, Angstrom	MBE: 0.2-3.3%, RMSE: 1.2-4.0%, MAE: 0.8-3.3% (validated with

		turbidity coefficient, Angstrom wavelength exponent, Aerosol single scattering albedo, Total column ozone amount, Total column nitrogen dioxide amount and Ground albedo.	several solarimetric stations on arid conditions). [120] MBE: ±10%, RMSE<20% (Prediction in Romania, Clear sky condition).[88]
Hargreaves and Samani	ASM	Temperature, Atmospheric pressure	r^2: 0.9543 (based on a validation study of Iran, best temperature based model (2004-2008).[121]
Angstrom-Prescott	ASM	Average monthly sky total irradiance/ Extraterrestrial monthly average irradiance, Angstrom coefficient.	r^2: 0.8582 (based on a validation study of Iran, best temperature based model (2004-2008).[121] RMSE: 9.32%, MBE: -0.30% (Compared with 5 sites measurements in Malaysia).[122]
ASHRAE	ASM	Latitude, longitude, solar angle, standard time.	MBE: 3-32%, RMSE: 7.5%-34% (monthly predictions for India).[123] MBE: ±10%, RMSE<20% (Prediction in Romania, Clear sky condition).[88]
Kasten-Czeplak	ASM	Cloud cover and Type of clouds	MBE: 9-39%, RMSE: 10-41% (monthly predictions for India).[123] MBE: ±10%, RMSE<20% (Prediction in Romania, Clear sky condition).[88] RMSE: 0.45-1.45 MJ/m^2*day (for several sites around the world).[124]
Ehnberg and Bollen	ASM	Solar elevation angle and Cloud cover	Standard deviation of 40 W/m^2(Model validated in Sweden)[102]
Heliostat	ASM	Satellite Images, Topography maps, Extraterrestrial irradiance, Albedo	RMSE: 10% (average on 51 sites in India).[107] RMSE: 10-16.6%(Annually for 6 sites in India).[106]
Sunny	ASM	Satellite Images, Topography maps, Extraterrestrial irradiance, Albedo	RMSE: 1-9% (1-5hrs forecasts)[125] MBE: 0-18%, MAE: 20-35%, RMSE: 32-50% (Validation on several sites of California).[113]
WRF	NWP	Selectable parameterization, Topography, albedo, land use, lesser resolution NWP data.	MAE: 16-37%, RMSE: 26-60% (2-3day forecast in different countries north hemisphere). [126] RMSE: 18-50% (Forecast in USA)[127] RMSE: 45% (Forecast in USA)[128] RMSE 22.6-66.2%(1-3 days forecasts in Europe)[65]

In the opposite direction, models as simplified SOLIS among the CSM or Kasten-Czeplak among the ASM, obtain acceptable results with a reduced number of external parameters. However the results are strongly dependent on the area of validation and therefore application. Another good candidate is the model Heliosat with good results in semi-humid climates; however it uses satellite data from Europe and Africa.

In this research the WRF model was selected due to the characteristics of the model. The different parameterizations allow to use the model in different climates and to have results according to the research. The input of the model consists in the output of a global scale NWP, and static data as orography, topography and land-use.

2.3 Current situation in the region

There are a significant number of maps and databases describing the solar resource distribution in Mexico[24], [129]–[133], developed by different universities and research centers, as stated in previous chapter. However in none of these studies confidence intervals of data are provided[22]. The main objective of this research is to create a solar radiation database of a region that has enough data to give a relative good confidence interval. In this instance we evaluate the solar radiation of the southern region of the state of Sonora Mexico, also described in Chapter 1.

2.4 Materials and Methods

2.4.1 Observational data

The region has two weather station networks, the agro-weather station network of the Board for Agricultural Research and Experimentation of Sonora (PIEAES for its acronym in Spanish) and the National Institute for Forest and Agricultural Research (INIFAP for its acronym in Spanish). Both are databases focused on supporting the activities of farmers of the region and offer the source weather data to feed the prediction models for researchers[134], [135]. The PIEAES network has 32 weather stations that give a range of different data (temperature, humidity, wind speed and direction, irradiation between others) every 10 minutes. According to PIEAES the weather stations have maintenance checks at least once a month [134]. The INIFAP network is a larger system that has more than 1000 weather stations around the country, but only four in this region. The irradiation sensor used on both weather networks is a SP-Lite pyranometer from Kipp & Zonen with a spectral range between 400nm to 1100nm. Even though the weather stations have periodical maintenance, calibration of the solar radiation sensors are not stated in none of the weather station web pages, giving a high uncertainty of the quality of the measurements, since the producer recommends calibration every 2 years[136].

To avoid erroneous validation data, three quality filters were applied to the observations. The first consist on having at least 80% of the data for each station. The second quality filter was

to have a minimal of three consecutive years. The last quality filter was applied to the monthly values, if within a month there were 10 daily missed records or 5 consecutive daily missed records, the monthly value was discarded.

Five to eight years of GHI data were used to validate the output of the model, depending on the data at disposal. 28 agro-weather stations from PIEAES and 4 from INIFAP were used to validate the WRF outputs. A list of the weather stations used and its coordinates is shown on Table 6 as well as a map of the localization of each station on Fig. 32.

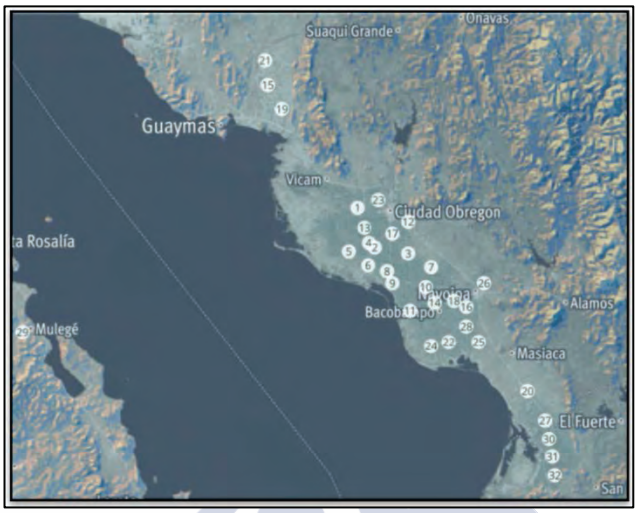

Fig. 32 Considered agro-weather stations.

Table 6 Weather Station List

Number	Name	Lon	Lat	Altitude (m)	Network
1	Block111	-110.12	27.50	37	PIEAES
2	Block1201	-110.02	27.30	20	PIEAES
3	Block1418	-109.83	27.27	45	PIEAES
4	Block1103	-110.05	27.32	35	PIEAES
5	Block1317	-110.17	27.28	9	PIEAES
6	Block1703	-110.05	27.21	35	PIEAES
7	Block1730	-109.70	27.20	46	PIEAES
8	Block1806	-109.95	27.18	15	PIEAES
9	Block2210	-109.92	27.12	4	PIEAES

10	Block2328	-109.73	27.10	16	PIEAES
11	Block2920	-109.82	26.98	9	PIEAES
12	Block414	-109.83	27.43	46	PIEAES
13	Block609	-110.08	27.40	25	PIEAES
14	Buaysiacobe	-109.68	27.02	17	PIEAES
15	Campo_52	-110.63	28.12	68	PIEAES
16	Cemay	-109.50	27.01	39	PIEAES
17	Ciano	-109.92	27.37	37	PIEAES
18	El_Chapote	-109.57	27.03	33	PIEAES
19	El_Norteno	-110.55	28.04	47	PIEAES
20	Estacion_Luis	-109.15	26.57	42	PIEAES
21	Gpe_Guaymas	-110.64	28.24	108	PIEAES
22	Huatabampo	-109.60	26.82	17	PIEAES
23	Jazmin	-110.01	27.54	37	PIEAES
24	Jupare	-109.70	26.80	11	PIEAES
25	Mumuncuera	-109.43	26.82	24	PIEAES
26	Tesia	-109.40	27.12	42	PIEAES
27	Torocobampo	-109.05	26.42	43	PIEAES
28	Tres_Carlos	-109.50	26.90	34	PIEAES
29	Valle_Mulege	-112.02	26.87	10	INIFAP
30	Chavez_Talamate	-109.02	26.32	27	INIFAP
31	Agri_Gotsis	-109.03	26.23	3	INIFAP
32	Carrizo	-108.99	26.14	25	INIFAP

2.4.2 Mean radiation year (MRY) methodology

One of the most common problems with using the WRF-model at high resolutions is the computational cost. In this chapter we consider to create a mean radiation year in order to reduce the amount of data to simulate (from 31 years to 1 year). Several types of methods to generate a typical weather data(or Typical Meteorological Year - TMY) like the Sandia National Laboratories method, the Danish method, the Festa-Ratto method or the Design reference year method are generally used to represent the long-term typical weather condition over a year[137]–[139] in a location. However in this research we developed a MRY in order to easily generate (with only one input, GHI in this case) and to analyze a complete region (not a single station or a single cell).

These arguments make this methodology ideal for this case, since a complete region is been analyzed. Moreover the use of this approach in comparison with the generally used methods, previously mentioned, helps to include irregularly periodical climate change events (like "ENSO") in the simulation period. Specifically these methods (TMY like methods) require a full contiguous month for each month of the year[138]; only considering 12 years of the total data at most to generate the year. However the method described below (MRY) has a daily variability in each month since it takes in consideration the closer day to the mean in a 31 year dataset. This variability allows including days that in other methods could be excluded since it will only include data from 12 years at most.

The methodology to produce the MRY is based on the arithmetic mean of surface solar radiation ($MeanSSDR_d$) from 31 days (each day corresponding to the same calendar day in a different year), calculated from the ERA-Interim GHI data ($SSDR_d$) of the total surface (area). Subsequently the $MeanSSDR_d$ is compared with each of the 31 days used before; the day that has the less difference with mean value, is selected. This is repeated for the 365 days of the year; the concatenated result gives the MRY for this region. The algorithm followed to generate the MRY is represented on Fig.33.

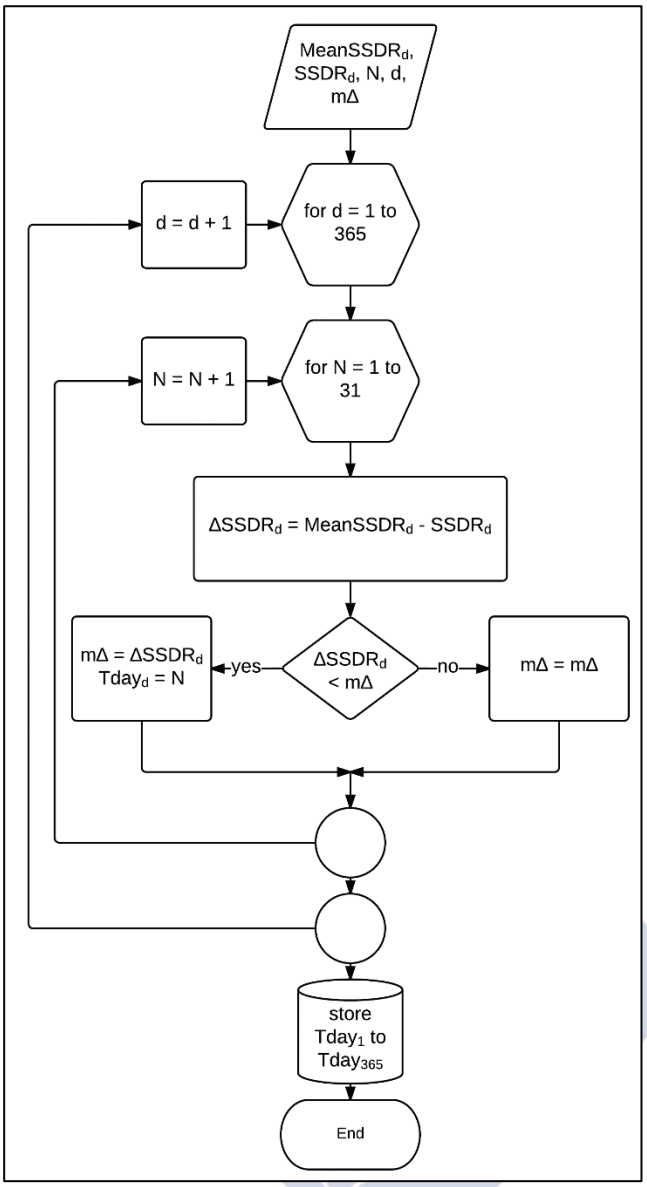

Fig.33 Flowchart for MRY methodology.

Where,

N is de number of years (1-31)

d is the selected day (1, 2...365)

mΔ = Minimal difference to the mean of each date

The mean radiation year is developed by the concatenation of the dates that have the lowest mΔ for the 365 days of the year in the 31 year data.

2.4.3 Validation metrics

The validation of modelled irradiation values against measurements are usually based on the root mean square error and the mean bias error[140]–[143], in this chapter both were used.

The mean bias error (MBE) is defined as the quantity used to measure how close the observed values are to the modelled ones. The MBE is given by

$$MBE = \frac{1}{n}\sum_{i=1}^{n}\frac{G_{MOD}-G_{OBS}}{G_{OBS}} \quad (1)$$

G_{MOD} represents the GHI given by the model

G_{OBS} represents the GHI given by the weather stations

n: samples

The relative root mean square error (rRMSE) is defined to be the square root of the totality of the squares of the difference between modeled and reference irradiances using some time interval over some time period divided by the number of observations. The rRMSE uses the following formula:

$$rRMSE = \sqrt{\frac{1}{n}\sum_{i=1}^{n}\left(\frac{G_{MOD}-G_{OBS}}{G_{OBS}}\right)^2} \quad (2)$$

2.4.4 Model and Setup

In this study, the Numerical Weather Prediction (NWP) model, advanced WRF model ver. 3.4 was used [144]. The model was run on the supercomputer *Finisterrae* in CESGA (Galicia, Spain). The spin-up time varies from different authors depending on the initial setup and resolution of the output. We do not take into account the first 12 hours because we consider that the WRF model needs time to stabilize.

The next 24 hours correspond to the selected day that interests us. The modelling setup including the selected domains and the initial and boundary conditions as well as the physics schemes are described below.

2.4.4.1 Domain setup

The WRF model was run in a series of one-way nested grids. The horizontal grid spacing was refined by a factor of 3 through 1 nested domain until 9 km resolution. The WRF model was built over a coarsest domain (Fig.34a) at 27 km, and a finest nested domain (Fig.34b) of 9 km spatial resolution.

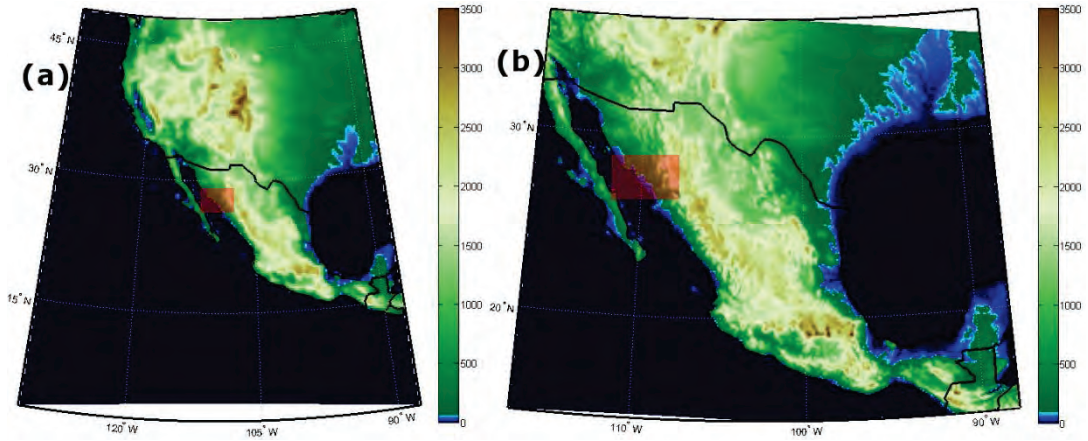

Fig.34 Domain 1(a) and domain 2 (b), topography models (Red rectangle: south of Sonora region).

2.4.4.2 Initial and boundary conditions.

The WRF model was used to improve the state of the estimated physical atmosphere magnitudes especially the planet boundary layers, by down-scaling the ERA-Interim reanalysis data provided by ECMWF. The ERA-Interim reanalysis project covers the period from 1979 to present and has a horizontal resolution of approximately 79km[70]. The initial conditions for the model were taken from the ERA-Interim date's selection of the MRY previously obtained. The static data used for all the WRF simulations had a horizontal resolution of 2 minutes (about 3.7 km).

2.4.4.3 Physics Schemes.

On Table 7 a summary of the configuration used on the model for each day is presented for reference. The physics schemes (in specific Cumulus, Shortwave and Longwave parametrizations) were selected, due to the characteristics of the region (climate and higher possibility of clear days) and the horizontal resolution of the grid. The rapid radiative transfer model [145] (a widely used scheme using look-up tables for efficiency) and the Dudhia [146] (a simple downward integration allowing for efficient cloud and clear-sky absorption and scattering) schemes were used for the longwave and shortwave radiation options, respectively. Finally, the cumulus physics was modelled with the New Kain-Fritsch[100] scheme that can be used on high resolution (in addition to coarser resolutions) and according to a study[147] is the parameterization that better performs in the country due to the types of cloud formation on rain season.

Table 7 Synopsis of the WRF model configuration used

Simulation period	365 days
Model version	V3.4
Domains	2
Horizontal resolution	27 and 9 km
Input data	ERA-Interim
Time step	100 s
Outputs frequency	120 (d01) and 10 minutes (d02)
Nesting	1-way nesting
Physics schemes	
Microphysics	WSM6 class
Cumulus	New Kain Fritsch
Shortwave	Dudhia
Longwave	Rapid Radiative Transfer Model
LSM	Noah
PBL	YSU

2.5 Results and Discussion

2.5.1 Model Results

The annual mean GHI for the south of Sonora region, calculated and taken from the daily WRF output[148] is presented in the map of Fig.35b. It's evidently noticed that the values and resolution on both cases (Fig.35a and Fig.35b) are different. The mean annual GHI found in the WRF output is 6.31kWh/m^2, slightly higher than the annual GHI of the ERA-Interim output (6.01kWh/m^2). The WRF simulation has a much higher resolution that better resolves the variability of the GHI on the eastern part of the region due to the mountains (Sierra Madre Occidental).

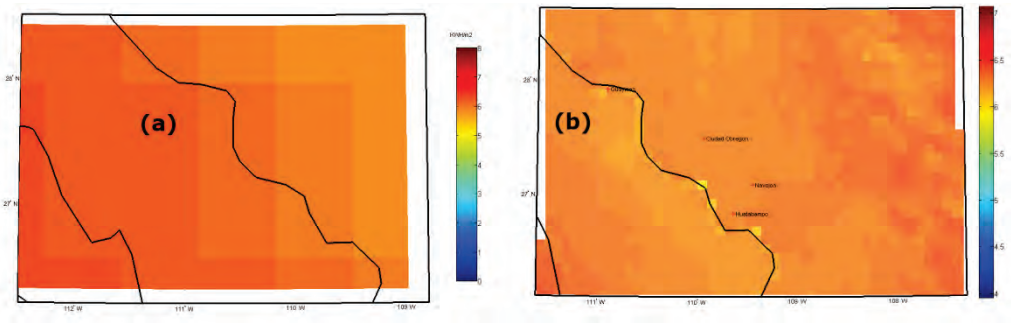

Fig.35 (a) ERA-Interim and (b) WRF output annual average GHI for the south of Sonora.

Additionally a mean monthly GHI representation for the WRF output was done, as shown in Fig.36. According to the figure the GHI is mainly driven by the sun position during the year.

The lower irradiation season during the months of autumn-winter is easily observed, as well as the higher irradiation season during spring – summer.

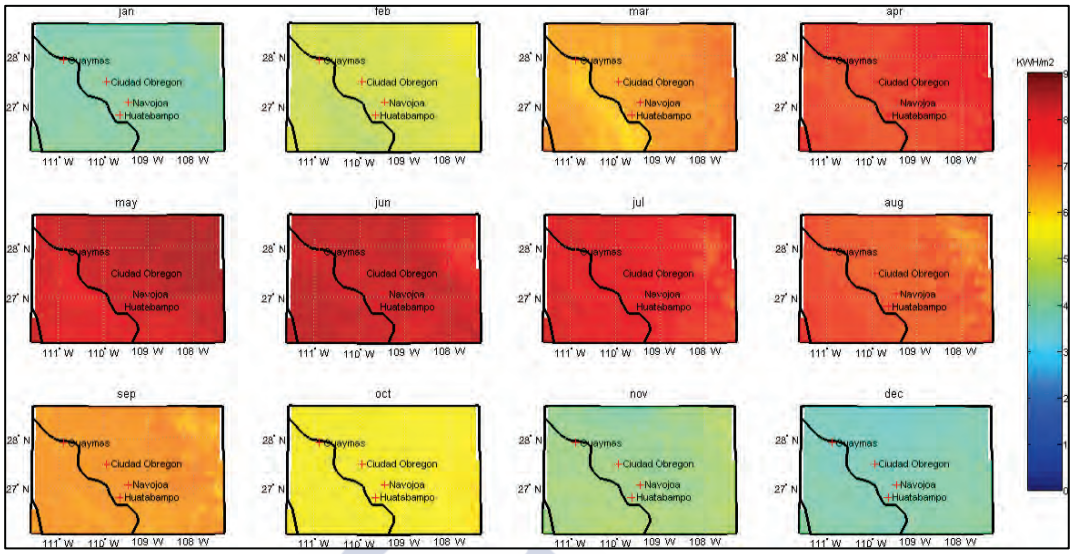

Fig.36 WRF output monthly average GHI for the south of Sonora.

2.5.2 Validation

In order to validate the GHI for the WRF model, a comparison between both the observations and the outputs were required, for the nearest geographical cell grid (latitude, longitude). In Fig.37 the mean monthly GHI for the region are represented, and were obtained from the observations, the WRF model output and the ERA-Interim data for each geographic location.

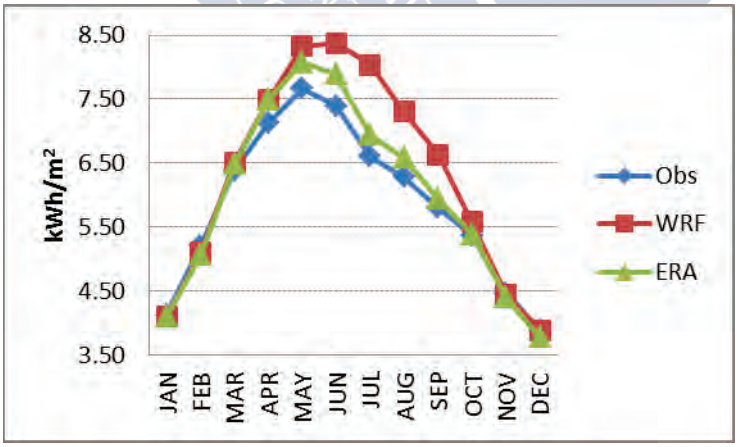

Fig.37 Mean Monthly GHI plot (Observations, WRF model and ERA-Interim output).

During 6 months (April to September) the WRF model over-estimate the GHI 0.88 kWh/m^2 on average; instead on the remaining months the model overestimate by 0.03 kWh/m^2 on average. Moreover, the model behavior during 6 months of the year is slightly closer to the observations than the ERA-Interim outputs.

In order to understand the behavior of the model and ERA-Interim output it's shown in Fig. 38 the monthly MBE and rRMSE. The minimal (4.38%) rRMSE obtained for the monthly validation period is on January and the maximum (22.32%) occurs on July, annual rRMSE is 9.61%. The MBE exhibits that there is a small underestimation on winter and a high overestimation on summer as shown in Fig. 38. Moreover the ERA-Interim output accuracy is also shown in Fig. 38 during spring-summer months has a closer trend than the WRF model. However, on fall-winter months the ERA-Interim output has an expected accuracy (less than 10% rRMSE), but lower accuracy than WRF model.

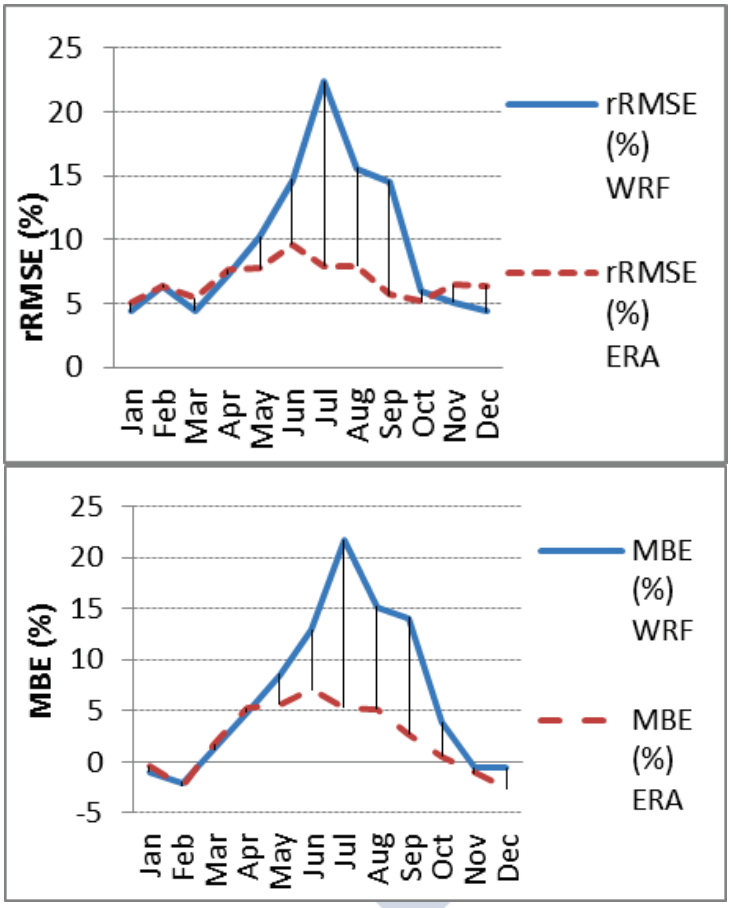

Fig. 38 (a) Monthly rRMSE WRF Model vs ERA-Interim, (b) MBE WRF Model vs ERA-Interim.

In Fig. 39, the monthly mean correlation between the models and the observations is presented. Is In the low radiation months between 3 and 5kWh/m^2 the WRF simulation represents the weather stations well, but on higher radiation months it tends to overestimate the irradiation. Overall the lineal correlation (R^2) for the WRF case is above 0.88, on the other case, the ERA-Interim correlation is above 0.93.

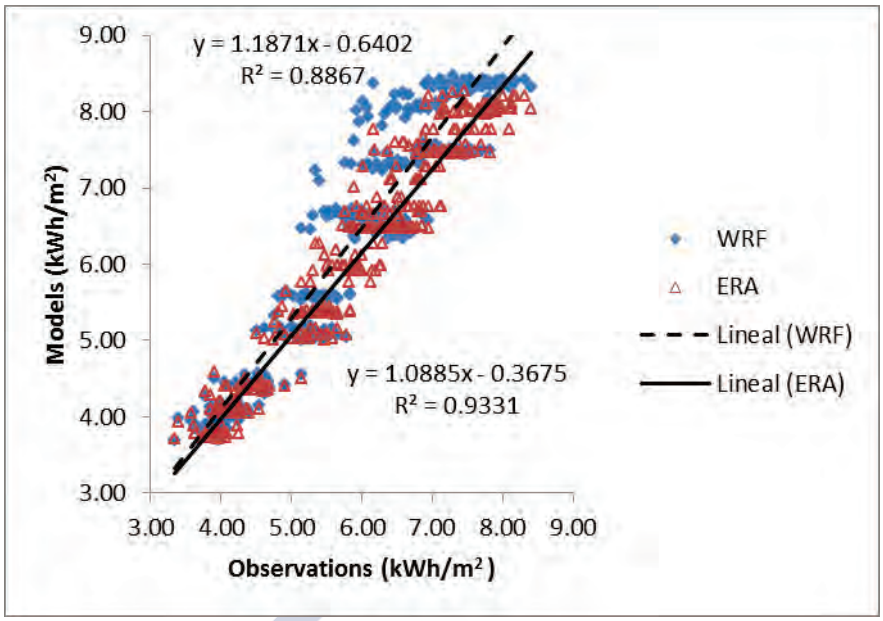

Fig. 39 Correlation plot of monthly GHI of Observation vs Models (WRF and ERA-Interim).

The observed effect could be related to the monsoon and hurricane season that covers the same time period (May – November). During the monsoon season (May – July) thunderstorms are formed due to a "desert heat low" that is formed in the Sonora desert, which pulls moisture into the region that contributes to their formation. Additionally during the hurricane season (May – November) many tropical storms strike the region, which could greatly impact the monthly GHI.

The observations clearly show that there is less radiation than estimated from the WRF model and it could be related that the model doesn't solve correctly this kind of storms with the cumulus parametrization chosen (New Kain-Fritsch) as shown by Gilliland and Rowe [149]. A possible evidence of this is shown in Fig. 40, the rRMSE doesn't increase proportionally with radiation; the green triangles are the rRMSE on the Monsoon/Hurricane season and it's evident that the greatest errors occur on that time.

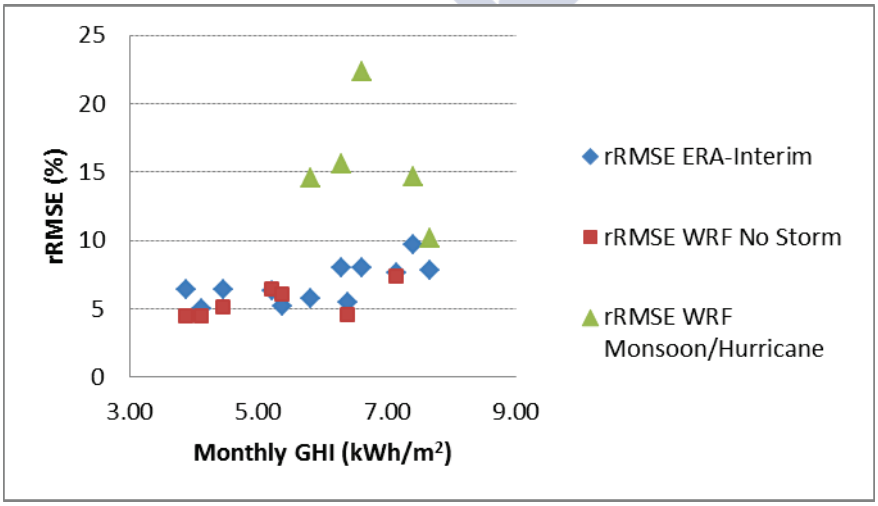

Fig. 40 Monthly rRMSE for ERA-Interim, WRF monsoon season and WRF No storm season.

Additionally, the monsoon system is a phenomenon that occurs on a larger scale than the one selected on the initial boundary conditions. Possibly, boundary conditions are not including clouds, which have to be entirely formed within the boundary domain. This lack of information on monsoon clouds could result in an underestimation of cloud cover over the region of study. Moreover, the resolution selected could also be a problem for the convective parameterization selected; according to various studies done, a higher resolution could solve the convective systems better[150]–[153]. In contrast, ERA-Interim, being a global analysis system, takes in consideration this kind of systems that develop outside of the area selected in the WRF model and also as an input has observational data that helps to improve the results output.

2.6 Conclusions

In this research a downscaling of the south of Sonora Mexico region was performed in order to obtain a highly temporal resolution solar potential assessment as well as a validation between the output and observations.

The graphical results processed from the WRF output indicate that the horizontal resolution for this example could be sufficient, in other words a higher resolution is not necessary for this region due to the homogeneity of the outputs and not drastic topographical changes. In general terms, the model represents the GHI of the region with a higher temporal resolution (10 min vs 12 hours).

Overall the results for the WRF present less accuracy, related to the weather stations, in annual terms. However in non-storm season WRF has better results than ERA-Interim outputs. Since the annual rRMSE values are low (average 9.91%) we conclude that the model has relatively good accuracy and could be an alternative to study the solar resource on regions where climate conditions are similar to the studied region; especially if high temporal resolution (10 min) is necessary. However the results of the validation were done mainly on the valley region of the south of Sonora, it is recommended to analyze the outputs on the sierra region (west and higher altitude) in order to understand if the results are biased only to that kind of climate.

The overestimation of the WRF model on the spring-summer period seems to be the storm solving problem of the initial configuration. In order to improve GHI accuracy during this season, it is necessary to carry out a sensitivity study on the different microphysics, cumulus and radiation parametrizations that the WRF model uses. Moreover, it is necessary to do a further research in different regions and climate conditions so as to compare the effects observed during the present study with the results in such conditions.

USC
UNIVERSIDADE
DE SANTIAGO
DE COMPOSTELA

CHAPTER 3 SENSIBILITY STUDY OF CUMULUS PARAMETERIZATION FOR A IRRADIATION ESTIMATE CASE IN A NUMERICAL WEATHER PREDICTION MODEL

3.1 Introduction

On Chapter 3 the results of sensibility study performed, of the convective parameterization on the prediction of GHI on a semi-desert region is presented. On Chapter 2 the results of the simulation of solar resource for the south of Sonora region are promising but improvable. Furthermore the results of the ERA-Interim output are slightly better. This kind of results is repeated on different solar radiation forecasts and assessments obtained by NWP models since the results depending on climate, season and location. We assume as a starting point that some of these problems could be solved by selecting the correct initial parametrizations for each case.

The design of these parametrizations on NWP models solves different atmospheric equations on different levels and resolutions of the simulation by diverse calculations. According to different authors, it should be noted that the skill of a simulation with a NWP model depends on factors such as the model itself[65], [126], [128], [154], soil specifications [155], spatial configuration [156], boundary conditions [157], region and season [61], [158], [159], and, particularly, on the physical options such as the parameterizations [160]–[163].

3.1.1 Convective or cumulus parameterizations

There is great importance of the clouds in the climate system and therefore in the renewable energy point of view. Though the solar irradiation is the main energy source for the atmospheric system, it impacts the atmosphere incidentally, mainly because the coupling of the atmosphere with oceans and moderately as a result of the presence of the clouds[95].

The importance of convection to both local and global processes suggests that without a reasonable representation of all types of moist convection in numerical models it is impossible to predict the atmospheric circulations correctly or to model the hydrological cycle adequately[164]. The effects of latent heat release, the transport of heat, moisture, and momentum, and the precipitation that convection produces need to be accounted within NWP models[165].

In accordance with Stensrud (2010), “it is convenient to divide the various forms of moist convection into just two major categories: deep convection and shallow convection.” Deep

convection refers to elements that vertically extent much of the troposphere. Though, shallow convection are convective elements that vertically extent only a smart portion of the troposphere[165].

To the extent of understanding convective parameterizations, is important to define the microphysics of the NWP's. According to Warner (2011), "cloud microphysics convective encompasses all cloud processes that occur on the scales of the cloud droplets and the hydrometeors, rather than on the cloud itself"[166]. In other words the microphysics schemes involve most of the physical processes of the atmosphere that could not be resolved on grid scale.

On the other hand, cloud parameterizations are the methods which the model takes into consideration the convective effects through the redistribution of temperature and moisture in a grid column, which reduces atmospheric instability[167]. Through the cloud parameterization the model controls the convective processes that lead to cloud formation and possibly to precipitation. In Fig. 41 a diagram with the processes that CP schemes need to take account for[168]. Some of these needs are covered by different ways on the CP parameterizations on NWP models; however the CP schemes have different results depending on the initialization input and the type of convective event[147], [167], [169], [170].

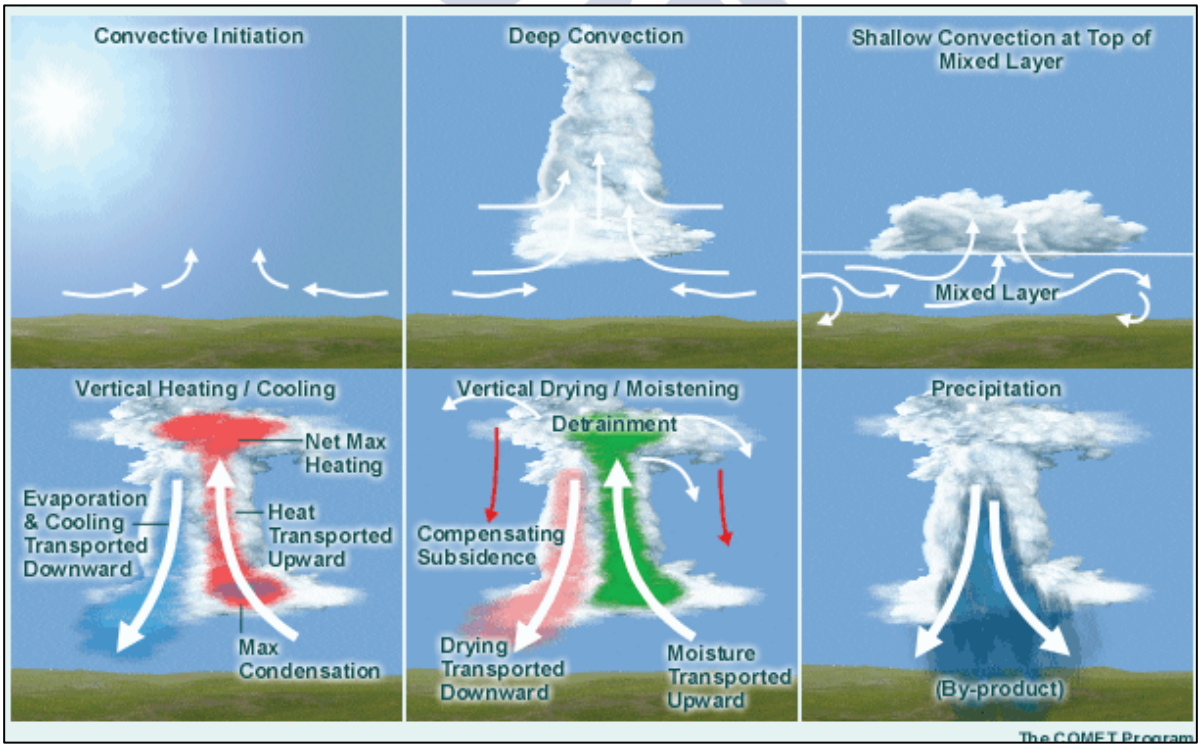

Fig. 41 Convective processes that need to account CP schemes.[168]

Therefore cloud parameterization impact indirectly the shortwave parameterization by interacting with the microphysics schemes and changing the cloud optical thickness that affect the GHI on the surface[171].

In this Chapter we are focused on solving the simulations with seven different convection parameterizations selected, to model the solar irradiation for an energy assessment standpoint of view. An analysis of the results and discussion is given on section 3.3 and conclusions on section 3.4.

3.2 Materials and Methods

The methodology followed in this chapter comprises the following steps: first the months of July (summer) and December (winter) were selected from the MRY previously developed, and perform all the simulations days with seven different convection parameterizations. From these results, a comparison of the mean solar irradiation output between them and the observations was performed.

The month of July, is selected, due to the past results, where this month had the highest differences (rRMSE and MBE) of the 12 months, in contrary as the month of December that had the lowest errors given by the simulation. This will give a higher chance to differentiate the GHI result of each simulation and to select which parameterization gives better results in such extreme conditions (winter-summer difference).

3.2.1 Brief regional description

The south of Sonora region was selected for this study due to the agro-weather and weather station density and its climatological characteristics. This region is located at the northwest of Mexico, in the state of Sonora. This research considers 13 municipalities of the south shown in the Fig.42.

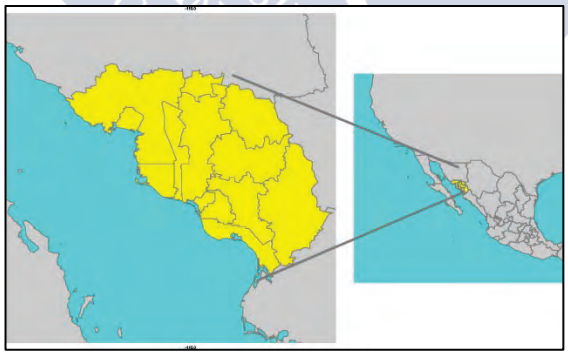

Fig.42 State of Sonora location (in yellow municipalities of the south region).

3.2.2 Observational data

In Chapter 2 only 32 agro-weather stations were used to validate the results GHI of the simulations. From this 32 weather station, 28 were taken from the PIEAES weather network used mainly to forecast crop disease and situated on the valley at the South of Sonora region, the last 4 weather stations were taken from the INIFAP weather station network and were selected to analyze the contour of the region selected.

However in this chapter, five weather stations from SMN were also considered[57] in order to increase of the area of validation from Chapter 1. The weather stations added in this research have high quality sensors and recalibrated solar sensors, according to Valdes et al.[133], since these weather stations were recalibrated in 2012. A list of the newly added weather stations used, its height and coordinates is shown in Table 8. The newest weather stations considered are marked in green on the south of Sonora map in Fig. 43.

Table 8 Weather stations added to this Chapter [57]

Number	Weather Station Name	Longitude	Latitude	Height	Network
33	Bahia de Kino	-111.136944	29.013333	10	SMN
34	Alamos	-108.937778	27.021667	409	SMN
35	Yecora	-108.933333	28.366667	1531	SMN
36	Basaseachi	-108.208889	28.199167	1973	SMN
37	Chinipas	-108.536389	27.392778	431	SMN

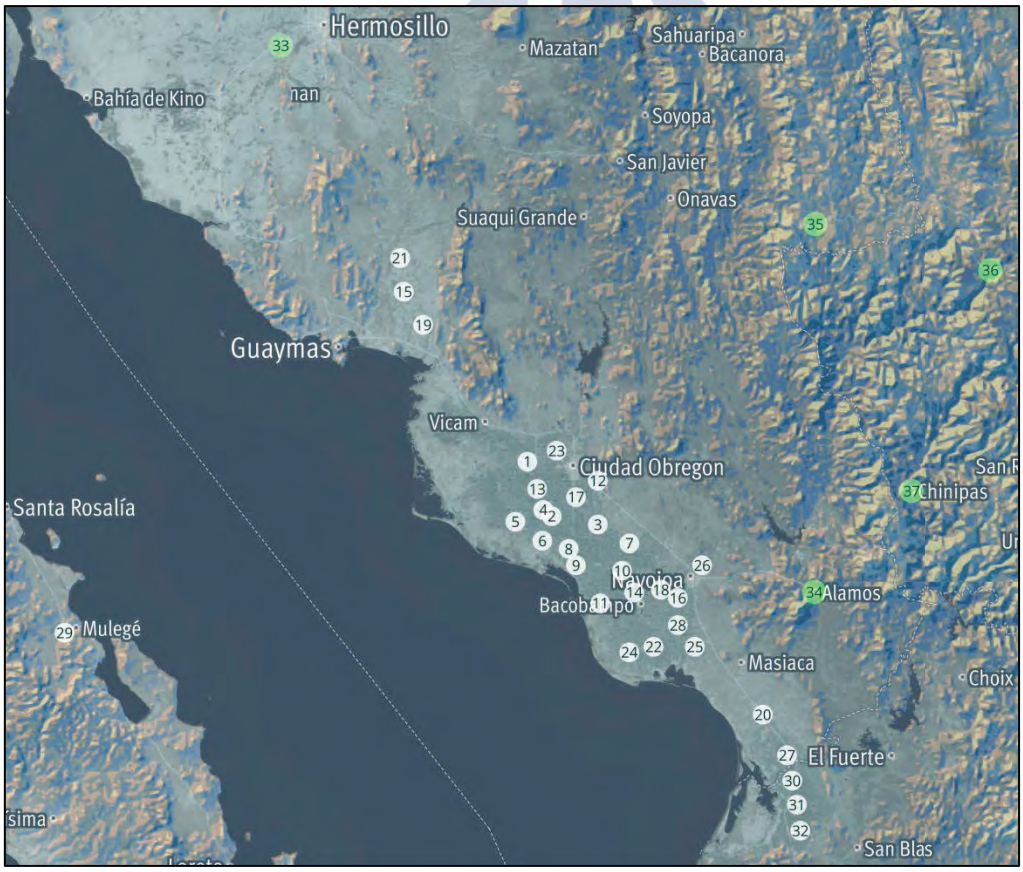

Fig. 43 Weather stations considered for the research. In green the weather stations from SMN network added for this chapter.

The quality filters used in this chapter are based in the same as Chapter one and are described next. The first consist on having at least 80% of the data for each station. The second quality filter was to have a minimal of three consecutive years for each weather station. The last quality filter was applied to the monthly values, if within a month there were 10 daily missed records or 5 consecutive daily missed records, the monthly value was discarded.

3.2.3 Model description and experimental setup

In this study, the numerical advanced weather prediction model (WRF model ver. 3.4) was used[144]. The modelling setup including the selected domains and the initial and boundary conditions as well as the physics schemes are based on Sosa-Tinoco et al. (2015) research and are listed below Table 9 [158].

Table 9 Synopsis of the WRF model configuration used

Simulation period	31 days of July and 31 days of December for each case
Model version	V3.4
Domains	2
Horizontal resolution	27 and 9 km
Input data	ERA-Interim
Time step	90 s
Outputs frequency	120 (d01) and 10 minutes (d02)
Nesting	1-way nesting
Physics schemes	**Option**
Microphysics	WSM6 class
Shortwave	Dudhia
Longwave	Rapid Radiative Transfer Model (RRTM)
LSM	Noah
PBL	YSU

It is noteworthy that the simulation period was of 36 hours and as well as in the Chapter 2, the first 12 hours were deduct since we consider this interval as appropriate time for spin up of the model and the results were driven by the characteristics of the model and not only the input data.

The cumulus parameterization used in Chapter 2 was Kain-Fritsch, the results of using it for the simulation, exhibited that in summer there were overestimations in contrast to all the weather stations. The Cumulus Parameterization (CP) schemes, chosen for this research, are shown in Table 9, as well as the abbreviations used in this Chapter. Also an ERA-Interim case

is considered just for comparison, the results were taken from Chapter 2. The abbreviation used for this Chapter for ERA-Interim GHI results is ERA.

Table 10 Cumulus Parameterization used

Scheme	Abbreviation	Added
Kain-Fritsch	KF	2000
Betts-Miller-Janjic	BMJ	2002
Grell-Freitas	GF	2013
Old Simplified Arakawa-Schubert	OSAS	2005
Grell-3	G3	2008
Tiedtke scheme	Ts	2011
New Simplified Arakawa-Schubert	NSAS	2011

3.3 Results and Discussion

The results from every day of each case were averaged in order to compare the GHI monthly mean with the observations. In Fig. 44 four cases are shown, the first KF shows a higher GHI than the other 3 cases, also is noticeable the poorest resolution on ERA however shows better differentiation between coast (west) and mountains (east). On the other hand OSAS and NSAS case show lower GHI on both maps and good differentiation between coast and mountain. NSAS case also shows similarly to ERA lower irradiation on the mountains.

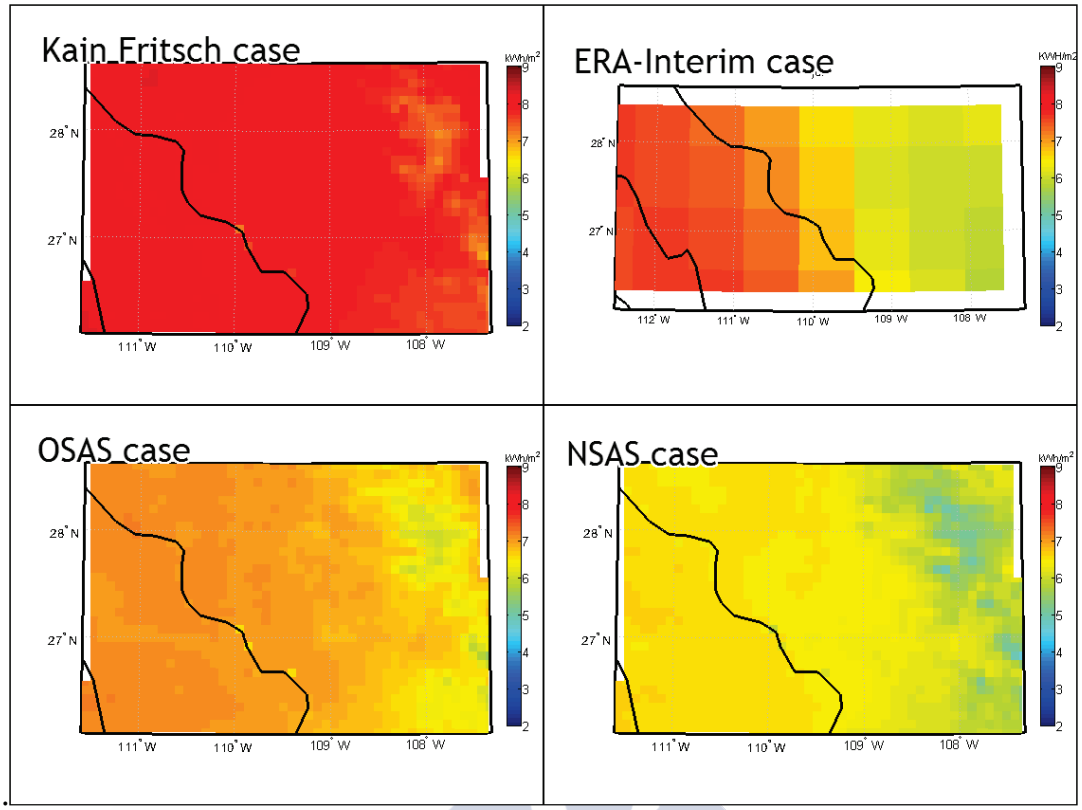

Fig. 44 Mean GHI maps in July for four cases (KF, NSAS, OSAS, Ts).

Likewise, in Fig. 45 GHI mean maps in July for the left cases (BM, GF, G3, and Ts) are shown. The four cases are shown together because the results are similar showing high (8kWh/m^2 approximately) GHI on most of the map but middle (6.5kWh/m^2) GHI on some parts of the mountains; however the G3 case has a higher contrast between the east and west. Is noticeable how the G3 performed better than GF case by reason of G3 scheme is an update of the later

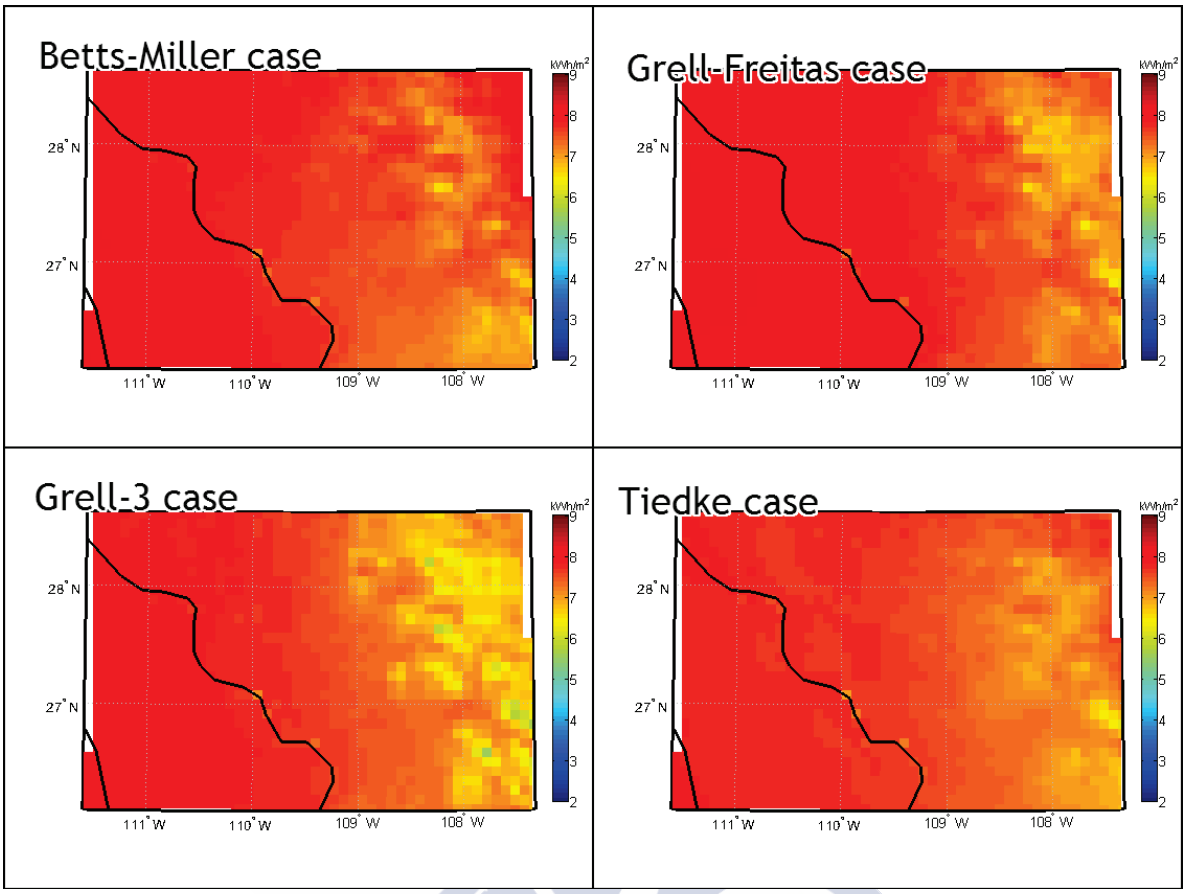

Fig. 45 Mean GHI maps in July for four cases (BM, ERA, G3 and GF).

From these results, each case was compared against the observations. In Fig. 46 the polar graph shows, in the red line the mean GHI on the month of July for the 32 observations, and in blue line the different mean GHI cases.

$$\overline{GHI}_{case} = \frac{1}{\#GridPoints}\sum GHI\_grid$$

Where,

GHI_grid is the mean of GHI on the grid point where the weather station is located on the simulation result.

$\#GridPoints$ is the number of grid points in this case 37 (the same number of observations.

Most of the cases shown have a clear overestimation of over 1kWh/m^2•day, similarly to the results previously presented in Chapter 2. Nevertheless the OSAS case has a lower overestimation of less than 500Wh/m^2•day in addition the NSAS case has the closest GHI to the observations with a low underestimation of 100Wh/m^2•day as shown in Fig. 46.

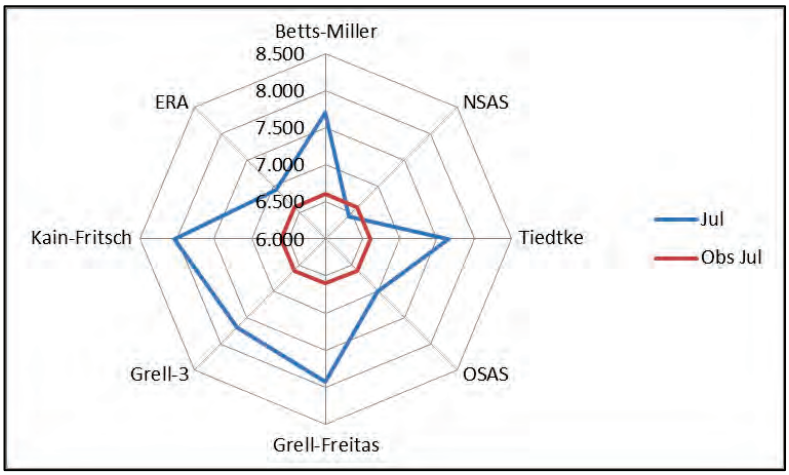

Fig. 46 Mean GHI on July for each case (kWh/m2) in comparison with observations.

The result shown hints that the hypothesis portrayed at the beginning of the chapter could be positive. On the other hand by the month of December, the difference between each case is not as considerable as in July. The eight cases show similar outputs (approximately 3.8kWh/m^2•day on most cases) as shown in Fig. 47. Since the results are similar the output where displayed together in contrast with the month of July that was shown in two different sets of maps. One particularity displayed in the Figure is the ERA case that as well as in July show less resolution.

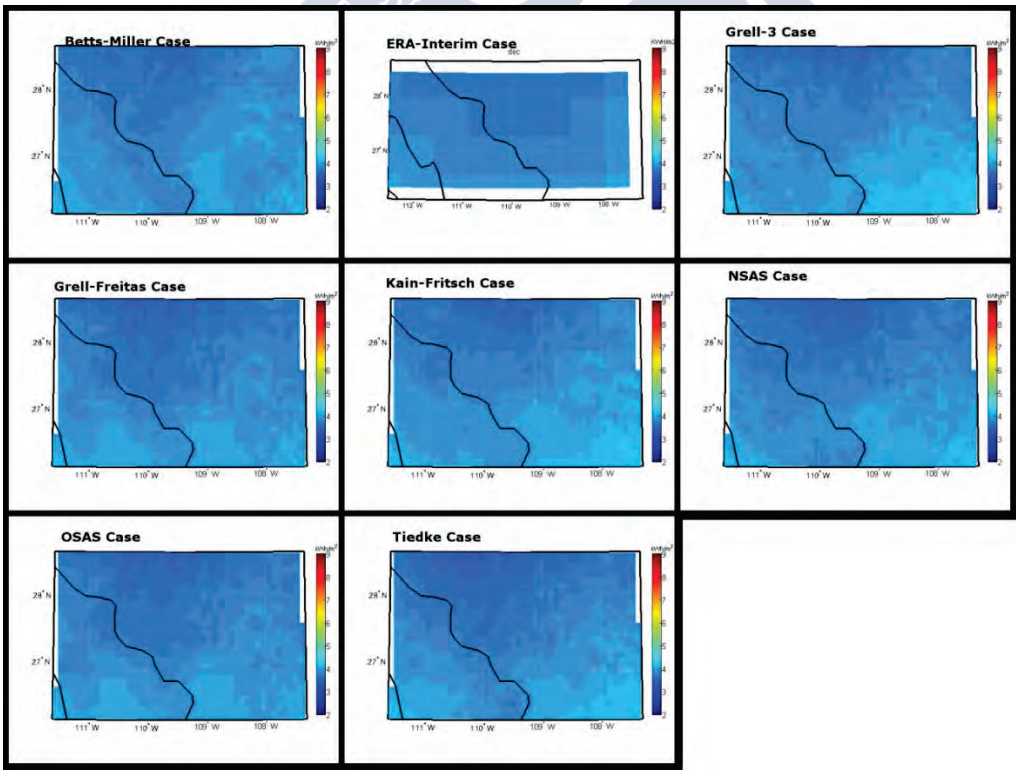

Fig. 47 Mean GHI maps in December for all cases.

In Fig. 48 the mean GHI observations are displayed at the outer red line in contrast with July due to in most of the cases had an underestimation; however the KF case had a slight overestimation of 20Wh/m^2. The cases with higher precision were KF, G3 and NSAS in order of precision, as shown in Fig. 48.

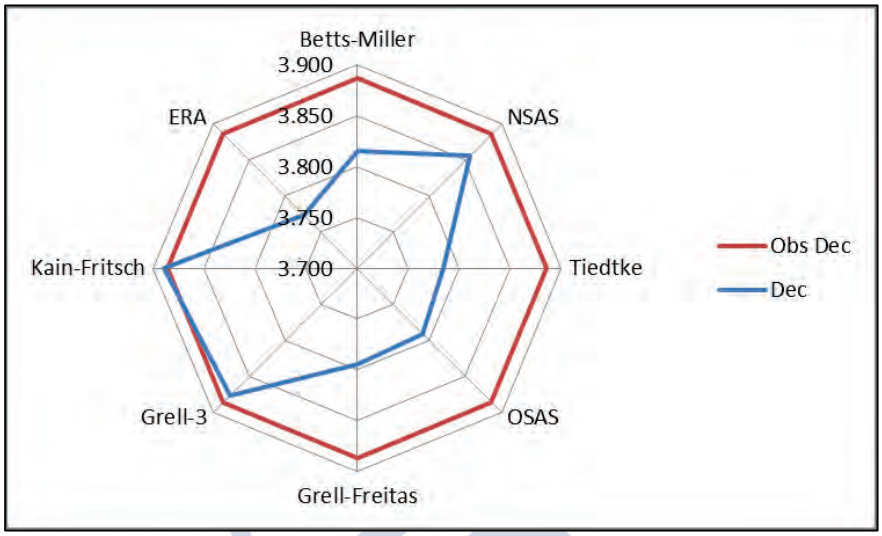

Fig. 48 GHI on December for each case (kWh/m2).

In order to understand the results during both seasons the rRMSE and MBE of each case are presented in Table 11. On the summer the CP that shows the best rRMSE is NSAS close by OSAS case, this could be related to the fact that NSAS is a developed scheme from OSAS parameterization. Furthermore the MBE shows a slight underestimation of the NSAS scheme on July.

In winter the rRMSE of three results is almost the same (~5.72%) for KF, Ts and G3. However the rRMSE of the rest of parameterizations presents not a bigger difference and in particular the NSAS output has only 5.76% of rRMSE Once more, the lowest MBE in December falls in the same three cases previously mentioned. Something worth to mention is that the NSAS case has the lowest sum of rRMSE on both season and both MBEs are negatives and small too.

Table 11 Validation metrics

Convective parameterization	rRMSE (%)		MBE (%)	
	July	**Dec**	**July**	**Dec**
ERA	7.96	6.36	5.34	-2.60
KF	22.88	**5.72**	22.05	**0.35**
BM	17.76	6.02	16.74	-1.58
NSAS	**5.46**	5.76	**-2.35**	-0.51

Ts	17.21	**5.72**	16.19	**0.35**
OSAS	8.22	6.51	6.20	-2.17
GF	21.10	6.46	20.23	-2.11
G3	17.71	**5.72**	16.73	**0.35**

In order to further understand these results we selected two cases, KF since is the parameterization used in Chapter 1 and NSAS case in consideration of the results of rRMSE and MBE. The precipitation of all the simulations on the month of July was extracted and added in order to represent the cumulative precipitation and to compare both cases. The variables taken from the simulation was RAINC and RAINNC and both were added in order to get the cumulative precipitation from each day of simulation. The variable RAINC is the rain produced by the CP scheme and RAINNC is the one produce by the microphysics parameterization.

The cumulative precipitation from both cases is presented as maps in Fig. 49. It is visible that, the KF case (Fig. 49a) has higher cumulative precipitation on the east (more red and yellow grid points) in comparison with NSAS case (Fig. 49b). On both cases there is less cumulative precipitation (<100mm), close to the coast line (west).

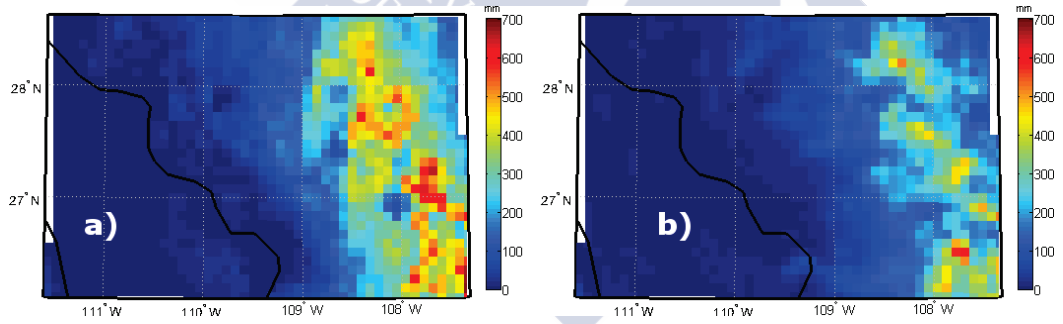

Fig. 49 Maps of cumulative precipitation on July a) Kain-Fritsch b) NSAS

If we analyze the precipitation on the points where there are weather stations against the simulations there seem to not have great differences for both simulation cases, but comparing with the observations there are higher differences, as much as four times greater in some cases, as shown in Fig. 50. The GHI on both simulations is stable between each point, in comparison with the observations that show some variability. In this figure, is visible that there is no high correlation between precipitation and GHI during this month but is also noticeable that the NSAS has better GHI prediction.

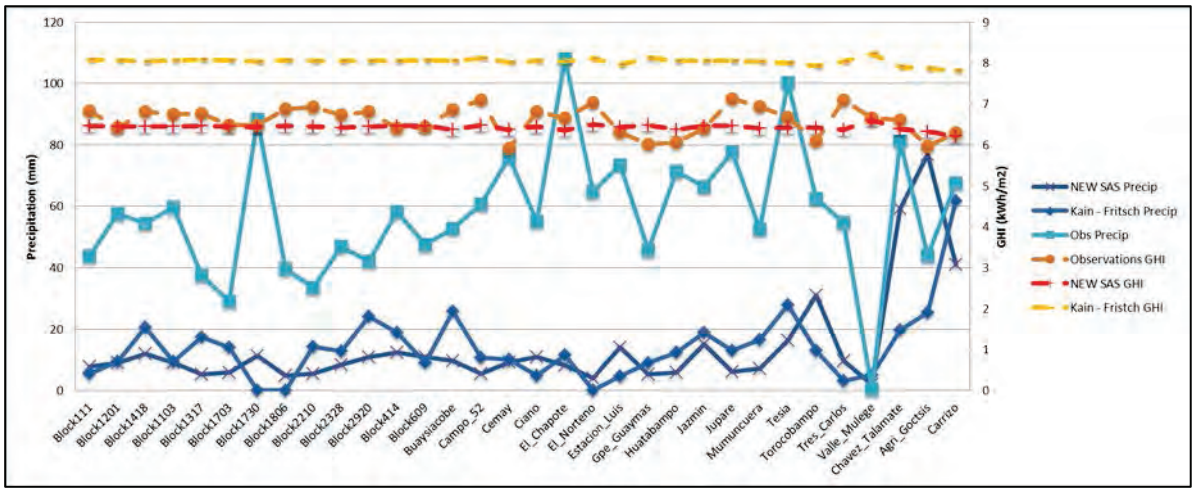

Fig. 50 GHI and Precipitation for each station (closer point) in July.

The main differences between each parametrization could be related to the persistency of the clouds (CP triggering), since in both schemes the amount of rain is similar but the solar irradiation is higher in KF case. The meaning of this is related of how each CP considers that convection leads to a shallow convection or deep convection and from that state to precipitation.

In order to analyze these results further, we took the model output that represent the hydrometeors simulated by the microphysics and represent them averaged in the month of July in a three-dimensional fashion (isosurface). The hydrometeors in this case are the particles of ice/water suspended on the atmosphere that the microphysics scheme produces due to the interaction with the rest of parameterizations in this case were considered ice (Q_{ICE}), rain (Q_{RAIN}), snow (Q_{SNOW}), graupel ($Q_{GRAUPEL}$) and clouds (Q_{CLOUD}). These outputs are four-dimensional variables that were necessary to average on time in order to represent in 3D, to reduce one dimension. Furthermore the importance of these hydrometeors to understand the GHI output is great after all they affect the cloud optical thickness directly and the shortwave parameterization accounts this property to calculate the shortwave irradiation (GHI) at the surface[172].

In Fig. 51 a representation of the five hydrometeors averaged during the month of July in isosurface/3D and in the same figure the precipitation averaged is shown on the bottom. First two figures (*a* and *b*) are top view planes, the last two figures (*c* and *d*) are horizontal 3D representations.

KF scheme (Fig. 51a and Fig. 51c) has less moist density (mostly blue clouds) and more precipitation (yellow/brown color) on the west side, however the NSAS representation shows that the clouds have higher moist density (yellow clouds) and less precipitation on the west. On Fig. 51c and Fig. 51d horizontal representations are shown, both parameterizations express deep convection, though NSAS presents higher deep convective clouds on the western limit of the area.

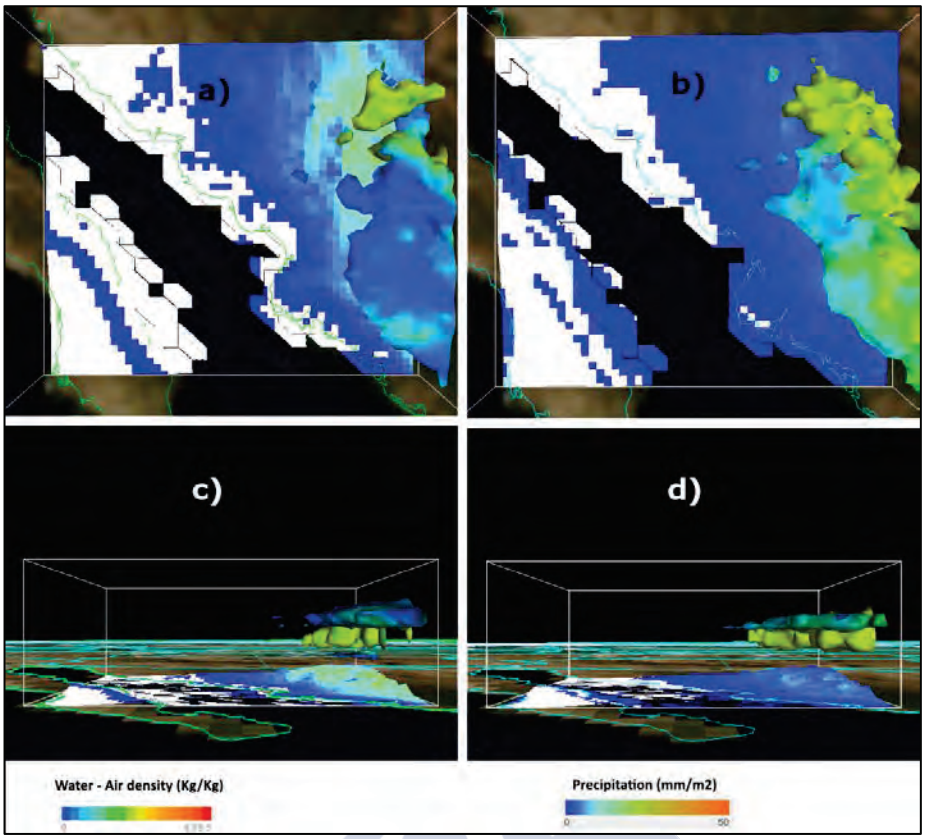

Fig. 51 Average clouds and precipitation on July, for KF (a, c) and NSAS (b, d).

A simulation in the month of March was performed, in order to validate the results on an intermediate season (spring), since in both time periods (summer and winter) are demonstrated that NSAS scheme has more than acceptable prediction for this region. Moreover on the monthly GHI observations March presents closer values, from the observations point of view, than any other month to July as shown in Fig. 52.

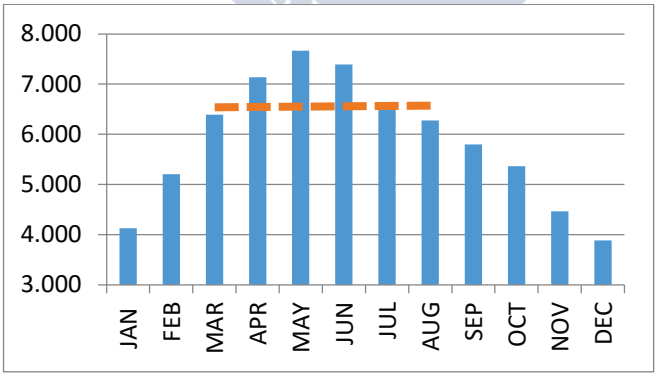

Fig. 52 Monthly GHI Observations

The results of the mean GHI map in March (Fig. 53) are similar between the parameterizations (KF and NSAS), having almost the same features and contrast between the coast line and the mountains. There is a low GHI in the sea that is hard to validate since there is no weather stations on the sea, which appears higher on the NSAS case.

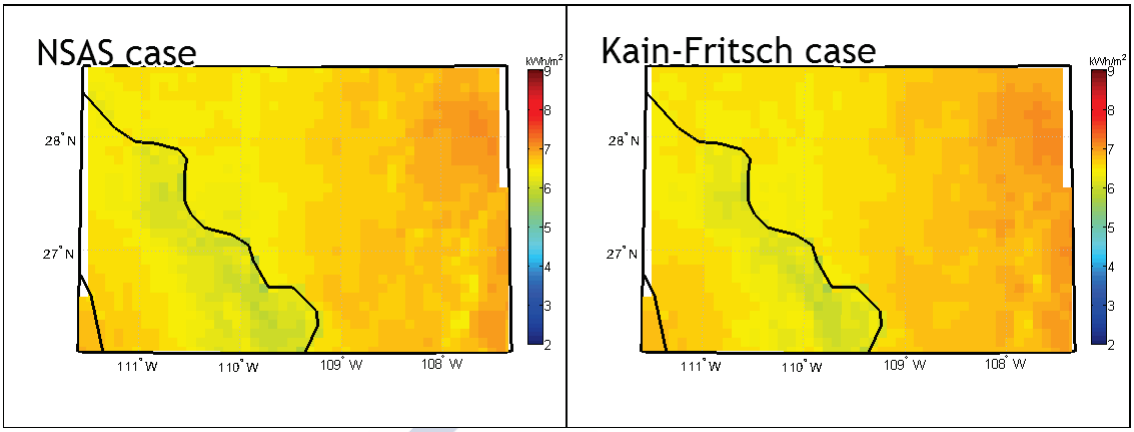

Fig. 53 Mean GHI maps in March for 3 cases (KF, ERA, and NSAS).

In Fig. 54 the average clouds and precipitation for both cases in March are shown. The results are similar to each other (NSAS and KF); probably because in March the weather is fairly clear and there are not many clouds or precipitation during this season. Apparently the month of March is cloudy, however the density of these clouds is minimal, and only small deep convection situation occur close to the mountains.

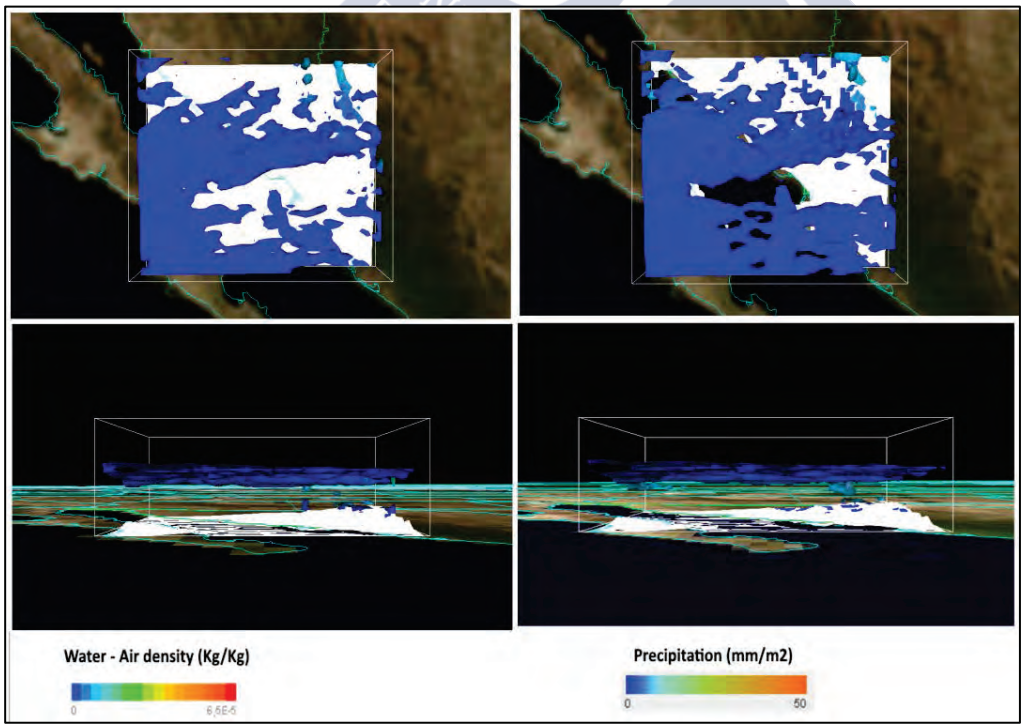

Fig. 54 Average clouds and precipitation on July, for KF (a, c) and NSAS (b, d).

These findings validates the NSAS scheme to be used during all the year to obtain irradiation levels closer to the observations. The validation metrics are shown in Table 12. The results show that the parameterization has better results than KF and ERA-interim both in rRMSE and MBE and the difference on the month between the Observations and the output of the simulation is only 0.07 kWh/m^2.

Table 12 March validation for KF, NSAS and ERA-interim (for comparison)

	rRMSE (%)	MBE (%)	Mean GHI (kWh/m^2)
KF	5.57	2.04	6.51
NSAS	5.30	1.35	6.46
Observations	-	-	6.39

3.4 Conclusions

Simulations in different seasons of the year, with seven convective parameterizations, where done thoroughly to select the CP for the region. The best CP for the region was selected in order to produce a database of GHI with the highest correlation with observations.

The first trial was to determine which CP could give results closer to observations on summer. The results were conclusive and the best CP for the south of Sonora region in summer was first NSAS and then OSAS, both parameterizations had higher confidence to the observation than any other parameterization. The second examination was done on winter, the results of the simulations showed that most parameterization has high correlation with the observations.

In order to understand the results a comparison between the precipitation of two CPs (KF and NSAS) and its GHI was performed. The result shows that KF scheme had higher precipitation on the east but the same precipitation on the weather stations as the NSAS scheme on the west. Moreover an analysis of the hydrometers generated by the model was done and it showed that the KF scheme had a lower density of moist on the atmosphere on average versus the NSAS scheme. The KF scheme seems to be in an overactive state. An overactive scheme produces too much rainfall in situ, and removes too much atmospheric moisture, which could have fallen as precipitation downstream like in most of the cases excepting the Arakawa-Schubert schemes.

The results obtained in this research are promising and could lead to have better results on the future in other regions by using NWP models to predict GHI. However is convenient to analyze the other physical parameterizations (shortwave, longwave, microphysics) in each scenario as well.

USC
UNIVERSIDADE
DE SANTIAGO
DE COMPOSTELA

CHAPTER 4: PHOTOVOLTAIC MODULES STUDIES AMONG DIFFERENT TECHNOLOGIES

4.1. Introduction

During the last 25 years, both the photovoltaic (PV) cumulative installed power and the annual electricity production have increased at an annual rate of about 38 %, resulting in an estimated 540 GW cumulative capacity in 2019[173], [11]. This tremendous growth has been mainly a consequence of the continuous decrease of the cost of solar systems, 70 % in the last 8 years[11]. Therefore, depending on the intensity of the solar resource, the PV electricity is reaching grid parity in many regions of the world.

One of the main uses that the solar resource provides is the energy conversion from the solar irradiance to electricity by means of the so called "photovoltaic effect"[174]–[176]. The present market offers different solar modules technologies which are able to carry that out in an efficient-durable enough way. Nevertheless, different technologies are expectable to show some differences when it comes to the main influent parameters: kind/amount of irradiance and temperature.

In a comparable manner to the previously studied solar energy mapping, a brief sort of solar module type distribution could be stated concerning this last's characteristics. This arises from the fact that, in each World's area, some specific meteorological conditions are predictable to be present and thus, when the specific PV systems' behavior is taken into account, a suitable choice is able to be established. In this way, a resource mapping could be accompanied by an optimum kind of PV generator by regions.

In this chapter, we developed a study of PV response and the most efficient types of solar cells depending on the production technologies. For that reason, in addition to a validation of models for predicting solar energy, it is important to choose the right technology depending on the climate zone. To do this, there are certainly worthwhile four parameters that should be considered: in response to variations in temperature, irradiation dependency, the cost and useful life-time, or by defect the aging modes. In order to carry this out, it is necessary to experimentally measure and compare under real conditions the main different kinds of solar module implementations. We compare the first-generation solar modules, produced from crystalline silicon, and the thin film or second-generation cells, which make use of much smaller quantities of semiconductor materials: CIS. Depending on the material substrate, its encapsulation, their properties and resilience, the effective electric performance under different meteorological conditions will vary from one to another.

This chapter includes a behavior comparison study between the main different technologies of photovoltaic modules, which is based on measurements under real sun conditions as well as on real operating installations. A study for the most common technologies in the considered region, that is, the South of Sonora, has been carried out. As it was previously detailed in the corresponding chapters, the climate characteristics of this region are high levels of direct irradiation, high temperatures and a noticeable seasonality.

4.1.1. PV's technologies state-of-the-art

To describe the state of the art for the photovoltaic technology is necessary to make a distinction between crystalline silicon cells and thin film cells based on inorganic semiconductors. The Crystalline Silicon Cells are based on crystalline silicon either as single crystal (mono-crystalline) or multi-crystalline with large grain sizes (about 1 cm side). These cells dominate the PV market and are called first-generation solar cells[177]. The maximum efficiency of converting solar radiation to electricity reached is 22.9±0.6 % world record for monocrystalline modules, very close to its theoretical limit. The multi-crystalline silicon solar panels have efficiencies somewhat lower than mono-crystalline, reaching a 18.5±0.4 % world record[178]. The lower efficiency is offset by cheaper production costs. In addition, during the last years, a more energy-efficient ways of achieving solar grade silicon for photovoltaic modules, such as the upgraded metallurgical grade silicon (UMG-Si) are becoming a good alternative to the most common technique (Czochralski method) [179]. The main advantage of the new method is the lower energy consumption. Although this kind of multi-crystalline implementation is still not currently very established commercially speaking, it is of interest since it reduces the costs and may present a suitable enough behavior.

Other ways of possible savings in cost are the so called Thin Film Cells or second generation modules. This technology implies a significant saving of semiconductor material. Although their efficiency is variable compared to silicon based solar cells and their production costs are relatively low, these cells are less used than first generation ones to produce electricity. The thin-film or amorphous cells are commonly constituted through a deposition of different substrates (mainly silicon-based) without any periodic order, whose properties are able to induce the photovoltaic effect. An interesting example of Thin Film are the CIS cells produced by evaporation of the constituent elements Cu, In and Se [180]. Although CIS cells efficiency currently reaches 17.5±0.5 %[178], problems arise due to the scarcity of In and its environmental impact[181].

During the last decades, the photovoltaic industry volume has been strongly increased. On the other hand, among the different technologies of implementation, the multi-crystalline one comprehends the highest amount of production [11], whereas the thin-film type represents the lowest in the market. As above mentioned, regarding such photovoltaic technologies, some aspects should be taken into account while considering their adequateness for a photovoltaic installation in a particular region: module's efficiency, their behavior with respect to different parameters such that cell's temperature and irradiance, electric characteristics, structural conditions (weight, flexibility...), robustness, expected ageing and maintenance needs.

In general, prices of crystalline modules have strongly decreased during de last years (see Fig. 1.), which is de so-called *Swanson Effect* [177], [182]. In practice, the Swanson effect affirms that for any duplication in production of PV cells, the corresponding price decreases in a 20% about.

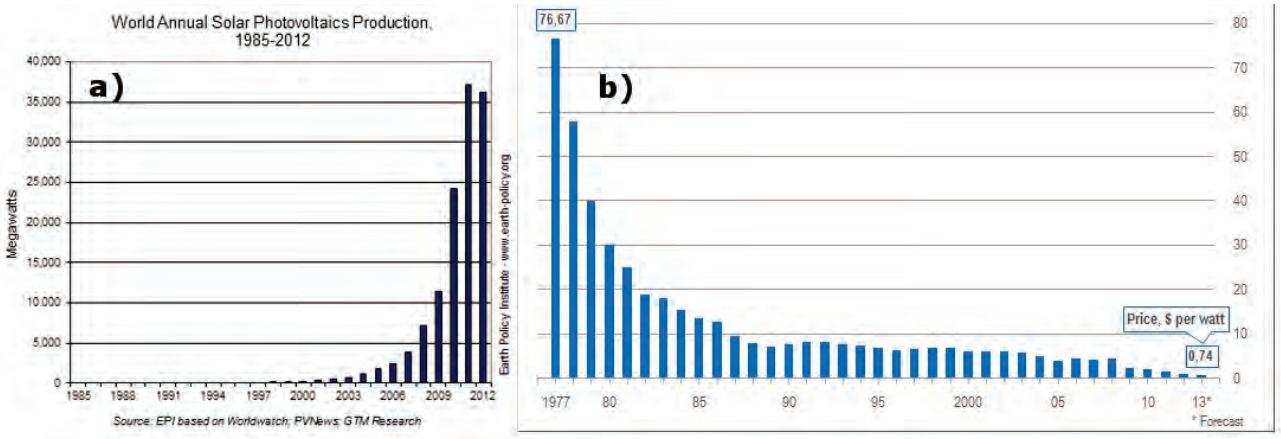

Fig. 55 a) Crystalline photovoltaic modules' prices from 1977 to 2012 [177] b) Yearly energy production for PV modules from 1984 to 2012.[182]

With respect to the future technological trends in PV the all move in the same direction: lowering the production cost of electricity produced. This objective is planned to be achieved through the two interrelated strategies:

1 Increasing the efficiency of the cells with the introduction of new concepts,

2) Increasing the durability of modules,

3) Simpler production processes and

4) The use of fewer and cheaper materials.

Specifically, in the case of Crystalline Silicon Solar Cells, trends in innovation are being made in improving the quality of metallurgical grade silicon (cheaper and of poorer quality than the solar grade silicon normally used)[183], and in the development of advanced manufacturing processes for wafers, primarily a greater penetration of epitaxial deposition process, so successful in the manufacture of multijunction solar cells.[184] Also, it is expected to intensify the effort in thinning the thickness of the cells (~30 mm) in order to save on material, but trying to maintain the efficiency values.

In the case of Thin Film Solar Cells, efforts are focused on increasing efficiency and durability and reducing the cost of the cells, which must be combined with a deep understanding of the properties of the materials that compose the cell. It is also necessary the replacement of some materials due to their high cost (mainly In and Te). There is also work ahead on the development of new multijunction structures, using lower purity materials and, consequently, lower cost, manufacturing in large areas, and on improving contacts and transparent conductive oxides. A special effort is focused on controlling the production content and morphology of the thin layers during the manufacturing process, to avoid the efficiency degradation of the cells when ageing [185].

4.1.2. Photovoltaic Modules and parameter definitions

A PV module is a series-parallel association of individual PV generators called solar cells. These cells are constituted by semiconductive materials which are able to generate electric energy from a fraction of light's photons that are absorbed by such device. The photons' energy is supplied to the material electrons if it is higher that their bandgap width and hence the electrons are free to generate electricity conduction [176].

A solar cell is basically a PN junction, which could be established in different ways/materials. As it is well known from solid state electronics, an internal electric field arises at the area surrounding the pn interface or spatial charge region. Therefore, if the incident photons from sunlight, with energies higher than the semiconductor bandgap, reach the pn interface, they will create electron–hole pairs. The electrons and holes thus created will move in opposite directions by the action of the field resulting in a current which will be the sum of the currents due to both types of carriers (recall that the holes are charged positively). From the above concepts, it is convenient to emphasize that a solar cell under illumination behaves like an electric generator. The solid curved line in Fig. 56 Characteristic curve of a standard solar cell. The corresponding power is also plotted, as well as the main parameters. [174]represents the I–V characteristic of a typical solar cell. If the cell is in open circuit (I = 0), the corresponding voltage is maximum and it is called the open circuit voltage Voc. On the contrary, if the terminals of the cell are shorted (V = 0), then the current is called the short circuit current Isc, and its value is maximum. It is usually desired that the output power is maximum (Pmp), as it is the case in power generation. Each solar cell and thus each solar module, under certain conditions of irradiance and temperature, have their specific "characteristic curve", which is directly related to the type of constituent solar cells, their association and the final result. This curve includes the current and voltage values that a solar module may present under such conditions of irradiation and temperature.

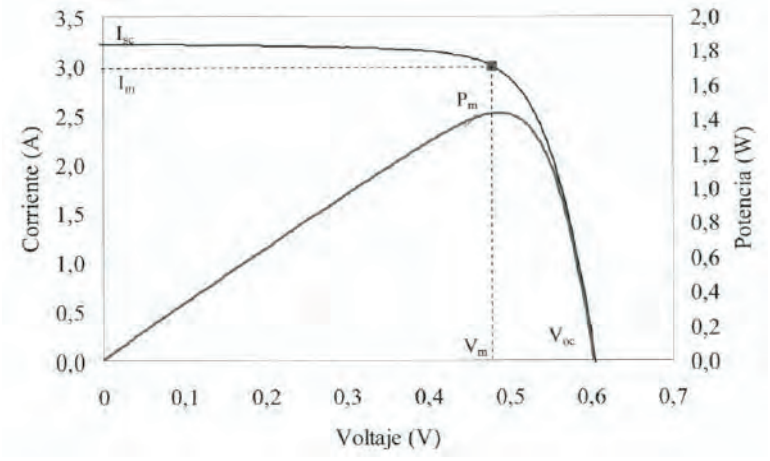

Fig. 56 Characteristic curve of a standard solar cell. The corresponding power is also plotted, as well as the main parameters. [174]

Equations (4) and (5) show how the temperature influences slightly the currents, since it narrows the band-gap width in a way that affects more positively the currents than the

increment of electron-hole recombination. On the other hand, the effect on voltages is noticeably higher, because of the increase in the reverse saturation current I_0 [176].

The irradiance is directly related to the energy production of solar modules, but the way under which this happens depends on the kind of cell or light spectra. All the main cell parameters (I, V, P) in our range have an approximately linear (see equations 4 and 5) behavior with irradiance for the typical real sun intensities. The more stable these parameters are, the more usable the photovoltaic modules will be, since the performance is relatively higher at lower irradiances.

$$I_{sc} = I'_{sc}\frac{G}{G'} + \alpha(T - T') \quad (4)$$

$$V_{oc} = V'_{oc} + mv_t \ln\frac{G}{G'} - \beta(T - T') \quad (5)$$

Where I_{SC} is the short-circuit current, VOC is the open circuit voltage, I_{SC}' V_{OC}' are the nominal values, T the ambient temperature (ºC); (T´, G´) the values correspondent to AMS (25°C,1000W/m^2) measurements; (m, $v_{t)}$ are characteristics of module material; $\propto$ β are constants.

4.2. Study and experimental setup

One of the relevant aspects to be taken into account throughout a performance study of different types of solar modules is the behavior they present under real operation conditions. This also correlates directly with the above mentioned PV adequateness regarding different geographic regions. In this sense, during the year 2014, the SEAG [186] has carried out a series of measurements in Santiago de Compostela under real sun conditions for any basic kind of photovoltaic technology: monocrystalline, thin film CIS and multicrystalline. Concerning this last case, UMG multicrystalline implementation modules were also analyzed in the same conditions. In Table 13 PV modules tested.a summary of the characteristics of the PV modules used is shown. In appendix 3 to 6 the datasheet of the PV modules is also displayed.

Table 13 PV modules tested.

PV module type	Brand	Model	Voc (V)	Isc (A)	Pmax (W)
Multicrystalline	Suntech	STP280-24	44.8	8.33	280
UMG	Ferrosolar	SFS-270	44.5	8.1	270
Monocrystalline	Isofoton	I-53	21.6	3.27	53
CIS	Wurth Solar	WSK0001	22	0.35	5.5

For the measurements, an IV tracer module characterization is obtained using a SOLARIV SOLAR300N curve tracer in real sun conditions[187], while irradiance and temperature were controlled. Furthermore, two different monitored installations that were operating under real conditions were also considered and analyzed. In these last cases, the working voltages, currents, irradiances and temperatures have been registered for the analysis. In Fig. 57, such installations are shown.

The main parameters to be studied concerning the operation of the different technologies were the behavior of the different solar modules' currents, voltages and power with respect to the temperatures and irradiance. This summarizes the whole study. Regarding the monitored installation, only the current's characteristics were possible to be studied, since the accumulators establish the voltage of operation.

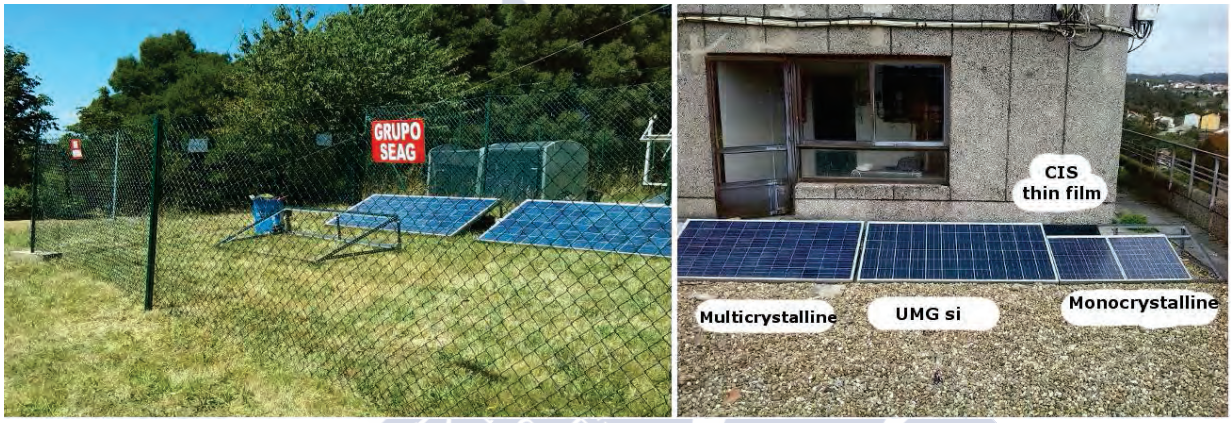

Fig. 57 Monitored photovoltaic installations in Santiago de Compostela, near to a MeteoGalicia [188] weather station.

4.3.Results

As previously seen, one of the relevant aspects to be considered when a photovoltaic installation is projected is the characteristic curve of the solar modules. Not only does it resume the expected behavior of the systems during their operation time, but also the predictable loses in this regime, as well as the most suitable choice for the different elements (such as charge regulator, convenience or not of a MPPT tracker and so forth).

The irradiance, and even more, the temperature effect over such characteristic curve, as well as, in general, over the photovoltaics' module way of operation is a matter of interest in this context. It is directly related to meteorological conditions and it should be taken into account once established the region of installation or vice versa.

4.3.1 Temperature dependence

In equations (4) and (5), if only the temperature terms were considered, the expressions take the form of equations (6) and (7). The temperatures effect on the maximum power is also linear and in this case, the slope under which it happens is usually named "Gamma" (γ).

$$I_{SC}\alpha(T - T') \quad (6)$$

$$V_{OC}\beta(T-T') \quad (7)$$

In Fig. 58a several IV test curves were done to a UMG photovoltaic module and show how the voltage is more affected by the temperature than the current and in Fig. 58b also shows the power dependence on the temperature. Each test was done on a difference in temperature of 3°C with a margin error of ±1°C. The same assessment was done to the four types of PV modules tested.

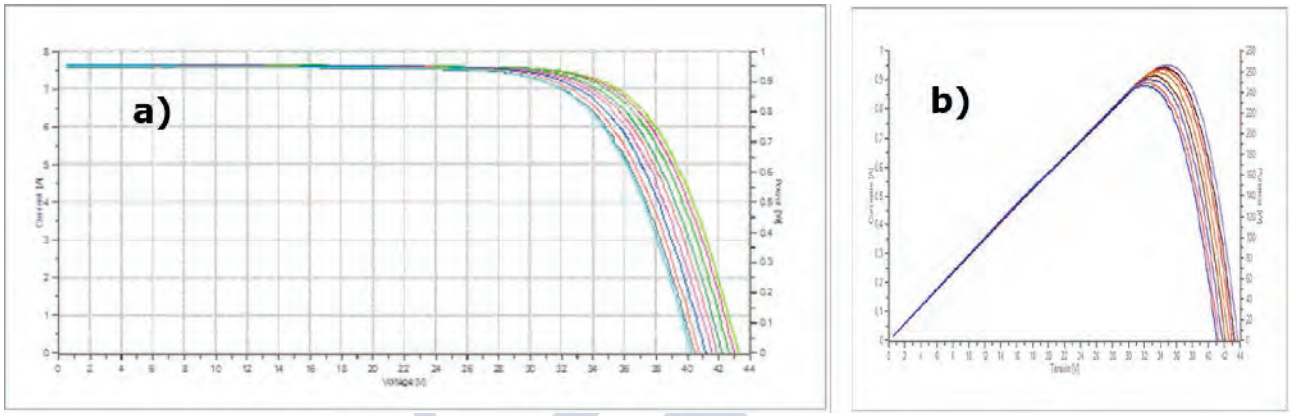

Fig. 58 I_V curves for different temperatures in UMG's modules tested at SEAG test site.

The solar modules' temperature is frequently high, in previous measurements, a range between 30 and 60 Celsius were considered [174], [189], so the less temperature dependent a photovoltaic module is, the more stable and solvent it is, and the three temperature dependence parameters are the basics in this section. In Fig. 59 it's shown the results of the series of test done to the photovoltaic modules. The test was done in quasi stable irradiation and only the temperature of the module was changed.

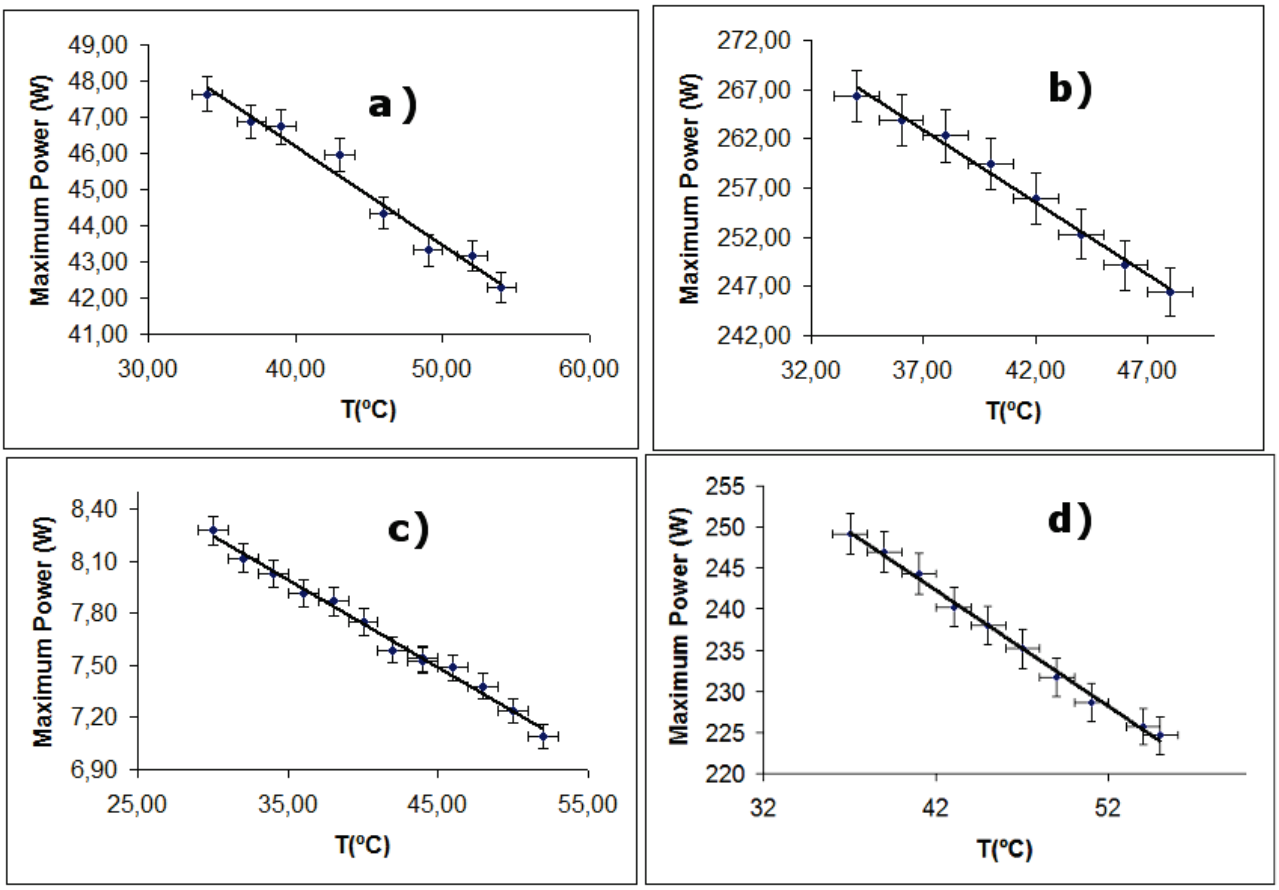

Fig. 59 Maximum power behavior vs temperature for the four kinds of solar module: from up-left to bottom right: monocrystalline, multicrystalline standard, thin-film and UMG multicrystalline.

When the maximum power behavior for each type of solar module was measured and analyzed, by means of an approximately stable irradiance (its variation during the measurements was lower than 30W/m^2, although the effect is corrected), the Fig. 60 is obtained. The values are the normalized Pmax vs T slopes in percentage with respect to standard temperature conditions. The results show that the maximum power of the thin film modules have shown the biggest dependency on temperature (worst behavior) whereas all the crystalline have a compatible dependence to each other in the same sense within the measurement errors.

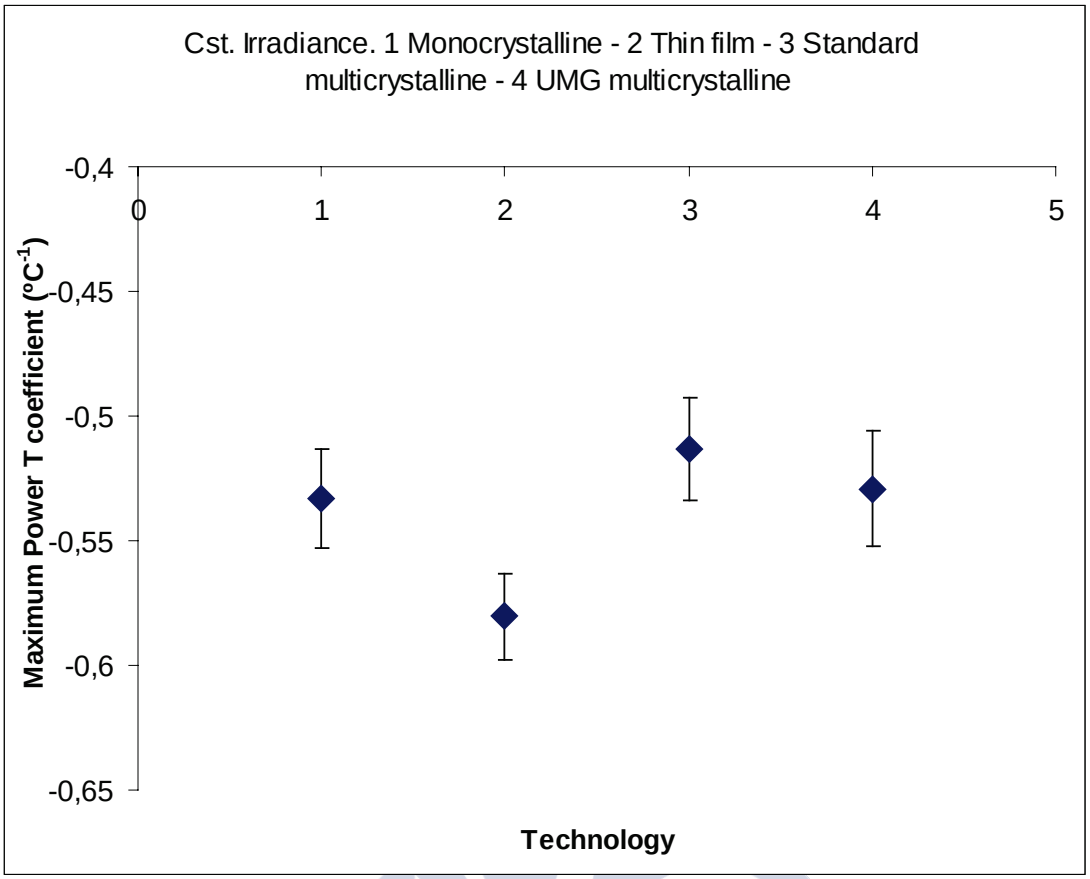

Fig. 60 Maximum power behavior with respect to temperature (Gamma factor) for the different studied technologies.

Regarding the open circuit voltage dependence on temperature (beta factor, see equations (7)), as it can be seen in Fig. 61, the results are noticeably different. In this case, the lower dependence on temperature is patent in monocrystalline modules, followed by thin film and UMG multicrystalline. The higher dependence was found in standard multi-crystalline modules for this case.

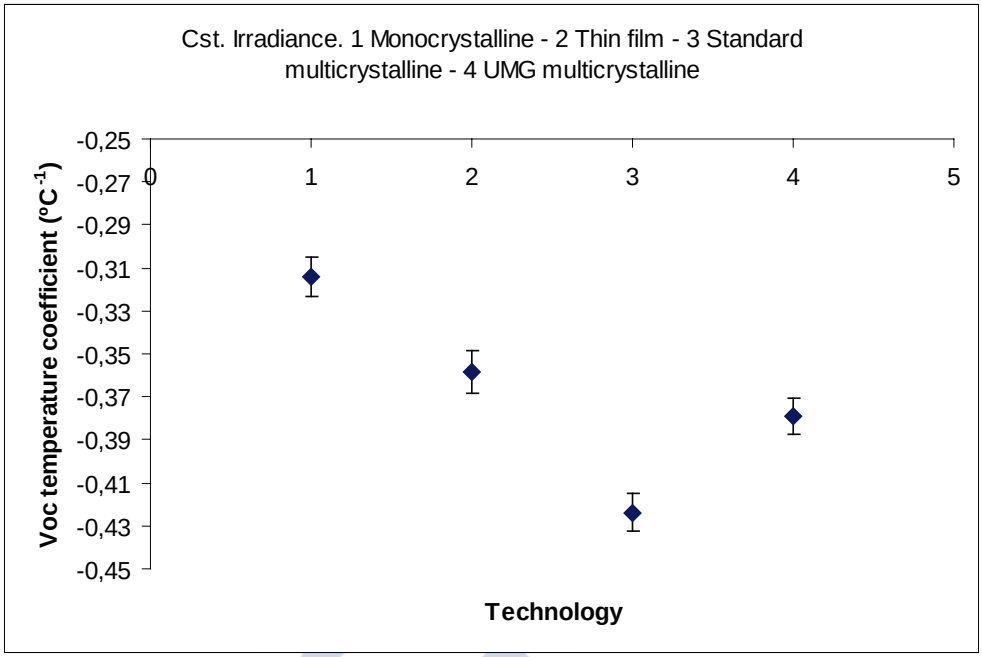

Fig. 61 Normalized open-circuit voltage dependence on temperature in percentage (Beta factor) for the different studied technologies.

When the dependences of the short circuit currents are considered in the same way, Fig. 62 shows the most stable behavior for the case of monocrystalline solar modules, whereas the biggest dependency is clearly patent for the thin-film samples. Concerning the results that were obtained on the multicrystalline photovoltaic modules' tests, the highest dependency was measured for UMG kind of implementation.

The sensitivities that were reached with these estimations are lower than that of the previous parameters, since the temperature influence on the currents is notably reduced, as well as higher on irradiance during the measurements (whose effect had to be corrected).

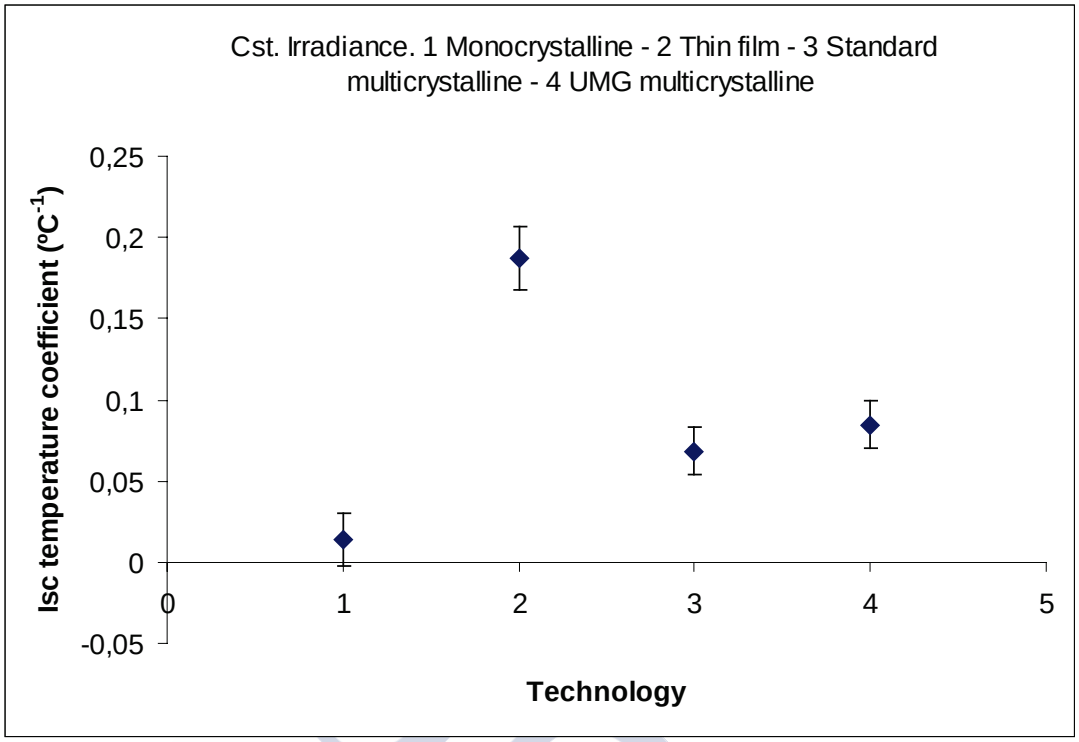

Fig. 62 Normalized short-circuit current dependence on temperature in percentage (Alpha factor) for the different studied technologies.

When Fig. 61 is considered, as well as the fact that the lower the temperature dependence is, the more stable is the solar panel's behavior is and, thus, more suitable are its characteristics for a desert region such the studied one, some conclusions could be drawn:

- The most suitable technology turns out to be the standard multi-crystalline one, showing UMG and monocrystalline type nearly the same results concerning this parameter, and compatible with standard's values within the errors.
- Thin film modules (CIS) have shown the worst results when high temperatures are considered.

4.3.2 Irradiance dependence

One of the important characteristics when it comes to the selection of a technology is its response at extremely different levels of irradiation. The region under study presents notably high levels of irradiance and relatively few cloudy days, which is, on the other hand, a notably different situation compared to World's regions with high amounts of clouds. That is the reason why the solar modules' energy production under different irradiance conditions is an aspect to be studied. In order to do so, several measurements (Fig. 63) were carried out at different irradiance levels (real sun) for each technology at stable temperature (36±1 Celsius).

The irradiance is directly related to the energy production of solar modules, but the way under which this happens depends on the kind of cell or light spectra. All the main cell parameters (I, V, P) in our range have an approximately linear behavior with irradiance for the typical real sun intensities (see equations (4, 5)). The more stable these parameters are, the more usable the photovoltaic modules will be, since the performance is relatively higher at lower

irradiances, but this is not in any situation the most preferable case, as it will be afterwards explained.

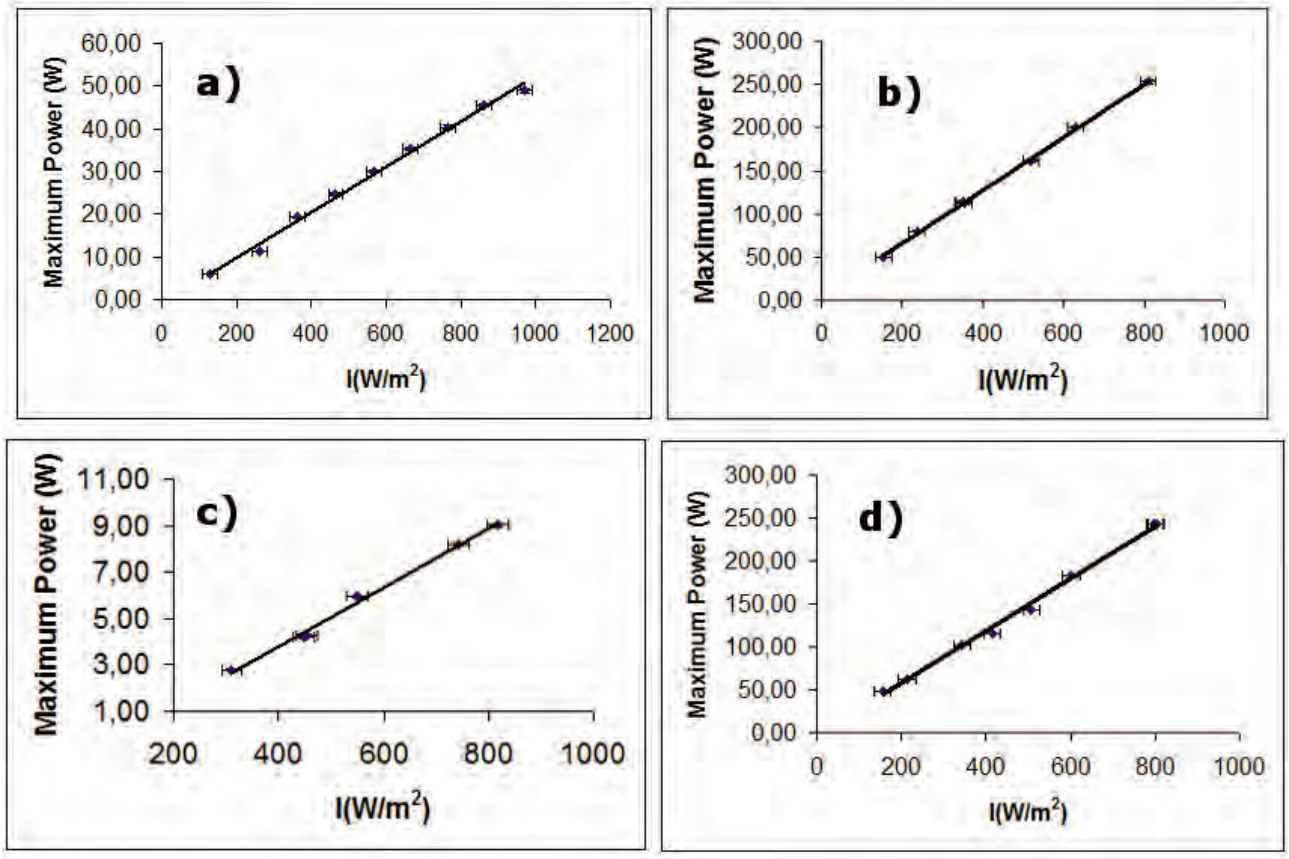

Fig. 63 Maximum power behavior vs irradiance for the four kinds of solar module: from up-left to bottom right: monocrystalline, multicrystalline standard, thin-film and UMG multicrystalline.

As it can be seen in Fig. 64, where the values are the normalized Pmax vs irradiance slopes in percentage with respect to standard irradiance conditions, the maximum power dependences of the different technologies that were analyzed on the irradiance are comparable to each other, with the exception of thin-film solar modules, whose behavior is around 10% more irradiance dependent.

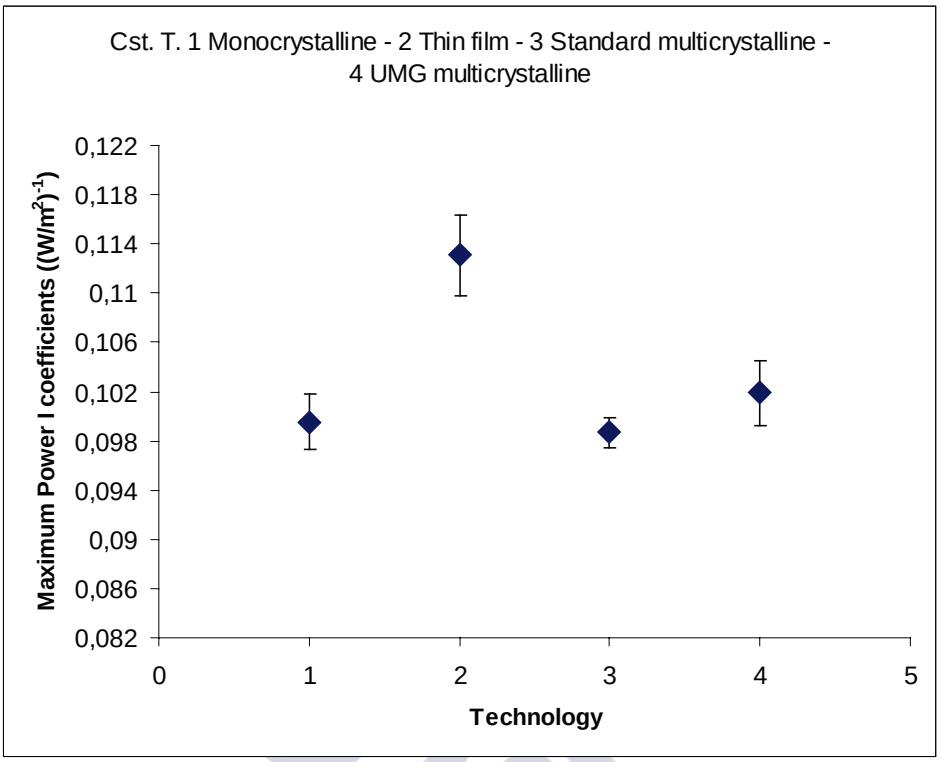

Fig. 64 Normalized maximum power behavior in percentage with respect to irradiance for different technologies.

Regarding the effect that irradiance has shown over the open-circuit voltage during the analysis, the results in Fig. 65 indicate again that the behaviors are compatible among the different technologies, being the highest dependence for the thin-film cells.

The situation concerning the short-circuit current is approximately equivalent, although in this case the differences between the thin-film cells and the others are sharper.

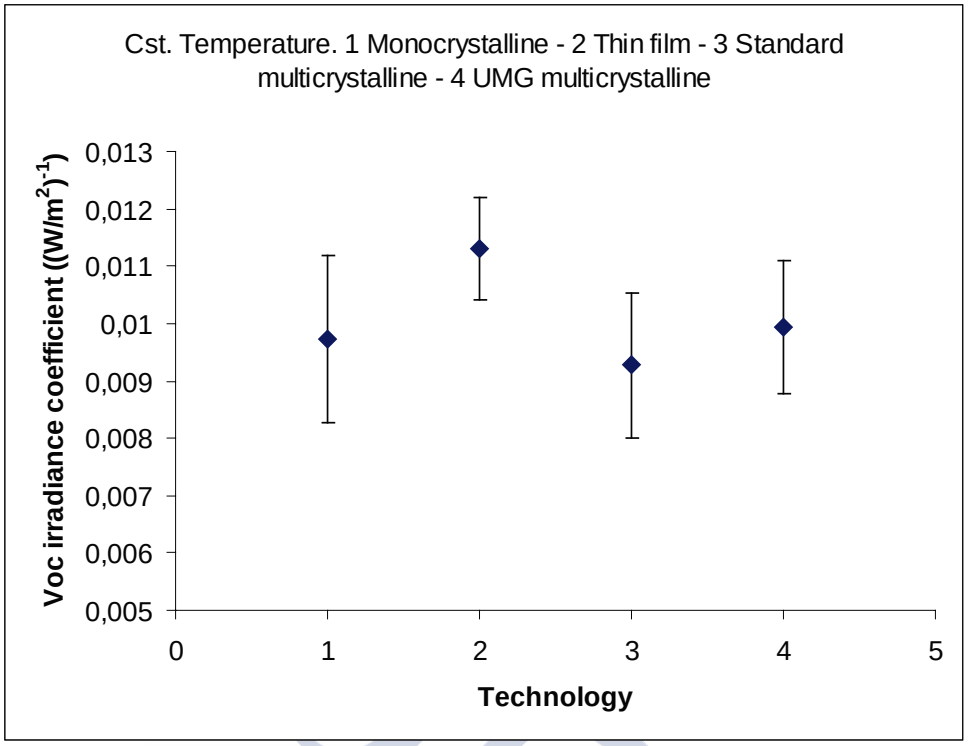

Fig. 65 Normalized open-circuit voltage dependence on irradiance in percentage for the different technologies.

The reason for this situation may be related to different aspects, such as the encapsulation, a slightly higher sensitivity to different angles in thin-film solar modules, spectral matters and so forth. In this sense further studies will be necessary for a thorough knowledge of these particular and non-trivial aspects.

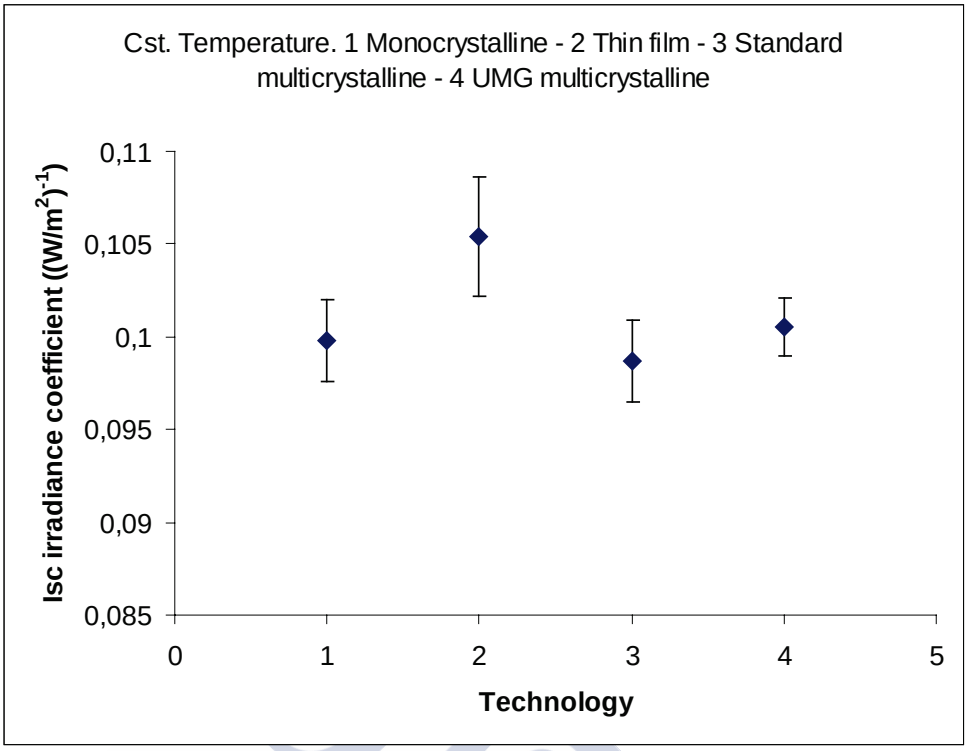

Fig. 66 Normalized short-circuit current dependence on irradiance in percentage for the different technologies.

The dependency or slope that the solar modules' energy capabilities show with respect to the irradiance is related to their adequateness when a site of installation is considered. In particular, if the region under consideration present high irradiance values (even more important for this purpose than the integrated solar energy during the day), the bigger such dependence is, the more suitable the solar panel will be. In areas such a big part of the studied region, values above 1000W/m^2 are typically reached on a daily basis, so such solar modules will take advantage under this situation and increase their relative power capabilities. On the other hand, for medium low irradiances, the more stable solar modules regarding irradiance are the most suitable ones.

By taking this fact into consideration, some conclusions could be derived from the past figures:

- Thin film solar modules would be the most suitable choice for a high-irradiance region such as the region under study.
- UMG multicrystalline type, as well as monocrystalline turns out to be the best choices among crystalline types.
- The standard multicrystalline solar modules present the best behavior for medium-low irradiances.

4.3.3. Combined temperature and irradiation dependence

When both dependences, on temperature and irradiance, are considered as a whole, a selection of the most suitable technology for regions could be established. In this way, as it was previously explained, higher maximum power slopes over irradiance are recommendable for sites that statistically present high irradiance values and the other way around when it comes to slopes (absolute value) over temperature. For medium-low irradiances, mainly during the months that are expectable to show lower values concerning solar resource, the lower the slopes with respect to irradiance, and the more favorable technology. Regarding temperature, lower dependences are also preferable in these last cases, although the requirement is not as significant as in other kind of region.

In Fig. 67, a match among all PV modules' tendencies is plotted. The regions of adequateness are also presented on the plot in the sense above detailed. The crystalline module' characteristics are placed at the good temperature-dependence area, whereas the thin-film case turns out to be on the best irradiance-dependence region. Regarding this last observation, it is important to take into account that thin-film modules present the inconvenience of being more sensitive to irradiance effect when it comes to ageing [190], [191], so this apparently preferment situation for high irradiances is not strict. It should be mentioned that the typical range of operation both for temperature and irradiance is not included, so the importance of the irradiance effect and that of the temperature could be somewhat lower or higher depending on this fact.

Under these last considerations, the multicrystalline solar modules arise as the most suitable choices for high irradiated areas such as the studied in the present work. Concerning both last's types, UMG case present a slightly higher advantage when the irradiance slope is considered that its disadvantage on temperatures' case. Furthermore, as it was above showed, UMG type's prices are lower.

In the next section, the fact that UMG modules present a slightly better ageing than other crystalline, which points in this same last's direction.

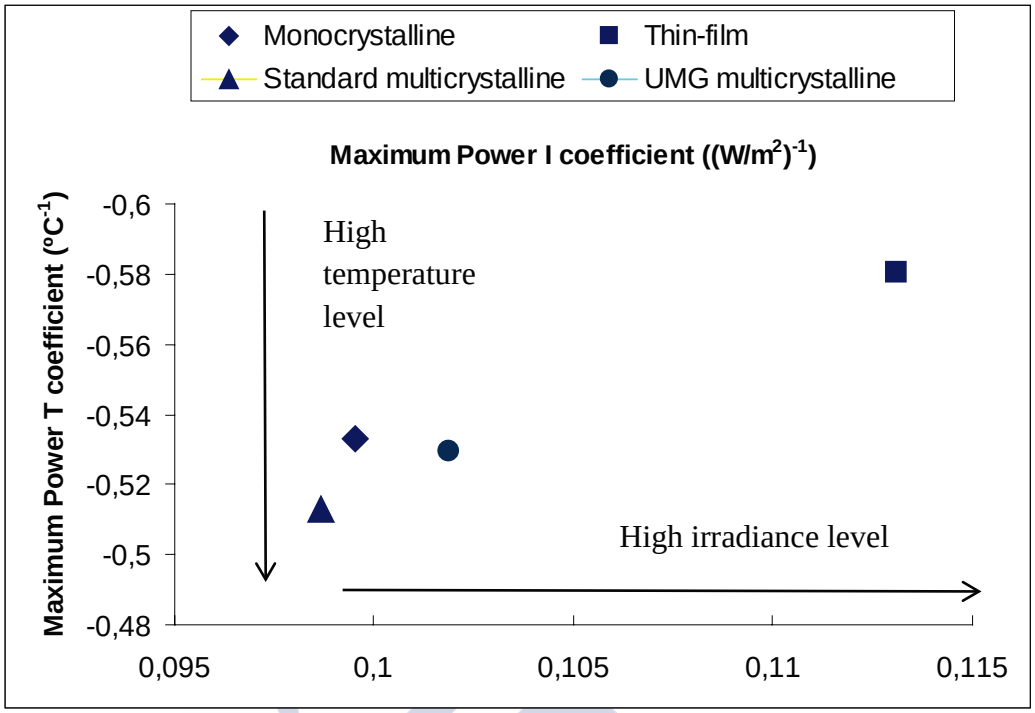

Fig. 67 Normalized temperature dependences (gamma) in percentage vs irradiance ones for all the PV module types under study.

As it was previously considered, both temperature and irradiance influence the solar modules behavior. The differences regarding those effects, when it comes to the different technologies, could describe which dependences are more variable from one solar module to another. Fig. 68 shows the normalized uniformity of such parameters concerning the maximum power by using the monocrystalline case as a reference. In general, the temperature influences have shown a slightly more variable behavior among the different technologies, except from the thin-film modules, in which the irradiation's dependence difference is clearly higher than that of the temperature (near to 15%). Moreover, the dots above the zero line indicate a better behavior than monocrystalline solar modules, in medium-low irradiation, whereas the contrary happens to the dots under it. This means that, for such climate regions, the standard multicrystalline modules have shown a better global behavior when the maximum power is considered, as well as that thin-film present the worst one. For high-irradiation areas, a bigger dependence on irradiance is better, so, as above explained; thin-film modules might be suitable. Nevertheless, their ageing rate for high irradiances is worse as well as the temperature dependence. The convenience regions are pointed in Fig. 68. Once again, the common irradiation/temperature ranges could be considered in each case for a more accurate evaluation.

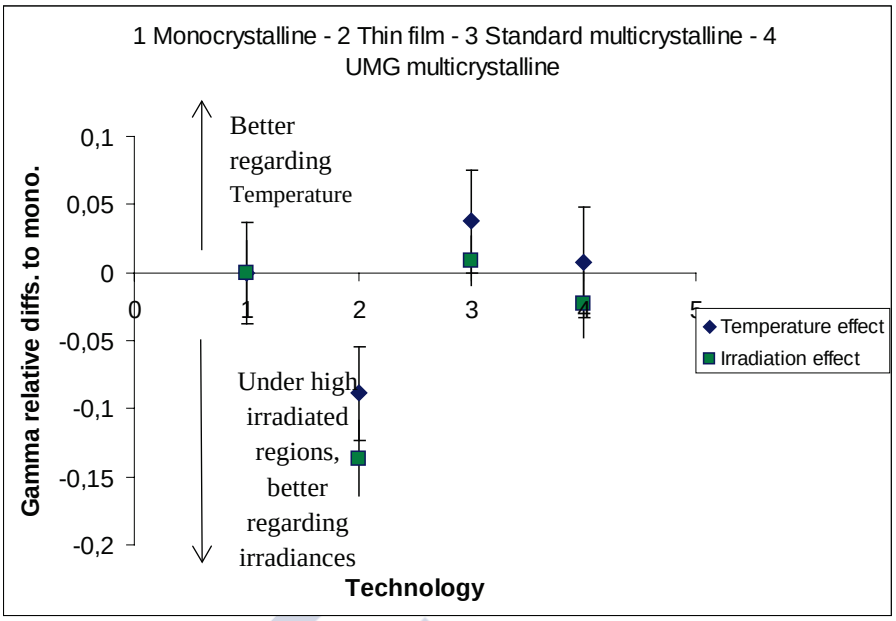

Fig. 68 Relative (to monocrystalline type) differences among the parameters that quantify the temperature/irradiance dependence for each technology.

Regarding the UMG polycrystalline case, the results are compatible to both monocrystalline and multicrystalline standard type within the error margins.

4.4.Conclusions

The main technologies of solar PV modules have been studied (monocrystalline, multicrystalline, and thin film) in order to establish a cataloguing of adequateness concerning the predicted climate conditions for the site under study. In addition to the standard multicrystalline type, the most efficient upgraded metallurgical grade silicon type was also analyzed.

The crystalline modules show a better performance if both the efficiency and the temperature is considered. When such dependence is analyzed only in irradiance, thin film modules turn out to present the most convenient characteristics for this region, followed by UMG case. Although is convenient to consider the ageing factor of the thin films that in most of the case is higher than in silicon crystalline based cases.

CHAPTER 5 GENERAL CONCLUSIONS AND FUTURE LINES OF RESEARCH

South of Sonora region in a Renewable Energy context

Even though, the renewable energy sector looks promising in Mexico, in particular wind, solar and geothermal energy, most of the studies of resource have been done without any validation and/or using inaccurate methods(linear interpolation of weather stations) to determine the resource in whole country as previously stated in Chapter 1. Another aspect of Mexico that difficult energy assessments is size of the country, its diverse climatology and its morphological features. Be choosing a micro-region, as the south of the Sonora state, resource assessment results in a better understanding of the energy possibilities and giving better tools for development on a scale that matters.

The wind assessment of the State of Sonora made by Vestas gave fewer wind power possibilities for the south region than to the north; however in the assessment made by CFE the wind power possibilities are better closer to the sierra in the south region. Moreover the methodology followed by these two recent studies is not clear, and validation for this kind of resource is necessary on a micro-scale level.

With respect to the solar resources, while in Sonora was believed to be significant based on limited past data, understanding the spatial and temporal variability requires significantly more data and analysis in order to optimize planning and placement of solar energy power plants.

From this remarks, we conclude, that is necessary to focus on a region that has enough data to have a convincing result and to have an energy resource analysis method that gave less uncertainty in comparison to past methods. For these reasons the south of Sonora seems like a suitable region to do this research because the region apparently has many resources but also has needs that could be cover by renewable energies.

Methodology for a solar energy assessment in the south of Sonora by a Numerical Weather Prediction Model

In this research a downscaling of the south of Sonora Mexico region was performed in order to obtain a highly temporal resolution solar potential assessment as well as a validation between the output and observations. A Numerical Weather Prediction Model has been implemented for this purpose.

The graphical results processed from the WRF output indicate that the horizontal resolution for this example could be sufficient for power plants placement. In other words a higher resolution is not necessary for this region due to the homogeneity of the outputs and not drastic topographical changes. In general terms, the model represents the GHI of the region with a high temporal resolution (10 min vs 12 hours).

Overall the results for the WRF present less accuracy than ERA-Interim, related to the weather stations, in annual terms. However in non-storm season WRF has better results than ERA-Interim outputs. Since the annual rRMSE values are low (average 9.91%) we conclude that the model has relatively good accuracy and could be an alternative to study the solar resource on regions where climate conditions are similar to the studied region; especially if high temporal resolution (10 min) is necessary. However the results of the validation were done mainly on the valley region of the south of Sonora, it is recommended to analyze the outputs on the sierra region (west and higher altitude) in order to understand if the results are biased only to that kind of climate. Moreover, it is necessary to do a further research in different regions and climate conditions so as to compare the effects observed during the present study with the results in such conditions.

Improvement of the Numerical Weather Prediction Result

Simulations in different seasons of the year, with seven convective parameterizations, where done thoroughly to select the CP for the region. The best CP for the region was selected in order to produce a database of GHI with the highest correlation with observations.

The first trial was to determine which CP could give results closer to observations on summer. The results were conclusive and the best CP for the south of Sonora region in summer was first NSAS and then OSAS. Both parameterizations had higher confidence to the observation than any other parameterization. The second examination was done on winter, the results of the simulations showed that most parameterization has high correlation with the observations. As remark, KF, which shows the worse resolution during summer, is the most powerful during the winter time.

In order to better understand the results a comparison between the precipitation of two CPs (KF and NSAS) and its GHI was performed. An analysis of the hydrometers generated by the model was done and it showed that the KF scheme had a lower density of moist on the atmosphere on average versus the NSAS scheme. The KF scheme seems to be in an overactive state. An overactive scheme produces too much rainfall in situ, and removes too much atmospheric moisture, which could have fallen as precipitation downstream like in most of the cases excepting the Arakawa-Schubert schemes.

The results obtained in this research are promising and could lead to have better results on the future in other regions by using NWP models to predict GHI. However is convenient to analyze the other physical parameterizations (shortwave, longwave, microphysics) in each cenario as well.

Selection of adequate PV technology according to the climate

The main technologies of solar PV modules have been experimentally studied (monocrystalline, multicrystalline, and thin film (CIS)) in order to establish a cataloguing of adequateness concerning the predicted climate conditions for the site under study. In particular, two multicrystalline production has been tested; standard (Czochralski method) and metallurgical extraction (UMG).

In particular, the efficiency losses associated to either GHI and working temperature has been studied. The crystalline modules show a better performance being the multicrystalline UGM consider the best candidate for power solar plants located in the Sonora climatic conditions.

Future lines of research

- With regard to the assessment of the predictive power of the model WRF, the future lines of work to consider are:
  - To conduct a comparative study of different settings associated with other physical processes that may lead changes in the predictive influence of the model GHI (short wave, long wave, microphysics and others) in the region of Sonora.
  - Develop a similar study in at least one other region of similar climate characteristics and which provided greater validation database (more historic weather stations and more measures). It would be interesting also to the availability only meteorological data and not engaged in agriculture weather stations database.
  - To extend the study to other regions with different climatic characteristics. Particularly wet or semi-wet areas where optimization study of convective parameterizations could be analyzed in depth.
- Another associated studies related with WRF technical improvements could be:
  - Assess the capacity of WRF to provide predictions of the direct and diffuse components of solar radiation separately.
  - To conduct a study of limits on the ability of both temporal and spatial model resolutions.
  - To perform a comparison between the MRY methodology and TMY methodologies seems also interesting since TMY is the most widely used methodology for typical meteorological years.
- With regard to the identification of appropriate photovoltaic technology depending on the climate zone of implementation:
  - To include in to the study other PV technologies (amorphous silicon technology or multilayer thin film solar panels).
  - To study of the influence of the resistivity in the response of the solar modules, allowing intra-production line, to change the resistivity of the modules according to their future climate location.

- To research the lifetime of different technologies, or otherwise aging studies in extreme conditions which would allow adding a crucial variable interest in making appropriate decisions about photovoltaic technology.

CONCLUSIONES GENERALES Y LÍNEAS FUTURAS DE INVESTIGACIÓN

El sur de Sonora en un contexto energético

A pesar de que el sector de las energías renovables resulta prometedor en México, en particular la eólica y la solar y la geotérmica, la mayor parte de los estudios de evaluación de recurso realizados en el país este momento no disponen de la necesaria validación y/o no han sido desarrollados usando métodos inadecuados (como interpolación lineal entre estaciones meteorológicas), tal como se ha recogido en el Capítulo 1. Otro de los aspectos negativos que dificultan la adquisición de información energética, es el tamaño del país, su ingente diversidad climatológica y su variada morfología. En ese sentido, haber elegido una micro-región, como el Sur del estado de Sonora, facilita la recogida de información, contribuye a una mejor comprensión de las posibilidades energéticas y facilita el desarrollo de herramientas de evaluación.

Las predicciones de viento para el estado de Sonora realizadas por Vestas dan una menor posibilidad de explotación de energía eólica en el sur que en el norte; sin embargo en las predicciones llevadas a cabo por CFE, las expectativas con mejores en el sur de la región cerca de la sierra. En ambos casos, la metodología usada en estos dos recientes estudios no es demasiado clara y sin duda una validación de este tipo de recursos debe hacerse a nivel de micro-escala.

En cuanto al recurso solar, si bien, basándose en datos antiguos, se considera que es abundante en Sonora, sería interesante disponer de datos con mejor resolución espacial y temporal que permitan optimizar la localización de posibles plantas de producción de energía solar. Un estudio de este tipo requiere sin duda tanto una cantidad significante mayor de datos como un análisis más profundo.

En resumen, se hace necesario centrar el estudio en una región que disponga de suficientes datos para permitir una validación adecuada que permita obtener un método de análisis capaz de ofrecer predicciones de mayor precisión que las obtenidas en el pasado. Por estas razones, el Sur de Sonora se perfila como una región adecuada ya que dispone aparentemente de muchos recursos renovables que necesita explotar.

Metodología para la elaboración de un atlas de recurso solar para una región semidesértica.

Es este trabajo, se ha obtenido un mapa de alta resolución temporal del potencial de recurso solar para la región del sur de Sonora mediante un modelo Numérico de Predicción climatológica (WRF). Los resultados obtenidos han sido validados mediante observaciones.

Los resultados gráficos obtenidos a partir del modelo WRF muestran que la resolución horizontal obtenida en este ejemplo es suficiente para el emplazamiento de plantas de producción. En otras palabras, no es necesaria mayor resolución, tanto por la homogeneidad de los resultados como la no existencia de cambios topográficos profundos. En términos generales, la resolución temporal del modelo es también alta (10 minutos) respecto a los modelos precedentes (12 horas).

A nivel global, en términos anuales, los resultados obtenidos por WRF muestran una menor exactitud en comparación con los datos de las estaciones meteorológicas, que los obtenidos por ERA-Interim. En todo caso, los valores anuales de rRMSE son bajos (una media de 9.91%) con lo cual podemos considerar que el WRF constituye una buena alternativa para el estudio del potencial de energía solar, al menos en regiones con unas condiciones climáticas semejantes a la región en estudio; sobre todo si necesitamos una buena resolución temporal (10 minutos). Ha de tenerse en cuenta además que, analizando los resultados más en detalle, en los meses exentos de fenómenos meteorológicos adversos (p.e. tormentas) WRF presenta mejores resultados que ERA-interim. En todo caso, el proceso de validación se ha realizado principalmente en zona de valle, donde existe el mayor número de observaciones, por lo cual sería recomendable extender el proceso a la región de sierra con el fin de estudiar posibles sesgos asociados a un determinado tipo de clima. A mayores, sería interesante generalizar el proceso de validación a otras zonas climáticas con el fin de analizar la validez de los resultados obtenidos.

Mejoramiento de la salida del Modelo Meteorológico Numérico

Con el fin de determinar la parametrización convectiva (PC) óptima para predecir la irradiación solar, se ha realizado un estudio en profundidad de los resultados obtenidos utilizando siete diferentes opciones en diferentes épocas del año.

En primer lugar se trató de determinar cuál es la PC que ofrece los resultados más cercanos a las observaciones durante el verano. La prueba fue concluyente, resultando la aproximación NSAS la de mejor predicción, seguida de OSAS. El mismo estudio realizado en el invierno muestra como la mayor parte de las parametrizaciones muestras un buen comportamiento. Como dato, KF es la de mejor resolución en este caso, mientras que en verano aparecía como la de peor nivel de predicción.

Con el fin de comprender mejor los resultados obtenidos se ha realizado un estudio comparativo de dos PC (KF y NSAS). Para ello, se ha estudiado el efecto de las variables de precipitación en la predicción de GHI. El análisis de los hidrómetros generados por el modelo

muestra como la parametrización KF muestra una menor densidad de humedad media en la atmosfera que la parametrización NSAS. O en otras palabras, KF parece ser un estado superactivo, lo cual produce una mayor cantidad de lluvia localmente removiendo demasiada humedad atmosférica, haciendo disminuir las precipitaciones. Este efecto se observa en casi todos los casos estudiados salvo en las parametrizaciones de Arakawa-Schubert.

Se han obtenido resultados prometedores que puede permitir a modelos NWP, obtener mejores resultados de GHI en otras regiones climáticas. En la misma línea, sería interesante analizar en el mismo escenario otras parametrizaciones físicas (onda corta, onda larga, microfísica).

Con el fin de identificar la tecnología fotovoltaica apropiada en función de las características climáticas, se ha realizado un estudio experimental de diferentes tecnologías de producción de módulos fotovoltaicos (monocristalino, policristalino y capa delgada). De hecho, en el caso de la tecnología policristalina, se han analizado módulos de dos tipos diferentes de modos de producción: el standard (método Czochralski) y el de extracción metalúrgica (UMG). Entre los paneles de capa delgada se ha analizado un panel CIS.

En particular, el estudio se ha focalizado en la perdida de eficiencia en los paneles con las variaciones en la irradiación solar y la temperatura de funcionamiento. En todos los casos, los módulos cristalinos han mostrado menos dependencia. Como resultado final, el módulo policristalino de producción metalúrgica presenta el mejor compromiso de funcionamiento a altas temperaturas y altos niveles de irradiación características de la región de Sonora en estudio.

Líneas futuras de investigación

- Con respecto a la evaluación de la capacidad de predicción del modelo WRF, las futuras líneas de trabajo a considerar serían :
    - Llevar a cabo un estudio comparativo de las diferentes parametrizaciones asociadas a otros procesos físicos que puedan conllevar variaciones en la capacidad de predicción de GHI del modelo (onda corta, onda larga, microfísica y otros) en la región de Sonora.
    - Repetir el estudio en al menos otra región de características climáticas semejantes y en la que se disponga de una mayor base de datos para validación (más estaciones meteorológicas y mayor histórico de medidas). Sería interesante además que se dispusiera de datos meteorológicos puros y no dedicados a la agricultura.
    - Extender el estudio a otras regiones con características climáticas diferentes. En particular zonas húmedas o semi-húmedas, donde el estudio realizado sobre optimización de parametrizaciones convectivas podría ser analizado en profundidad.
- Otros estudios asociados de cara a mejoras técnicas del WRF podrían ser:

- Evaluar la capacidad del modelo WRF para proporcionar predicciones de las componentes directa y difusa de la radiación solar separadamente.
- Realizar un estudio de límites en la capacidad de resoluciones tanto temporal como espacial del modelo.
- Una comparación entre la metodología MRY y TMY también es atractiva ya que el TMY es la metodología más encontrada en la literatura.

➢ Con respecto a la identificación de la tecnología fotovoltaica apropiada en función de la zona climática de implantación :

- Incorporación al estudio de otras tecnologías a (tecnología de silicio amorfo de capa delgada o paneles solares multicapa).
- Estudio de la influencia de la resistividad en la respuesta de los módulos solares, lo que permitiría dentro de una misma línea de producción, modificar la resistividad de los módulos en función de su futuro emplazamiento climático.
- Estudio de tiempo de vida útil de las diferentes tecnologías, o en su defecto estudios de envejecimiento en condiciones extremas lo que permitiría añadir una variable de crucial interés en la toma de decisiones sobre tecnología fotovoltaica apropiada.

REFERENCES

[1] International Energy Agency, “Mexico Energy Statistics,” 2013. [Online]. Available: http://www.iea.org/statistics/statisticssearch/report/?country=Mexico&product=balances&year=2012. [Accessed: 02-Jul-2015].

[2] Secretería de Energía, “Balance nacional de energía 2013,” México DF, 2013.

[3] DOF, “DECRETO por el que se reforman y adicionan diversas disposiciones de la Constitución Política de los Estados Unidos Mexicanos, en Materia de Energía.,” *D. Of. la Fed.*, vol. 723, no. 17, pp. 2 – 13, 2013.

[4] DOF, “DECRETO por el que se expide la Ley General de Cambio Climático,” *D. Of. la Fed.*, vol. 705, no. 4, pp. 1–29, 2012.

[5] DOF, “Decreto por el que se expide la Ley de los Órganos Reguladores Coordinados en Materia Energética; se reforman, adicionan y derogan diversas disposiciones de la Ley Orgánica de la Administración Pública Federal y, se expide la Ley de la Agencia Nacional de,” *D. Of. la Fed.*, vol. 741, no. 8, pp. 102–136, 2014.

[6] “Sistema de Información Energética.” [Online]. Available: http://sie.energia.gob.mx/bdiController.do?action=temas. [Accessed: 05-Aug-2015].

[7] J. Agredano and J. M. Huacuz, “Pv Technology Status and Prospects in Mexico,” 2009.

[8] GTZ, “Nichos de mercado para sistemas FV en conexión a red en méxico,” Eschborn, 2009.

[9] P. W. (NASA L. R. C. Stackhouse, “Surface meteorology and Solar Energy,” *NASA*, 2008. [Online]. Available: http://ntrs.nasa.gov/search.jsp?R=20080012200. [Accessed: 03-Jul-2015].

[10] L. G. Sanchez Stone, “La energía solar distribuida, ya es mas barata que la energía convencional.,” *Rev. Energías Renov.*, no. 25, pp. 14–16, 2015.

[11] Iea-Pvps (International Energy Agency), “Snapshot of Global PV Markets 2014,” 2015.

[12] PV Magazine Latam, “México: CRE aprueba 2 GW fotovoltaicos en lo que va de año,” *PV Magazin Latam*, 2015. [Online]. Available: http://www.pv-magazine-latam.com/noticias/detalles/articulo/mxico--cre-aprueba-2-gw-fotovoltaicos-en-lo-que-

va-de-ao_100018854/. [Accessed: 03-Aug-2015].

[13] Comisión Reguladora de Energía (CRE), “RENOVABLES, HIDROELÉCTRICAS Y COGENERACIÓN EFICIENTE,” *CRE*, 2015. [Online]. Available: http://www.cre.gob.mx/pagina_a.aspx?id=88. [Accessed: 03-Aug-2015].

[14] Latin America PV Playbook, “Latin America Country Markets 2014-2015E,” 2015.

[15] Comisión Federal de Electricidad, “Informe Anual 2014,” Ciudad de México, 2015.

[16] OPDE, “OPDE Portal,” *OPDE*, 2015. [Online]. Available: http://www.opde.net/en/. [Accessed: 03-Aug-2015].

[17] NREL, “NREL: Concentrating Solar Power Projects - Agua Prieta II,” *NREL*, 2015. [Online]. Available: http://www.nrel.gov/csp/solarpaces/project_detail.cfm/projectID=135. [Accessed: 03-Aug-2015].

[18] G. Urdiales, “Elecnor cumple dos décadas de éxito en México - economiahoy.mx,” *Economia Hoy*, 2013. [Online]. Available: http://www.economiahoy.mx/economia-eAm-mexico/noticias/5007232/07/13/Elecnor-cumple-dos-decadas-de-exito-en-Mexico.html#.Kku8rk1XWibGleZ. [Accessed: 03-Aug-2015].

[19] D. Riveros-Rosas, J. Herrera-Vázquez, C. A. Pérez-Rábago, C. A. Arancibia-Bulnes, S. Vázquez-Montiel, M. Sánchez-González, F. Granados-Agustín, O. A. Jaramillo, and C. A. Estrada, “Optical design of a high radiative flux solar furnace for Mexico,” *Sol. Energy*, vol. 84, no. 5, pp. 792–800, May 2010.

[20] C. a Arancibia-Bulnes, M. I. Peña-Cruz, D. Marroquín-García, R. E. Cabanillas, C. a Pérez-Rábago, D. Riveros-Rosas, J. F. Hinojosa, and C. a Estrada, “Heliostat testing at a new facility in Sonora, Mexico,” *Proc. SolarPACES 2011 Congr.*, p. 23489, 2011.

[21] CENTRO DE INVESTIGACIÓN DE ENERGÍA – UNIVERSIDAD NACIONAL AUTÓNOMA DE MÉXICO (CIE-UNAM), “Heliostats Testbed (CPH),” 2011. [Online]. Available: http://lacyqs.cie.unam.mx/en/index.php/facilities/heliostats-field-test.

[22] M. Valdes-Barrón, D. Riveros-Rosas, C. A. a Arancibia-Bulnes, and R. Bonifaz, “The solar Resource Assessment in Mexico : State of the Art,” *Energy Procedia*, vol. 57, pp. 1299–1308, 2014.

[23] Instituto de Investigaciones Eléctricas and Secretaría de Energía, “POTENCIAL EÓLICO Y SOLAR PARA UN MÉXICO MÁS FUERTE,” *SENER*, 2010. [Online]. Available: http://www.energia.gob.mx/portal/Default.aspx?id=1803. [Accessed: 04-Aug-2015].

[24] SENER, “INVENTARIO NACIONAL DE ENERGÍAS RENOVABLES (INERE),”

2015. [Online]. Available: http://inere.energia.gob.mx/publica/version3.6/. [Accessed: 06-Aug-2015].

[25] CONUEE, “Las Energías Renovables en México y el mundo,” Mexico DF, 2009.

[26] Q. Hernández-Escobedo, R. Saldaña-Flores, E. R. R. Rodríguez-García, and F. Manzano-Agugliaro, “Wind energy resource in Northern Mexico,” *Renew. Sustain. Energy Rev.*, vol. 32, pp. 890–914, Apr. 2014.

[27] Q. Hernández-Escobedo, F. Manzano-Agugliaro, and A. Zapata-Sierra, “The wind power of Mexico,” *Renew. Sustain. Energy Rev.*, vol. 14, no. 9, pp. 2830–2840, Dec. 2010.

[28] Y. Cancino-Solórzano, A. J. Gutiérrez-Trashorras, and J. Xiberta-Bernat, “Current state of wind energy in Mexico, achievements and perspectives,” *Renew. Sustain. Energy Rev.*, vol. 15, no. 8, pp. 3552–3557, Oct. 2011.

[29] D. Elliott, M. Schwartz, G. Scott, S. Haymes, D. Heimiller, and R. George, “Wind Energy Resource Atlas of Oaxaca,” 2003.

[30] NREL, “NREL: International Activities - Climate and Environmental Initiatives,” 2010. [Online]. Available: http://www.nrel.gov/international/climate_initiatives.html. [Accessed: 24-Aug-2015].

[31] L. Gulstad, “Velocidad de Viento a 120 metros de altura (Anual),” *Vestas*, 2013. [Online]. Available: http://inere.energia.gob.mx/documentos/METADATOS/Eolico_Vestas/Velocidad/120m_Altura.htm. [Accessed: 06-Jun-2015].

[32] L. Carmona Sánchez, E. D. Ortega Cobarrubias, and A. Zitacuaro Contreras, “Velocidad de Viento a 120 metros de altura (Anual) - Etapa I,” *INERE*, 2014. [Online]. Available: http://inere.energia.gob.mx/documentos/METADATOS/Eolico_CFE/Velocidad/120m_Altura.htm. [Accessed: 06-Jun-2015].

[33] C. G. Justus and A. Mikhail, “Height Variation of Wind Speed and Wind Distributions Statistics,” *Geophys. Res. Lett.*, vol. 3, no. 5, pp. 261–264, May 1976.

[34] X. Lu, M. B. McElroy, and J. Kiviluoma, “Global potential for wind-generated electricity.,” *Proc. Natl. Acad. Sci. U. S. A.*, vol. 106, no. 27, pp. 10933–8, Jul. 2009.

[35] A. A. Ghilardi, E. Riegelhaupt, and F. R. Saldaña, “Los recursos bioenergéticos de México. La Bioenergía en México. Un catalizador del desarrollo sustentable.,” 2006.

[36] M. E. González Ávila, “Producción de bioenergía en el norte de México: Tan lejos y tan cerca...,” *Front. norte*, vol. 21, no. 41, pp. 177–183.

[37] SAGARPA/FIRCO, “Diagnóstico General de la Situación Actual de los Sistemas de

Biodigestión en México," p. 35, 2011.

[38] J. López González, G. Hiriart Le Bert, and R. Silva Casarín, "Cuantificación de energía de una planta mareomotriz," *Ingeniería Investigación y Tecnología*, vol. 11, no. 002. 2010.

[39] The Executive Committee of Ocean Energy Systems, "2014 ANNUAL REPORT," Lisbon, 2015.

[40] CONUEE, "Comisión Nacional para el Uso Eficiente de la Energía," 2015. [Online]. Available: http://www.conuee.gob.mx/wb/. [Accessed: 06-Aug-2015].

[41] CONAGUA, "Atlas Digital del Agua México 2012," 2012. [Online]. Available: http://www.conagua.gob.mx/atlas/index.html. [Accessed: 06-Aug-2015].

[42] G. Hiriart Le Bert, L. C. a. Gutiérrez Negrín, J. L. Quijano León, A. Ornelas Celis, S. Espíndola, and I. Hernández, "Evaluación de la Energía Geotérmica en México," p. 164, 2011.

[43] INEGI, "Anuario estadístico y geográfico de Sonora 2014," México DF, 2015.

[44] INEGI, "Sitio del INEGI en Internet. Mapa digital de México," *Online*, 2014. [Online]. Available: http://gaia.inegi.org.mx/mdm6/. [Accessed: 01-Jan-2014].

[45] INEGI, "División municipal. Sonora," *INEGI*, 2010. [Online]. Available: http://cuentame.inegi.org.mx/monografias/informacion/son/territorio/div_municipal.aspx?tema=me&e=26. [Accessed: 05-Aug-2015].

[46] S. De la Vega Estrada, R. Romo Viramontes, and A. L. Gonzáles Barrera, "Índice de marginación por entidad Federativa y municipio 2010," Mexico DF, 2010.

[47] SEDESOL, "INFORME ANUAL SOBRE LA SITUACION DE POBREZA Y REZAGO SOCIAL 2015 Sonora," *SEDESOL*, 2015. [Online]. Available: http://www.sedesol.gob.mx/work/models/SEDESOL/Informes_pobreza/2015/Estados/Sonora.pdf. [Accessed: 05-Aug-2015].

[48] E. Lee and R. Van Schoik, "Arizona y Sonora : una región fronteriza establecida que trabaja para encontrar un lugar significativo en la cambiante economía global," 2014.

[49] Comision de Energia del Estado de Sonora, "Reunión Plenaria Comisión Sonora-Arizona Comité de Energía Información General del Estado de Sonora." 2011.

[50] Secretaría de Turismo del Estado de Sonora., "Sonora Turismo," 2014. [Online]. Available: http://www.sonoraturismo.gob.mx/. [Accessed: 24-Aug-2015].

[51] M. Hallack-Alegria and D. W. Watkins Jr., "Drought Frequency Analysis and Prediction in Sonora, Mexico," in *Impacts of Global Climate Change*, 2005, pp. 1–9.

[52] K. Averyt, J. Fisher, A. Huber-Lee, A. Lewis, J. Macknick, N. Madden, J. Rogers, and

S. Tellinghuisen, “Freshwater Use by U.S. Power Plants: Electricity’s Thirst for a Precious Resource,” *Energy Water a Warm. World Initiat. - Union Concerned Sci.*, pp. 1–62, 2011.

[53] J. Macknick, R. Newmark, G. Heath, and K. C. Hallett, “Operational water consumption and withdrawal factors for electricity generating technologies: a review of existing literature,” *Environ. Res. Lett.*, vol. 7, no. 4, p. 045802, Dec. 2012.

[54] J.-L. E. Cartron, G. Ceballos, and R. S. Felger, *Biodiversity, Ecosystems, and Conservation in Northern Mexico*. 2005.

[55] G. S. Alemán-Nava, A. Meneses-Jacome, D. L. Cardenas-Chavez, R. Díaz-Chavez, N. Scarlat, J.-F. Dallemand, N. Ornelas-Soto, R. García-Arrazola, and R. Parra, “Bioenergy in Mexico: Status and perspective,” *Biofuels, Bioprod. Biorefining*, vol. 9, pp. 8–20, 2015.

[56] D. Valdez-zamudiol, A. Castellanos-villegas, and S. E. Mash, “Land Cover Changes in Central Sonora , Mexico,” no. 1994, 2000.

[57] Comisión Nacional del Agua, “Servicio Meteorológico Nacional - CONAGUA,” 2015. [Online]. Available: http://smn.cna.gob.mx/. [Accessed: 25-Aug-2015].

[58] A. Energia Sonora, “Energia Sonora programs | Energía Sonora,” 2012. [Online]. Available: http://energiasonora.org/en/energia-sonora-programs/. [Accessed: 24-Aug-2015].

[59] A. López-Agüera, J. Domingues-Azevedo, I. Rodríguez-Cabo, D. Rey-Rey, V. Gándara-Villadoniga, E. Vieites-Montes, J. Peralta, I. Sosa, J. Guerra, and M. Alguacil, “Ecoaldeas or Self-Sustainable Communities and renewable energy solutions (SSC). First approach Ecuador and Mexico,” in *RENEWABLE ENERGY & POWER QUALITY JOURNAL*, 2012, pp. 487–494.

[60] J. Peralta, C. Otero, Á. López, I. Sosa, D. Emérita, and B. Alfredo, “Identificación y Evaluación del Potencial de Recursos Renovables en el Ecuador y su Viabilidad de Desarrollo Local,” in *Tercer Congreso Argentino de Ingeniería Mecánica III CAIM 2012*, 2012, pp. 1–12.

[61] J. Peralta-Jaramillo, “Modelamiento Computacional del Recurso Solar y Eólico para aplicación de Sistemas de Energía Renovable,” Universidad de Santiago de Compostela, 2015.

[62] J. Peralta, Á. Lopez, A. Barriga, I. Sosa, and E. Delgado, “Análisis estadístico de la información meteorológica para la explotación de energías renovables en el Ecuador,” in *Primer Congreso Internacional y Expo Cientifica Investigacion Sostenible: Energías Renovables y Eficiencia Energética*, 2013, pp. 1–9.

[63] A. Hammer, D. Heinemann, C. Hoyer, R. Kuhlemann, E. Lorenz, R. Müller, and H. G.

Beyer, “Solar energy assessment using remote sensing technologies,” *Remote Sens. Environ.*, vol. 86, no. 3, pp. 423–432, Aug. 2003.

[64] E. Lorenz, J. Hurka, D. Heinemann, and H. G. Beyer, “Irradiance Forecasting for the Power Prediction of Grid-Connected Photovoltaic Systems,” *IEEE J. Sel. Top. Appl. Earth Obs. Remote Sens.*, vol. 2, no. 1, pp. 2–10, Mar. 2009.

[65] E. Lorenz, J. Remund, S. C. Müller, W. Traunmüller, G. Steinmaurer, D. Pozo, J. Antonio, V. L. Fanego, L. Ramirez, M. G. Romeo, C. Kurz, L. M. Pomares, and C. G. Guerrero, “Benchmarking of different approaches to forecast solar irradiance,” in *24th European photovoltaic solar energy conference*, 2009, pp. 25–34.

[66] T. Prabha and G. Hoogenboom, “Evaluation of solar irradiance at the surface—inferences from in situ and satellite observations and a mesoscale model,” *Theor. Appl. Climatol.*, vol. 102, no. 3–4, pp. 455–469, Aug. 2010.

[67] R. Perez, S. Kivalov, J. Schlemmer, K. Hemker, D. Renné, and T. E. Hoff, “Validation of short and medium term operational solar radiation forecasts in the US,” *Sol. Energy*, vol. 84, no. 12, pp. 2161–2172, Dec. 2010.

[68] K. Angela, S. Taddeo, and M. James, “Predicting Global Solar Radiation Using an Artificial Neural Network Single-Parameter Model,” *Adv. Artif. Neural Syst.*, vol. 2011, pp. 1–7, 2011.

[69] P. Mathiesen and J. Kleissl, “Evaluation of numerical weather prediction for intra-day solar forecasting in the continental United States,” *Sol. Energy*, vol. 85, no. 5, pp. 967–977, May 2011.

[70] D. P. Dee, S. M. Uppala, a. J. Simmons, P. Berrisford, P. Poli, S. Kobayashi, U. Andrae, M. a. Balmaseda, G. Balsamo, P. Bauer, P. Bechtold, a. C. M. Beljaars, L. van de Berg, J. Bidlot, N. Bormann, C. Delsol, R. Dragani, M. Fuentes, a. J. Geer, L. Haimberger, S. B. Healy, H. Hersbach, E. V. Hólm, L. Isaksen, P. Kållberg, M. Köhler, M. Matricardi, a. P. McNally, B. M. Monge-Sanz, J.-J. Morcrette, B.-K. Park, C. Peubey, P. de Rosnay, C. Tavolato, J.-N. Thépaut, and F. Vitart, “The ERA-Interim reanalysis: configuration and performance of the data assimilation system,” *Q. J. R. Meteorol. Soc.*, vol. 137, no. 656, pp. 553–597, Apr. 2011.

[71] A. Ortega, R. Escobar, S. Colle, and S. L. de Abreu, “The state of solar energy resource assessment in Chile,” *Renew. Energy*, vol. 35, no. 11, pp. 2514–2524, Nov. 2010.

[72] V. Lara-Fanego, J. A. Ruiz-Arias, D. Pozo-Vázquez, F. J. Santos-Alamillos, and J. Tovar-Pescador, “Evaluation of the WRF model solar irradiance forecasts in Andalusia (southern Spain),” *Sol. Energy*, vol. 86, no. 8, pp. 2200–2217, Aug. 2012.

[73] R. J. Zamora, E. G. Dutton, M. Trainer, S. a. McKeen, J. M. Wilczak, and Y.-T. Hou, “The Accuracy of Solar Irradiance Calculations Used in Mesoscale Numerical Weather

Prediction," *Mon. Weather Rev.*, vol. 133, no. 4, pp. 783–792, 2005.

[74] D. R. Myers, "Solar radiation modeling and measurements for renewable energy applications: data and model quality," *Energy*, vol. 30, no. 9, pp. 1517–1531, Jul. 2005.

[75] C. Rigollier, O. Bauer, and L. Wald, "ON THE CLEAR SKY MODEL OF THE ESRA — EUROPEAN SOLAR RADIATION ATLAS — WITH RESPECT TO THE HELIOSAT METHOD," *Sol. Energy*, vol. 68, no. 1, pp. 33–48, 2000.

[76] A. Meinel and M. Meinel, *Applied Solar Energy*. Addison Wesley Publishing Co., 1976.

[77] E. G. Laue, "The measurement of solar spectral irradiance at different terrestrial elevations," *Sol. Energy*, vol. 13, no. 1, pp. 43–57, Apr. 1970.

[78] F. Linke, "Transmissions-koeffizient und Trübungsfaktor," *Beitr. Phys. Fr. Atmos*, no. 10, pp. 91–103, 1922.

[79] Lord Rayleigh, "XXXIV. On the transmission of light through an atmosphere containing small particles in suspension, and on the origin of the blue of the sky," *Philos. Mag. Ser. 5*, vol. 47, no. 287, pp. 375–384, May 1899.

[80] A. T. Young, "On the Rayleigh-Scattering Optical Depth of the Atmosphere.pdf," *J. Appl. Meteorol.*, vol. 20, pp. 328–330, 1981.

[81] E. P. Shettle and R. W. Fenn, "Models for the Aerosols of the Lower Atmosphere and the Effects of Humidity Variations on their Optical Properties," Sep. 1979.

[82] B. Molineaux, P. Ineichen, and J. J. Delaunay, "Direct luminous efficacy and atmospheric turbidity—Improving model performance," *Sol. Energy*, vol. 55, no. 2, pp. 125–137, Aug. 1995.

[83] J. Betcke, "Energy-Specific Solar Radiation Data from Meteosat Second Generation (MSG): The Heliosat-3 Project," Oldenburg, 2005.

[84] C. A. Gueymard, "REST2: High-performance solar radiation model for cloudless-sky irradiance, illuminance, and photosynthetically active radiation – Validation with a benchmark dataset," *Sol. Energy*, vol. 82, no. 3, pp. 272–285, Mar. 2008.

[85] M. J. Reno, C. W. Hansen, and J. S. Stein, "Global Horizontal Irradiance Clear Sky Models: Implementation and Analysis," no. March, pp. 1–66, 2012.

[86] P. Ineichen, "Comparison of eight clear sky broadband models against 16 independent data banks," *Sol. Energy*, vol. 80, no. 4, pp. 468–478, Apr. 2006.

[87] P. Ineichen, "Comparison and validation of three global-to-beam irradiance models against ground measurements," *Sol. Energy*, vol. 82, no. 6, pp. 501–512, Jun. 2008.

[88] V. Badescu, C. A. Gueymard, S. Cheval, C. Oprea, M. Baciu, A. Dumitrescu, F.

Iacobescu, I. Milos, and C. Rada, “Computing global and diffuse solar hourly irradiation on clear sky. Review and testing of 54 models,” *Renew. Sustain. Energy Rev.*, vol. 16, no. 3, pp. 1636–1656, Apr. 2012.

[89] D. R. Myers, *SOLAR RADIATION Practical Modeling for Renewable Energy Applications*, 1st Editio. Boca Raton, FL, 2013.

[90] G. H. Hargreaves and Z. A. Samani, “Estimating Potential Evapotranspiration,” *J. Irrig. Drain. Div.*, vol. 108, no. 3, pp. 225–230.

[91] A. Ångström, “On the Atmospheric Transmission of Sun Radiation. II,” *Geogr. Ann.*, vol. 12, pp. 130–159, 1930.

[92] J. Prescott, “Evaporation from a water surface in relation to solar radiation,” *Trans. R. Soc. South Aust.*, vol. 64, pp. 114–118, 1940.

[93] American Society of Heating Refrigeration and Air-conditioning Engineers., *ASHRAE Applications Handbook (SI)*, 2nd ed. Atlanta: ASHRAE, 2005.

[94] C. Furlan, A. P. de Oliveira, J. Soares, G. Codato, and J. F. Escobedo, “The role of clouds in improving the regression model for hourly values of diffuse solar radiation,” *Appl. Energy*, vol. 92, pp. 240–254, Apr. 2012.

[95] S. Manabe and R. F. Strickler, “Thermal Equilibrium of the Atmosphere with a Convective Adjustment,” *J. Atmos. Sci.*, vol. 21, no. 4, pp. 361–385, Jul. 1964.

[96] A. Arakawa and W. H. Schubert, “Interaction of a Cumulus Cloud Ensemble with the Large-Scale Environment, Part I,” *J. Atmos. Sci.*, vol. 31, no. 3, pp. 674–701, Apr. 1974.

[97] M. Tiedtke, “A Comprehensive Mass Flux Scheme for Cumulus Parameterization in Large-Scale Models,” *Mon. Weather Rev.*, vol. 117, no. 8, pp. 1779–1800, Aug. 1989.

[98] A. K. Betts and M. J. Miller, “The Betts-Miller Scheme,” pp. 107–121, 1993.

[99] J. S. Kain and J. M. Fritsch, “Convective Parameterization for Mesoscale Models: The Kain-Fritsch Scheme,” pp. 165–170, 1993.

[100] J. S. Kain, “The Kain–Fritsch Convective Parameterization: An Update,” *J. Appl. Meteorol.*, vol. 43, no. 1, pp. 170–181, Jan. 2004.

[101] F. Kasten and G. Czeplak, “Solar and terrestrial radiation dependent on the amount and type of cloud,” *Sol. Energy*, vol. 24, no. 2, pp. 177–189, 1980.

[102] J. S. G. Ehnberg and M. H. J. Bollen, “Simulation of global solar radiation based on cloud observations,” *Sol. Energy*, vol. 78, no. 2, pp. 157–162, Feb. 2005.

[103] C. Rigollier, M. Lefèvre, and L. Wald, “The method Heliosat-2 for deriving shortwave solar radiation from satellite images,” *Sol. Energy*, vol. 77, no. 2, pp. 159–169, 2004.

[104] R. Perez, P. Ineichen, K. Moore, M. Kmiecik, C. Chain, R. George, and F. Vignola, “A new operational model for satellite-derived irradiances: description and validation,” *Sol. Energy*, vol. 73, no. 5, pp. 307–317, Nov. 2002.

[105] J. S. Bojanowski, A. Vrieling, and A. K. Skidmore, “Calibration of solar radiation models for Europe using Meteosat Second Generation and weather station data,” *Agric. For. Meteorol.*, vol. 176, pp. 1–9, Jul. 2013.

[106] J. Polo, L. F. Zarzalejo, M. Cony, A. A. Navarro, R. Marchante, L. Martín, and M. Romero, “Solar radiation estimations over India using Meteosat satellite images,” *Sol. Energy*, vol. 85, no. 9, pp. 2395–2406, Sep. 2011.

[107] M. Cony, L. Singal, L. Martin, and J. Polo, “Modeling of Solar Resource from VIS Images of Meteosat First Generation over India,” *EGU Gen. Assem. 2012*, 2012.

[108] M. Al-rasheedi, C. a Gueymard, A. Ismail, and S. Al-hajraf, “Solar Resource Assessment over Kuwait : Validation of Satellite-derived Data and Reanalysis Modeling,” *EuroSun*, no. September, pp. 16–19, 2014.

[109] M. a. Shamim, M. Bray, R. Remesan, and D. Han, “A hybrid modelling approach for assessing solar radiation,” *Theor. Appl. Climatol.*, 2014.

[110] J. Garatuza-Payán, W. J. Shuttleworth, and R. T. Pinker, “Satellite measurements of solar radiation in the Yaqui Valley , northern Mexico,” *Geofísica Int.*, vol. 40, no. 3, pp. 207–218, 2001.

[111] A. Pettazzi and S. Salsón, “Introducing the Solar Radiation Atlas of Galicia , the ultimate resource to assess and exploit solar radiation in Galicia (NW Spain),” in *ICREPQ’12*, 2012.

[112] P. Ineichen, “Long Term Satellite Global, Beam and Diffuse Irradiance Validation,” *Energy Procedia*, vol. 48, pp. 1586–1596, 2014.

[113] A. Nottrott and J. Kleissl, “Validation of the NSRDB–SUNY global horizontal irradiance in California,” *Sol. Energy*, vol. 84, no. 10, pp. 1816–1827, Oct. 2010.

[114] P. Lynch, “The origins of computer weather prediction and climate modeling,” *J. Comput. Phys.*, vol. 227, no. 7, pp. 3431–3444, 2008.

[115] P. Berrisford, D. Dee, K. Fielding, M. Fuentes, P. Kallberg, S. Kobayashi, and S. Uppala, “The ERA-Interim Archive,” Reading, Berkshire, 2009.

[116] NOAA, “National Centers for Environmental Prediction,” 2015. [Online]. Available: http://www.emc.ncep.noaa.gov/index.php?branch=GFS. [Accessed: 19-Aug-2015].

[117] NOAA, “NOAA National Operational Model Archive & Distribution System - Data Access,” 2015. [Online]. Available: http://nomads.ncdc.noaa.gov/data.php?name=access#hires_weather_datasets.

[Accessed: 19-Aug-2015].

[118] W. C. Skamarock, J. B. Klemp, and J. Dudhia, “PROTOTYPES FOR THE WRF (WEATHER RESEARCH AND FORECASTING) MODEL,” Boulder, Colorado.

[119] J. Dudhia, “Overview of WRF Physics NCAR.” .

[120] C. a. Gueymard and J. A. Ruiz-Arias, “Validation of direct normal irradiance predictions under arid conditions: A review of radiative models and their turbidity-dependent performance,” *Renew. Sustain. Energy Rev.*, vol. 45, pp. 379–396, 2015.

[121] F. Besharat, A. A. Dehghan, and A. R. Faghih, “Empirical models for estimating global solar radiation: A review and case study,” *Renew. Sustain. Energy Rev.*, vol. 21, pp. 798–821, May 2013.

[122] T. Khatib, A. Mohamed, and K. Sopian, “A review of solar energy modeling techniques,” *Renew. Sustain. Energy Rev.*, vol. 16, no. 5, pp. 2864–2869, Jun. 2012.

[123] M. J. Ahmad and G. N. Tiwari, “Solar radiation models—A review,” *Int. J. Energy Res.*, vol. 35, no. 4, pp. 271–290, Mar. 2011.

[124] J. a. Davies and D. C. McKay, “Evaluation of selected models for estimating solar radiation on horizontal surfaces,” *Sol. Energy*, vol. 43, no. 3, pp. 153–168, Jan. 1989.

[125] J. Kleissl, *Solar Energy Forecasting and Resource Assessment*. 2013.

[126] R. Perez, E. Lorenz, S. Pelland, M. Beauharnois, G. Van Knowe, K. Hemker, D. Heinemann, J. Remund, S. C. Müller, W. Traunmüller, G. Steinmauer, D. Pozo, J. A. Ruiz-Arias, V. Lara-Fanego, L. Ramirez-Santigosa, M. Gaston-Romero, and L. M. Pomares, “Comparison of numerical weather prediction solar irradiance forecasts in the US, Canada and Europe,” *Sol. Energy*, vol. 94, pp. 305–326, Aug. 2013.

[127] J. Remund, R. Perez, and E. Lorenz, “Comparison of solar radiation forecasts for the USA,” *Eur. PV Conf.*, vol. 2, pp. 3–5, 2008.

[128] R. Perez, M. Beauharnois, E. Lorenz, S. Pelland, and J. Schlemmer, “Evaluation of numerical weather prediction solar irradiance forecasts in the US,” in *Proc. ASES Annual Conference*, 2011.

[129] R. Almanza and S. López, “Radiación solar global en la República mexicana mediante datos de insolación,” *Ser. del Inst. Ing.*, no. 357, 1975.

[130] R. Almanza-Salgado, V. Estrada-Cajigal-Ramírez, and J. Barrientos-Avila., “Actualización de los mapas de irradiación global solar en la Republica Mexicana.,” *Ser. del Inst. Ing.*, no. 543, 1992.

[131] I. Galindo-Estrada and G. Cifuentes-Nava, “Radiación Solar Global en la República Mexicana: Valores Horarios Medios,” Ciudad de México, 1996.

[132] J. Garatuza-Payán, R. T. Pinker, W. J. Shuttleworth, and C. J. Watts, “Solar radiation and evapotranspiration in northern Mexico estimated from remotely sensed measurements of cloudiness,” *Hydrol. Sci. J.*, vol. 46, no. 3, pp. 465–478, Jun. 2001.

[133] M. Valdes, D. Riveros-Rosas, and R. Bonifaz, “Solarimetric Network for Solar Radiation Assessment in Mexico,” in *SolarPACES 2012*, 2012.

[134] PIEAES, “Red Agrometeorológica del Sur de Sonora,” *Online*, 2014. [Online]. Available: http://pieaes.dyndns.org. [Accessed: 15-Jun-2014].

[135] INIFAP, “Red de estaciones del INIFAP,” *Onlilne*, 2014. [Online]. Available: http://clima.inifap.gob.mx/redinifap/. [Accessed: 15-Jun-2014].

[136] Kipp & Zonen B.V., “SP Lilte2 pyranometer - Kipp & Zonen,” 2015. [Online]. Available: http://www.kippzonen.es/Product/217/SP-Lite2-Piranometro#.VfYAL_meDGc. [Accessed: 13-Sep-2015].

[137] T. Lhendup and S. Lhundup, “Comparison of methodologies for generating a typical meteorological year (TMY),” *Energy Sustain. Dev.*, vol. 11, no. 3, pp. 5–10, Sep. 2007.

[138] S. Janjai and P. Deeyai, “Comparison of methods for generating typical meteorological year using meteorological data from a tropical environment,” *Appl. Energy*, vol. 86, no. 4, pp. 528–537, Apr. 2009.

[139] A. L. S. Chan, T. T. Chow, S. K. F. Fong, and J. Z. Lin, “Generation of a typical meteorological year for Hong Kong,” *Energy Convers. Manag.*, vol. 47, no. 1, pp. 87–96, Jan. 2006.

[140] J. A. Davies, D. C. McKay, G. Luciani, and M. Abdel-Wahab, “Validation of Models for Estimating Solar Radiation on Horizontal Surfaces: Final Report,” 1988.

[141] A. B. Djemaa and C. Delorme, “A comparison between one year of daily global irradiation from ground-based measurements versus METEOSAT images from seven locations in Tunisia,” *Sol. Energy*, vol. 48, no. 5, pp. 325–333, 1992.

[142] I. Supit and R. R. van Kappel, “A simple method to estimate global radiation,” *Sol. Energy*, vol. 63, no. 3, pp. 147–160, 1998.

[143] C. Schillings, R. Meyer, and H. Mannstein, “Validation of a method for deriving high resolution direct normal irradiance from satellite data and application for the Arabian Peninsula,” *Sol. Energy*, vol. 76, no. 4, pp. 485–497, 2004.

[144] W. C. Skamarock, J. B. Klemp, J. Dudhia, D. O. Gill, D. M. Barker, M. G. Duda, X.-Y. Huang, W. Wang, and J. G. Powers, “A Description of the Advanced Research WRF Version 3,” Boulder, 2008.

[145] E. J. Mlawer, S. J. Taubman, and S. a Clough, “RRTM : A Rapid Radiative Transfer Model,” in *PROCEEDINGS OF THE 18th ANNUAL CONFERENCE ON*

ATMOSPHERIC TRANSMISSION MODELS, 1995, pp. 150–157.

[146] J. Dudhia, "Numerical Study of Convection Observed during the Winter Monsoon Experiment Using a Mesoscale Two-Dimensional Model," *Journal of the Atmospheric Sciences*, vol. 46, no. 20. pp. 3077–3107, 1989.

[147] R. Lobato, "Esquema de asimilación y verificación del modelo de mesoescala MM5," 2003.

[148] I. Sosa-Tinoco, J. Peralta-Jaramillo, and C. Otero-Casal, "WRF GHI Mexico daily," Santiago de Compostela, 2015.

[149] E. K. Gilliland and C. M. Rowe, "A comparison of cumulus parameterization schemes in the WRF model," in *Proceedings of the 87th AMS Annual Meeting & 21th Conference on Hydrology*, 2007, no. P2.16.

[150] J. Done, C. A. Davis, and M. Weisman, "The next generation of NWP: Explicit forecasts of convection using the weather research and forecasting (WRF) model," *Atmos. Sci. Lett.*, vol. 5, no. 6, pp. 110–117, 2004.

[151] M. L. Weisman, W. C. Skamarock, and J. B. Klemp, "The Resolution Dependence of Explicitly Modeled Convective Systems," *Mon. Weather Rev.*, vol. 125, no. 4, pp. 527–548, 1997.

[152] C. R. Homeyer, "Numerical simulations of extratropical tropopause-penetrating convection: Sensitivities to grid resolution," *J. Geophys. Res. Atmos.*, vol. 120, no. 14, pp. 7174–7188, Jul. 2015.

[153] L. Li, W. Li, and J. Jin, "Improvements in WRF simulation skills of southeastern United States summer rainfall: physical parameterization and horizontal resolution," *Clim. Dyn.*, vol. 43, no. 7–8, pp. 2077–2091, Jan. 2014.

[154] J. P. Evans, R. J. Oglesby, and W. M. Lapenta, "Time series analysis of regional climate model performance," *J. Geophys. Res.*, vol. 110, no. D4, pp. 1–23, 2005.

[155] S. Pielke R.A., "Influence of the spatial distribution of vegetation and soils on the prediction of cumulus convective rainfall," *Rev. Geophys.*, vol. 39, no. 2, pp. 151–177, 2001.

[156] A. Beck, B. Ahrens, and K. Stadlbacher, "Impact of nesting strategies in dynamical downscaling of reanalysis data," *Geophys. Res. Lett.*, vol. 31, no. 19, pp. 1–5, 2004.

[157] B. Denis, R. Laprise, and D. Caya, "Sensitivity of a regional climate model to the resolution of the lateral boundary conditions," *Clim. Dyn.*, vol. 20, pp. 107–126, 2003.

[158] I. Sosa-Tinoco, J. Peralta-Jaramillo, C. Otero-Casal, A. López-Agüera, G. Miguez-Macho, and I. Rodríguez-Cabo, "VALIDATION OF A GLOBAL HORIZONTAL IRRADIATION ASSESSMENT FROM A NUMERICAL WEATHER PREDICTION

MODEL IN THE SOUTH OF SONORA-MEXICO.,” 2015.

[159] P. L. Vidale, “Predictability and uncertainty in a regional climate model,” *J. Geophys. Res.*, vol. 108, no. D18, pp. 1–23, 2003.

[160] B. H. Lynn, L. Druyan, C. Hogrefe, J. Dudhia, C. Rosenzweig, R. Goldberg, D. Rind, R. Healy, J. Rosenthal, and P. Kinney, “Sensitivity of present and future surface temperatures to precipitation characteristics,” *Clim. Res.*, vol. 28, no. 1, pp. 53–65, 2004.

[161] W.-T. Tao, J. Simpson, D. Baker, S. Braun, M.-D. Chou, B. Ferrier, D. Johnson, A. Khain, S. Lang, B. Lynn, C.-L. Shie, C.-H. Sui, Y. Wang, and P. Wetzel, “Microphysics, Radiation and Surface in the Goddard Cumulus Ensemble (GCE) Model,” *Meteorol. Atmos. Phys.*, vol. 82, no. 1, pp. 97–137, 2003.

[162] J. Fernández, J. P. Montávez, J. Sáenz, J. F. González-Rouco, and E. Zorita, “Sensitivity of the MM5 mesoscale model to physical parameterizations for regional climate studies: Annual cycle,” *J. Geophys. Res. Atmos.*, vol. 112, no. 4, pp. 1–18, 2007.

[163] J. A. Ruiz-Arias, D. Pozo-Vázquez, N. Sánchez-Sánchez, J. P. Montávez, A. Hayas-Barru, and J. Tovar-Pescador, “Evaluation of two MM5-PBL parameterizations for solar radiation and temperature estimation in the South-Eastern area of the Iberian Peninsula,” *Nuovo Cim. della Soc. Ital. di Fis. C*, vol. 31, no. 5–6, pp. 825–842, 2008.

[164] J. Peixoto and A. Oort, *Physics of Climate*. New York, New York, USA: American Institute of Physics, 1992.

[165] D. J. Stensrud, *Parameterization Schemes: Keys to Understanding Numerical Weather Prediction Models*. 2007.

[166] T. T. Warner, *Numerical Weather and Climate Prediction*. 2011.

[167] A. Arakawa, “The cumulus parameterization problem: Past, present, and future,” *J. Clim.*, vol. 17, no. 13, pp. 2493–2525, 2004.

[168] A. Laing and J.-L. Evans, “Introduction to Tropical Meteorology, Ch. 9: Observation, Analysis, and Prediction: 9.4 Numerical Weather Prediction in the Tropics » 9.4.6 Cumulus Convection in NWP,” 2011. [Online]. Available: http://www.goes-r.gov/users/comet/tropical/textbook_2nd_edition/navmenu.php_tab_10_page_4.6.0.htm. [Accessed: 12-Sep-2015].

[169] W. Wang and N. L. Seaman, “A Comparison Study of Convective Parameterization Schemes in a Mesoscale Model,” *Mon. Weather Rev.*, vol. 125, no. 2, pp. 252–278, 1997.

[170] A. Laing and J.-L. Evans, “Introduction to Tropical Meteorology,” 2011. [Online].

Available: http://www.goes-r.gov/users/comet/tropical/textbook_2nd_edition/index.htm. [Accessed: 12-Sep-2015].

[171] P. Mathiesen, C. Collier, and J. Kleissl, "A high-resolution, cloud-assimilating numerical weather prediction model for solar irradiance forecasting," *Sol. Energy*, vol. 92, pp. 47–61, Jun. 2013.

[172] G. L. Stephens, G. W. Paltridge, and C. M. R. Platt, "Radiation Profiles in Extended Water Clouds. III: Observations," *Journal of the Atmospheric Sciences*, vol. 35, no. 11. pp. 2133–2141, 1978.

[173] Solar Power Europe, "Global Market Outlook For Solar Power / 2015 - 2019," 2015.

[174] M. A. Abella, *SISTEMAS FOTOVOLTAICOS. INTRODUCCIÓN AL DISEÑO Y DIMENSIONADO DE INSTALACIONES DE ENERGÍA SOLAR FOTOVOLTAICA*, Ediciones . Publicaciones Técnicas S.L., 2005.

[175] Iea-Pvps (International Energy Agency), "Photovoltaic and Solar Forecasting:," 2013.

[176] E. Lorenzo and G. L. Araujo, *Electricidad solar: ingeniería de los sistemas fotovoltaicos*. 1994.

[177] R. M. Swanson and I. Way, "A vision for crystalline silicon solar cells," 2006.

[178] M. A. Green, K. Emery, Y. Hishikawa, W. Warta, and E. D. Dunlop, "Solar cell efficiency tables (Version 45)," *Prog. Photovoltaics Res. Appl.*, vol. 23, no. 1, pp. 1–9, Jan. 2015.

[179] K. Yasuda, K. Saegusa, and T. H. Okabe, "Production of solar-grade silicon by halidothermic reduction of silicon tetrachloride," *Metall. Mater. Trans. B Process Metall. Mater. Process. Sci.*, vol. 42, no. 1, pp. 37–49, Oct. 2011.

[180] M. Raugei, S. Bargigli, and S. Ulgiati, "Life cycle assessment and energy pay-back time of advanced photovoltaic modules: CdTe and CIS compared to poly-Si," *Energy*, vol. 32, no. 8, pp. 1310–1318, Aug. 2007.

[181] G. Phipps, C. Mikolajczak, and T. Guckes, "Indium and gallium supply sustainability," in *22nd European Union Photovoltaic Solar Energy Conference, Milan*, 2007, no. September, pp. 1–7.

[182] G. Carr, "Sunny uplands | Alternative energy will no longer be alternative," *The economist*, 2012. [Online]. Available: http://www.economist.com/news/21566414-alternative-energy-will-no-longer-be-alternative-sunny-uplands. [Accessed: 24-Sep-2015].

[183] S. Pizzini, "Towards solar grade silicon: Challenges and benefits for low cost photovoltaics," *Sol. Energy Mater. Sol. Cells*, vol. 94, no. 9, pp. 1528–1533, 2010.

[184] T. Saga, “Advances in crystalline silicon solar cell technology for industrial mass production,” *NPG Asia Mater.*, vol. 2, no. 3, pp. 96–102, Jul. 2010.

[185] T. J. McMahon, “Accelerated testing and failure of thin-film PV modules,” *Prog. Photovoltaics Res. Appl.*, vol. 12, no. 23, pp. 235–248, 2004.

[186] I. Rodríguez-Cabo, “El Proyecto Pierre Auger como Red de Sistemas Fotovoltaicos Aislados de Alta Estadística,” Universidad de Santiago Compostela, 2015.

[187] H. Instruments, “SOLAR300N I-V CURVE TRACERS AND PV TESTERS SOLAR300N,” 2015. [Online]. Available: http://www.ht-instruments.com/en/products-ht/i-v_curve_tracers_and_pv_testers/solar300n. [Accessed: 24-Sep-2015].

[188] Meteogalicia, “MeteoGalicia.” [Online]. Available: http://www.meteogalicia.es/web/index.action. [Accessed: 24-Sep-2015].

[189] Ferroatlantica and Silicio FerroSolar, “Silicio FerroSolar,” 2014. [Online]. Available: http://www.ferroatlantica.es/index.php/es/ferrosolar-home. [Accessed: 26-Sep-2015].

[190] U. Malm, *Modelling and Degradation Characteristics of Thin-film CIGS Solar Cells*, vol. Doctor of . 2008.

[191] M. Vazquez and I. Rey-stolle, “Photovoltaic Module Reliability Model Based on Field Degradation Studies,” *Prog. Photovoltaics Res. Appl.*, vol. 16, no. 5, pp. 419–433, 2008.

USC
UNIVERSIDADE
DE SANTIAGO
DE COMPOSTELA

APPENDIX

USC
UNIVERSIDADE
DE SANTIAGO
DE COMPOSTELA

Appendix 1

USC
UNIVERSIDADE
DE SANTIAGO
DE COMPOSTELA

Day	Month	Year	Day	Month	Year	Day	Month	Year	Day	Month	Year
1	1	1996	1	4	1998	1	7	1996	1	10	2000
2	1	1996	2	4	1998	2	7	1999	2	10	1992
3	1	1982	3	4	1995	3	7	2005	3	10	1992
4	1	1996	4	4	1999	4	7	1992	4	10	1982
5	1	1994	5	4	1986	5	7	2010	5	10	2001
6	1	1992	6	4	1984	6	7	2005	6	10	1990
7	1	1996	7	4	2011	7	7	2010	7	10	2002
8	1	1998	8	4	2004	8	7	2006	8	10	1986
9	1	2002	9	4	1990	9	7	2009	9	10	1987
10	1	1986	10	4	2000	10	7	1999	10	10	2005
11	1	1997	11	4	1982	11	7	2007	11	10	2005
12	1	2004	12	4	1991	12	7	1983	12	10	2001
13	1	1986	13	4	2011	13	7	2006	13	10	1983
14	1	2006	14	4	1981	14	7	2009	14	10	2005
15	1	1988	15	4	1981	15	7	1992	15	10	1989
16	1	1991	16	4	1995	16	7	2009	16	10	2005
17	1	1989	17	4	2004	17	7	1991	17	10	1990
18	1	1993	18	4	2003	18	7	2004	18	10	2001
19	1	1997	19	4	1988	19	7	2004	19	10	2008
20	1	2010	20	4	1988	20	7	1996	20	10	1989
21	1	2010	21	4	1996	21	7	1995	21	10	1984
22	1	2010	22	4	2006	22	7	1996	22	10	1997
23	1	1991	23	4	1999	23	7	2003	23	10	2004
24	1	2003	24	4	2010	24	7	2010	24	10	2005
25	1	2003	25	4	2005	25	7	1999	25	10	1997
26	1	1989	26	4	2010	26	7	1985	26	10	2003
27	1	1985	27	4	1991	27	7	1988	27	10	2011
28	1	2004	28	4	1992	28	7	2008	28	10	2001
29	1	1997	29	4	1987	29	7	2003	29	10	1981
30	1	1996	30	4	2006	30	7	2008	30	10	1991
31	1	1996	1	5	1987	31	7	2003	31	10	2001
1	2	1998	2	5	1987	1	8	2007	1	11	1999
2	2	1996	3	5	2008	2	8	2007	2	11	1999
3	2	1997	4	5	2011	3	8	2007	3	11	1995
4	2	1998	5	5	2011	4	8	2001	4	11	1982
5	2	2010	6	5	1983	5	8	1994	5	11	2009
6	2	1998	7	5	1996	6	8	2006	6	11	1982
7	2	1990	8	5	1996	7	8	1985	7	11	1990
8	2	1996	9	5	1981	8	8	1994	8	11	1981
9	2	2004	10	5	1986	9	8	1988	9	11	2011
10	2	1997	11	5	1999	10	8	1983	10	11	1983
11	2	1985	12	5	1986	11	8	2004	11	11	1992
12	2	2003	13	5	1982	12	8	2007	12	11	1988
13	2	1985	14	5	2006	13	8	1983	13	11	1995
14	2	2010	15	5	2000	14	8	2006	14	11	2004
15	2	1995	16	5	2006	15	8	1998	15	11	1993
16	2	2010	17	5	2006	16	8	1986	16	11	1997
17	2	2010	18	5	1993	17	8	1990	17	11	2001
18	2	1992	19	5	2004	18	8	1990	18	11	1990
19	2	1995	20	5	1995	19	8	1987	19	11	2008
20	2	2006	21	5	1997	20	8	1987	20	11	2008

21	2	1988	22	5	1987	21	8	1984	21	11	1994
22	2	2010	23	5	2002	22	8	1988	22	11	2010
23	2	1988	24	5	1984	23	8	2005	23	11	1983
24	2	2007	25	5	1993	24	8	1988	24	11	1983
25	2	1987	26	5	1997	25	8	1988	25	11	1994
26	2	1983	27	5	1987	26	8	2002	26	11	1985
27	2	1983	28	5	1991	27	8	1988	27	11	2008
28	2	1992	29	5	2011	28	8	1994	28	11	2008
1	3	2005	30	5	1991	29	8	1989	29	11	1993
2	3	2010	31	5	2006	30	8	1989	30	11	1987
3	3	1996	1	6	1994	31	8	2011	1	12	1995
4	3	1996	2	6	2009	1	9	1997	2	12	2000
5	3	2008	3	6	2009	2	9	2002	3	12	1982
6	3	1988	4	6	2004	3	9	1986	4	12	1989
7	3	1990	5	6	2009	4	9	2001	5	12	1991
8	3	1983	6	6	2003	5	9	2002	6	12	2005
9	3	1987	7	6	2004	6	9	1988	7	12	2005
10	3	1987	8	6	1982	7	9	1996	8	12	2005
11	3	1991	9	6	1999	8	9	2003	9	12	1999
12	3	2010	10	6	1999	9	9	2004	10	12	2000
13	3	1981	11	6	1998	10	9	2001	11	12	2010
14	3	1983	12	6	2008	11	9	1995	12	12	1997
15	3	1987	13	6	2008	12	9	1983	13	12	1989
16	3	2004	14	6	1997	13	9	1988	14	12	2010
17	3	2007	15	6	2006	14	9	1984	15	12	2002
18	3	1986	16	6	1991	15	9	1984	16	12	2003
19	3	2002	17	6	1986	16	9	1984	17	12	1986
20	3	1996	18	6	1986	17	9	2008	18	12	1994
21	3	2004	19	6	1993	18	9	1982	19	12	2003
22	3	1985	20	6	1993	19	9	1996	20	12	2009
23	3	1988	21	6	1999	20	9	2000	21	12	2009
24	3	1981	22	6	2003	21	9	1989	22	12	2010
25	3	1981	23	6	2009	22	9	2002	23	12	1981
26	3	1981	24	6	1985	23	9	1989	24	12	2011
27	3	1981	25	6	1990	24	9	1989	25	12	2010
28	3	1981	26	6	1985	25	9	2000	26	12	1983
29	3	2000	27	6	2006	26	9	1992	27	12	1995
30	3	1998	28	6	1982	27	9	1992	28	12	1989
31	3	2001	29	6	1983	28	9	2001	29	12	1987
			30	6	2004	29	9	2009	30	12	1995
						30	9	1985	31	12	1995

Appendix 2

USC
UNIVERSIDADE
DE SANTIAGO
DE COMPOSTELA

Elsevier Editorial System(tm) for Renewable Energy
Manuscript Draft

Manuscript Number: RENE-D-15-01675

Title: VALIDATION OF A GLOBAL HORIZONTAL IRRADIATION ASSESSMENT FROM A NUMERICAL WEATHER PREDICTION MODEL IN THE SOUTH OF SONORA-MEXICO.

Article Type: Research Paper

Keywords: solar resource; global irradiation; Sonora Mexico; WRF; validation

Corresponding Author: Mr. Ian Mateo Sosa Tinoco, Ph.D. candidate

Corresponding Author's Institution: Universidade de Santiago Compostela

First Author: Ian Mateo Sosa Tinoco, Ph.D. candidate

Order of Authors: Ian Mateo Sosa Tinoco, Ph.D. candidate; Juan M Peralta-Jaramillo, PhD; Carlos Otero-Casal, Master; Ángeles López-Agüera, PhD; Gonzalo Miguez-Macho, PhD; Iago Rodriguez-Cabo, PhD

Abstract: The present work illustrates the methodology followed to generate a high spatial (9 km) and high temporal resolution (10 min) global solar irradiance assessment, based on a numerical weather prediction model, for the south of Sonora region in Mexico and its validation with observational data. At the same time a comparison with an ERA-Interim output data was performed in order to determine if downscaling was necessary. The methodology used starts with obtaining the mean radiation year in order to strongly reduce computational cost. Each day of the mean radiation year defines the initial and boundary conditions of the simulations. The simulation outputs were used to create the monthly and the annual irradiation maps. The grid cells are compared with the correspondent observation and the precision of the model is evaluated. The correlation of the model with the observation data is higher than 0.88. It's observed that on fall and winter the rRMSE of the model is lower than 6.4% but during the months of spring-summer the rRMSE increases. The results show that the downscaling using the configuration selected was correct.

Suggested Reviewers: Chris Gueymard PhD
President, Solar Consulting Services
Chris@SolarConsultingServices.com
Expert in the area, one of the best researchers in solar assessment.

Frank Vignola PhD
Laboratory Head, Materials Science Institute/Solar Energy Center, University of Oregon
fev@uoregon.edu
He is one of the most referenced authors in solar energy assessment.

Cover Letter

Ian Mateo Sosa Tinoco
Universidad de Santiago Compostela
Rúa Xosé María Fernández Núñez S/N
Santiago de Compostela, A Coruña, Spain, 15706
(+34) 881814000
Ianmateo.sosa@usc.es, erroba@gmail.com

Renewable Energy Journal Editor
July 23, 2015

Dear Editor:

I am pleased to submit an original research article entitled "Validation of a global horizontal irradiation assessment from a numerical weather prediction model in the south of Sonora-Mexico" by, Juan Peralta, Carlos Otero, Angeles López, Gonzalo Miguez-Macho, Iago Rodríguez and Ian Sosa Tinoco for publication in the Renewable Energy Journal. This manuscript was proposed after doing an evaluation of the south of Sonora region for the renewable energy resource (solar and wind), in order to create a sustainable community.

After studying the characteristics of the region we evaluated to use the same tool (WRF) as we did for the wind resource assessment due to the optimal results as compared to the weather stations. In this manuscript, we show that the WRF model could be used to develop solar maps in a semi-desert region with extremely good results.

We believe that this paper is appropriate for publication by the Renewable Energy Journal, because the manuscript has a profound base in the knowledge and development of GHI maps and could be used as a methodology tool for the creation of this kind of maps globally.

This manuscript has not been published and is not under consideration for publication elsewhere. We have no conflicts of interest to disclose. If you feel that the manuscript is appropriate for your journal, we suggest the following reviewers:

Frank Vignola, Laboratory Head, University of Oregon. fev@uoregon.edu

Christian Gueymard, President of Solar Consulting Services.

chris@solarconsultingservices.com

Thank you for your consideration!

Sincerely,

PhD Candidate at Physics Department

Universidad de Santiago Compostela

***Highlights**

Highlights

A solar map developed with a numerical weather prediction model was validated in the south of Sonora region.

A mean radiation year was developed to select the dates to construct the solar map.

Monthly errors were analyzed for both outputs (WRF and ERA-Interim).

GHI overestimation for monsoon/hurricane season was found in both cases.

VALIDATION OF A GLOBAL HORIZONTAL IRRADIATION ASSESSMENT FROM A NUMERICAL WEATHER PREDICTION MODEL IN THE SOUTH OF SONORA-MEXICO.

Sosa-Tinoco, Ian[1, 2], Peralta-Jaramillo, Juan[1, 3], Otero-Casal, Carlos [4], López- Agüera, A. [1], Miguez-Macho, G. [4], Rodríguez-Cabo, I. [1]

[1] SEAG, Facultad de Física Universidad de Santiago Compostela, Rúa Xosé María Fernández Núñez S/N, Santiago de Compostela 15782 E-mail: ianmateo.sosa@usc.es Phone number: +34 881 814000

[2]Instituto Tecnológico de Sonora, Ave. Antonio Caso S/N, Col. Villa ITSON, Cd. Obregón, México.

[3]Escuela Superior Politécnica del Litoral, CDTS-FIMCP, Vía Perimetral Km. 30.5 Guayaquil, Ecuador.

[4]Grupo de Física No Lineal, Universidad de Santiago Compostela

Abstract

The present work illustrates the methodology followed to generate a high spatial (9 km) and high temporal resolution (10 min) global solar irradiance assessment, based on a numerical weather prediction model, for the south of Sonora region in Mexico and its validation with observational data. At the same time a comparison with an ERA-Interim output data was performed in order to determine if downscaling was necessary. The methodology used starts with obtaining the mean radiation year in order to strongly reduce computational cost. Each day of the mean radiation year defines the initial and boundary conditions of the simulations. The simulation outputs were used to create the monthly and the annual irradiation maps. The grid cells are compared with the correspondent observation and the precision of the model is evaluated. The correlation of the model with the observation data is higher than 0.88. It's observed that on fall and winter the rRMSE of the model is lower than 6.4% but during the months of spring-summer the rRMSE increases. The results show that the downscaling using the configuration selected was correct.

Keywords: solar resource, global irradiation, Sonora Mexico, WRF, validation

Nomenclature

CESGA: Supercomputer Center of Galicia (Centro de Supercomputación de Galicia).

ECMWF: European Centre for Medium-Range Weather Forecasts.

ERA-Interim: It's the latest global atmospheric reanalysis produced by the ECMWF.

GHI: Global Horizontal Irradiation per day.

INIFAP: National Institute of Forestry, Agricultural and Livestock Research (Instituto Nacional de Investigaciones Forestales, Agricolas y Pecuarias).

MBE: Mean bias error.

rRMSE: Relative root mean square error.

$SSDR_d$: Surface solar downwards radiation by day output from ERA-Interim.

WRF: Weather Research and Forecasting Model.

1. Introduction

During the last 7 years the Sustainable Energy Applications Group (SEAG) in collaboration with the Non Lineal Physics Group at the Santiago Compostela University and different associate researchers, several actions have been done in order to create a procedure protocol based in the parametric study of different micro-regions around the world, so as to the establishment of a self-sustainable communities network [1].

The procedure protocol comprehends the identification and evaluation of local energy resources. The solar energy is one of the key resources to be evaluated in each region. A solar map lets us determine the solar energy potential for the region in study. The current state of development of solar energy technologies is increasing the need for more detailed radiation information.

There are many methodologies to develop a solar map and/or forecast (inference from in situ data, satellite observations and models)[2–9]. In this work the GHI was estimated by a numerical weather forecast model and from the solar data given of the ERA-Interim reanalysis[10]. The use of similar approaches has been assessed by some authors[8,11–13]; yet, variations in the output depend upon the location due to variable weather conditions and partially cloudy days.

There are a significant number of maps and databases describing the solar resource distribution in Mexico[14–18], developed by different universities and research centers. However in none of these studies confidence intervals of data are provided[19]. The main objective of this research is to create a solar radiation map of a region that has enough data to give a relative good confidence interval.

In this instance we evaluate the solar radiation of the southern region of the state of Sonora Mexico, where there is evidence[20], that the region has the highest energy return factor of the country for grid connected PV systems and could be an important case of study due to its particular characteristics.

2. Materials and Methods

2.1 Regional description

Sonora is one of the 31 states that Mexico is divided; the state is situated at the northwest of the country. The state is bordered to the north by Arizona, to the east by Chihuahua, to the northwest by Baja California, to the by south Sinaloa and to the west by the sea of Cortez. This research takes in consideration 13 municipalities of the south shown in the Figure 1. The south of Sonora region has three main climates, very dry, dry and semi-dry, according to the climate classification of the National Institute of Statistics and Geography from Mexico[21].

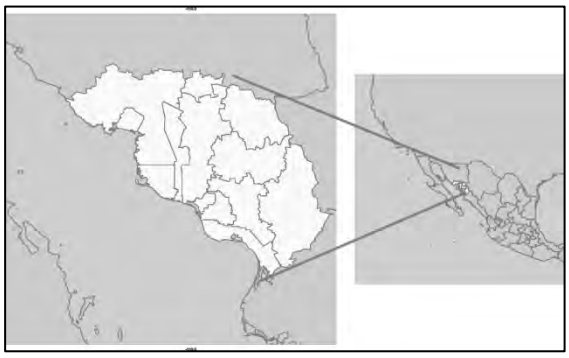

Fig.1 State of Sonora location (in yellow municipalities of the south region).

2.2 Observational data

The region has two weather station networks, the agro-weather station network of the Board for Agricultural Research and Experimentation of Sonora (PIEAES for its acronym in Spanish) and the National Institute for Forest and Agricultural Research (INIFAP for its acronym in Spanish). Both are databases focused on supporting the activities of farmers of the region and offer the source weather data to feed the prediction models for researchers[22,23]. The PIEAES network has 32 weather stations that give a range of different data (temperature, humidity, wind speed and direction, irradiation between others) every 10 minutes. According to PIEAES the weather stations have maintenance checks at least once a month [22]. The INIFAP network is a larger system that has more than 1000 weather stations around the country. The irradiation sensor used on both weather networks is a SP-Lite pyranometer from Kipp & Zonen with a spectral range between 400nm to 1100nm.

Five to eight years of GHI data were used to validate the output of the model, depending on the data at disposal. 28 agro-weather stations from PIEAES and 4 from INIFAP were used to validate the WRF outputs. A list of the weather stations used and its coordinates is shown on Table 1 as well as a map of the localization of each station on Fig. 2.

To avoid erroneous validation data, three quality filters were applied to the observations. The first consist on having at least 80% of the data for each station. The second quality filter was to have a minimal of three consecutive years. The last quality filter was applied to the monthly values, if within a month there were 10 daily missed records or 5 consecutive daily missed records, the monthly value was discarded.

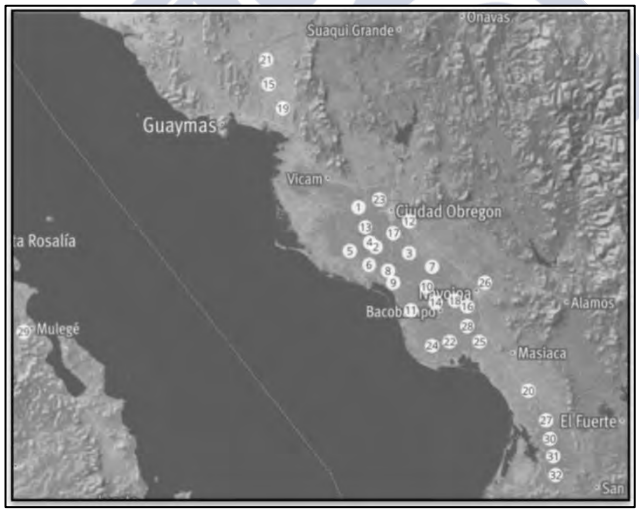

Fig. 2 Considered agro-weather stations.

Table 1 Weather Station List

Number	Name	Lon	Lat	Altitude (m)	Network
1	Block111	-110.12	27.50	37	PIEAES
2	Block1201	-110.02	27.30	20	PIEAES
3	Block1418	-109.83	27.27	45	PIEAES
4	Block1103	-110.05	27.32	35	PIEAES

5	Block1317	-110.17	27.28	9	PIEAES
6	Block1703	-110.05	27.21	35	PIEAES
7	Block1730	-109.70	27.20	46	PIEAES
8	Block1806	-109.95	27.18	15	PIEAES
9	Block2210	-109.92	27.12	4	PIEAES
10	Block2328	-109.73	27.10	16	PIEAES
11	Block2920	-109.82	26.98	9	PIEAES
12	Block414	-109.83	27.43	46	PIEAES
13	Block609	-110.08	27.40	25	PIEAES
14	Buaysiacobe	-109.68	27.02	17	PIEAES
15	Campo_52	-110.63	28.12	68	PIEAES
16	Cemay	-109.50	27.01	39	PIEAES
17	Ciano	-109.92	27.37	37	PIEAES
18	El_Chapote	-109.57	27.03	33	PIEAES
19	El_Norteno	-110.55	28.04	47	PIEAES
20	Estacion_Luis	-109.15	26.57	42	PIEAES
21	Gpe_Guaymas	-110.64	28.24	108	PIEAES
22	Huatabampo	-109.60	26.82	17	PIEAES
23	Jazmin	-110.01	27.54	37	PIEAES
24	Jupare	-109.70	26.80	11	PIEAES
25	Mumuncuera	-109.43	26.82	24	PIEAES
26	Tesia	-109.40	27.12	42	PIEAES
27	Torocobampo	-109.05	26.42	43	PIEAES
28	Tres_Carlos	-109.50	26.90	34	PIEAES
29	Valle_Mulege	-112.02	26.87	10	INIFAP
30	Chavez_Talamate	-109.02	26.32	27	INIFAP
31	Agri_Gotsis	-109.03	26.23	3	INIFAP
32	Carrizo	-108.99	26.14	25	INIFAP

2.3 Mean radiation year (MRY) methodology

One of the most common problems with using the WRF-model at high resolutions is the computational cost. In this paper we consider to create a mean radiation year in order to reduce the amount of data to simulate (from 31 years to 1 year). Several types of methods to generate a typical weather data like the Sandia National Laboratories method, the Danish method, the Festa-Ratto method and the Design reference year method between others are generally used to represent the long-term typical weather condition over a year[24–26]. However in this research we used an average radiation year in order to easily generate (with only GHI) and to analyze a complete region (not a station or a cell).

The methodology to produce the MRY is based on the arithmetic mean of surface solar radiation ($MeanSSDR_d$) from 31 days (each day corresponding to the same calendar day in a different year), calculated from the ERA-Interim GHI data ($SSDR_d$) of the total surface (area). Subsequent the $MeanSSDR_d$ is compared with each of the 31 days used before; the day that has the less difference with mean value, is selected. This is repeated for the 365 days of the year; the concatenated result gives the MRY for this region. The algorithm followed to generate the MRY is

represented on Fig.3.

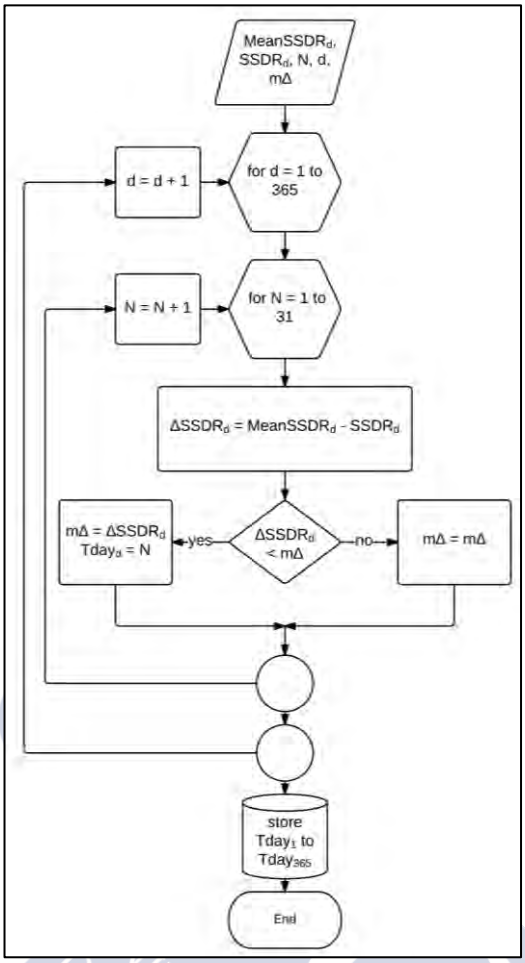

Fig.3 Flowchart for MRY methodology.

Where,

N is de number of years (1-31)

d is the selected day (1,2,...365)

mΔ = Minimal difference to the mean of each date

The mean radiation year is developed by the concatenation of the dates that have the lowest mΔ for the 365 days of the year in the 31 year data.

2.4 Validation metrics

The validation of modelled irradiation values against measurements are usually based on the root mean square error and the mean bias error[27–30], in this article both were used.

The mean bias error (MBE) is defined as the quantity used to measure how close the observed values are to the modelled ones. The MBE is given by

$$MBE = \frac{1}{n}\sum_{i=1}^{n}\frac{G_{MOD}-G_{OBS}}{G_{OBS}} \quad (1)$$

G_{MOD} represents the GHI given by the model

G_{OBS} represents the GHI given by the weather stations

n: number data

The relative root mean square error (rRMSE) is defined to be the square root of the totality of the squares of the difference between modeled and reference irradiances using some time interval over some time period divided by the number of observations. The rRMSE uses the following formula:

$$rRMSE = \sqrt{\frac{1}{n}\sum_{i=1}^{n}\left(\frac{G_{MOD}-G_{OBS}}{G_{OBS}}\right)^2} \quad (2)$$

2.5 WRF Model and Setup.

In this study, the numerical weather prediction model, advanced WRF model ver. 3.4 was used [31]. The model was run on the supercomputer *Finisterrae* in CESGA (Galicia, Spain). We do not take into account the first 12 hours because we consider that the WRF model needs time to stabilize. The next 24 hours correspond to the selected day that interests us. The modelling setup including the selected domains and the initial and boundary conditions as well as the physics schemes are described below.

2.5.1 Domain setup.

The WRF model was run in a series of one-way nested grids. The horizontal grid spacing was refined by a factor of 3 through 1 nested domain until 9 km resolution. The WRF model was built over a coarsest domain (Fig. 4a) at 27 km, and a finest nested domain (Fig. 4b) of 9 km spatial resolution.

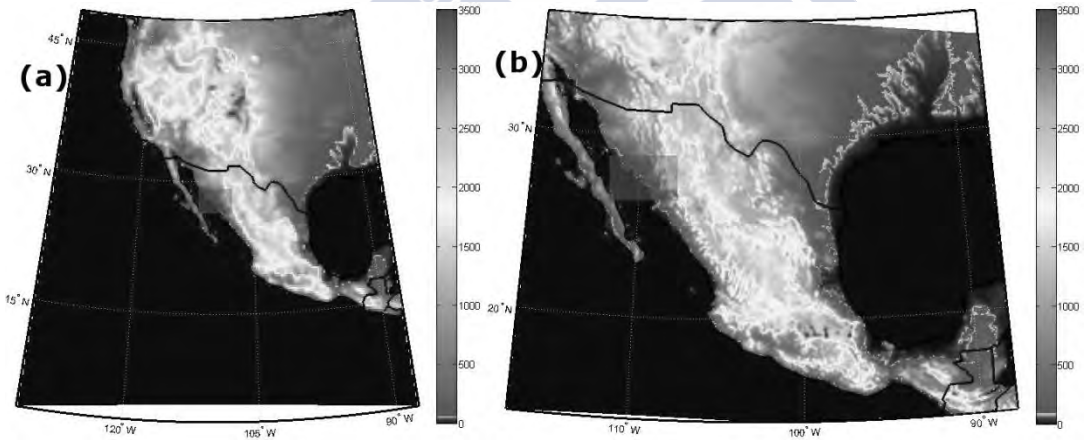

Fig.4 Domain 1(a) and domain 2 (b), topography models (Red rectangle: south of Sonora region).

2.5.2 Initial and boundary conditions.

The WRF model was used to improve the state of the estimated physical atmosphere magnitudes especially the planet boundary layers, by down-scaling the ERA-Interim reanalysis data provided by ECMWF. The ERA-Interim reanalysis project covers the period from 1979 to present and has a horizontal resolution of approximately 79km[10]. The initial conditions for the model were taken from the ERA-Interim date's selection of the MRY previously obtained.

2.5.3 Topographic Inputs.

The topographic data with a resolution of 2 minutes (about 3.7 km) were used for all the WRF simulations.

2.5.4 Physics Schemes.

On Table 2 a summary of the configuration used on the model for each day is presented for reference. The physics schemes (in specific Cumulus, Shortwave and Longwave parametrizations) were selected, due to the characteristics of the region (climate and higher possibility of clear days) and the horizontal resolution of the grid. The rapid radiative transfer model [32] (a widely used scheme using look-up tables for efficiency) and the Dudhia [33] (a simple downward integration allowing for efficient cloud and clear-sky absorption and scattering) schemes were used for the longwave and shortwave radiation options, respectively. Finally, the cumulus physics was modelled with the New Kain-Fritsch[34] scheme that can be used on high resolution (in addition to coarser resolutions).

Table 2. Synopsis of the WRF model configuration used.

Simulation period	365 days
Model version	V3.4
Domains	2
Horizontal resolution	27 and 9 km
Input data	ERA-Interim
Time step	100 s
Outputs frequency	120 (d01) and 10 minutes (d02)
Nesting	1-way nesting
Physics schemes	
Microphysics	WSM6 class
Cumulus	New Kain Fritsch
Shortwave	Dudhia
Longwave	Rapid Radiative Transfer Model
LSM	Noah
PBL	YSU

3. Results and Discussion

3.1 Model Results

The annual GHI for the south of Sonora region, calculated and taken from the daily WRF output[35] is presented in the map of Fig. 5b. It's evidently noticed that the values and resolution on both cases (Fig. 5a and Fig. 5b) are different. The mean annual GHI found in the WRF output is 6.31kWh/m^2, slightly higher than the annual GHI of the ERA-Interim output (6.01kWh/m^2). The WRF simulation has a much higher resolution that better resolves the variability of the GHI on the eastern part of the region due to the mountains (Sierra Madre Occidental).

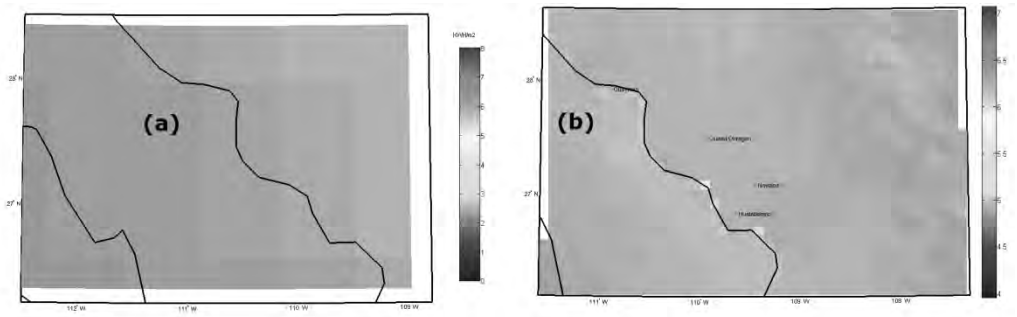

Fig.5 (a) ERA-Interim and (b) WRF output annual average GHI for the south of Sonora.

Additionally a mean monthly GHI representation for the WRF output was done, as shown in Fig.6. According to the figure the GHI is mainly driven by the sun position during the year. The lower irradiation season during the months of autumn-winter is easily observed, as well as the higher irradiation season during spring – summer.

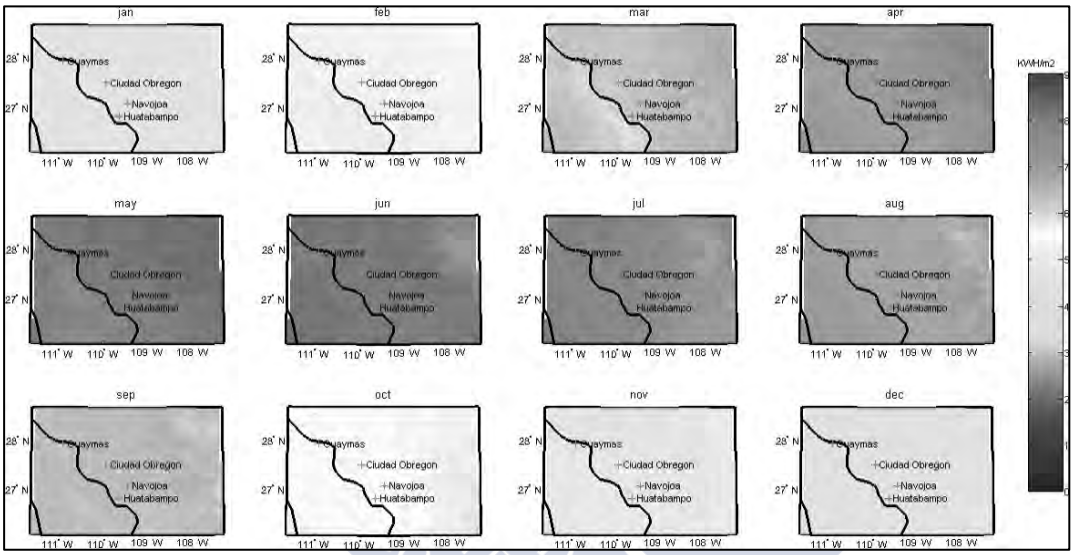

Fig.6 WRF output monthly average GHI for the south of Sonora.

3.2 Validation

In order to validate the GHI for the WRF model, a comparison between both the observations and the outputs were required, for the nearest geographical cell grid (latitude, longitude). In Fig.7 the mean monthly GHI for the region are represented, and were obtained from the observations, the WRF model output and the ERA-Interim data for each geographic location, where the stations are situated.

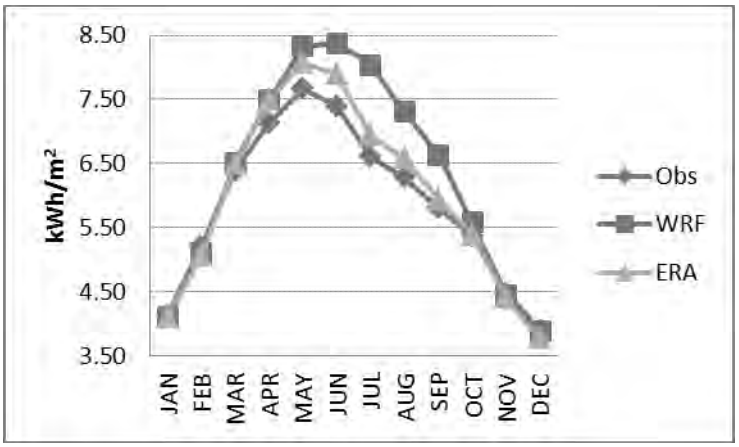

Fig.7 Monthly average GHI chart of observations, WRF model and ERA-Interim output.

During 6 months (April to September) the WRF model over-estimate the GHI 0.88 kWh/m^2 on average; instead on the remaining months the model overestimate by 0.03 kWh/m^2 on average. Moreover, the model behavior during 6 months of the year is slightly closer to the observations than the ERA-Interim outputs.

In order to understand the behavior of the model and ERA-Interim output it's shown in Fig. 8 the monthly MBE and rRMSE. The minimal (4.38%) rRMSE obtained for the monthly validation period is on January and the maximum (22.32%) occurs on July, annual rRMSE is 9.61%. The MBE demonstrates that there is a small underestimation on winter and a high overestimation on summer as shown in Fig. 8. Moreover the ERA-Interim output precision is also shown in Fig. 8 during spring-summer months has a better trend than the WRF model. However, on fall-winter months the ERA-Interim output has a good precision (less than 10% rRMSE), but lower precision than WRF model.

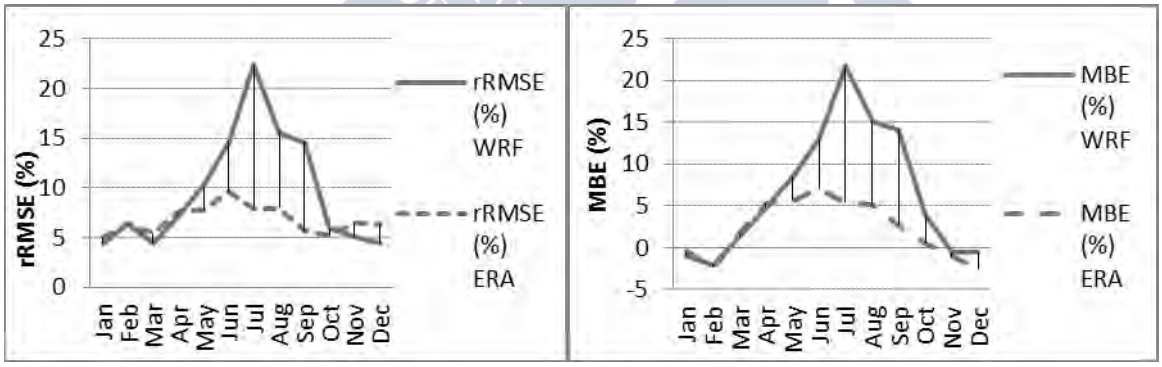

Fig. 8 (a) Monthly rRMSE WRF Model vs ERA-Interim, (b) MBE WRF Model vs ERA-Interim.

In Fig. 9, the monthly mean correlation between the models and the observations is presented. Is In the low radiation months between 3 and 5kWh/m^2 the WRF simulation represents the weather stations well, but on higher radiation months it tends to overestimate the irradiation. Overall the lineal correlation for the WRF case is above 0.88, on the other case, the ERA-Interim correlation is above 0.93.

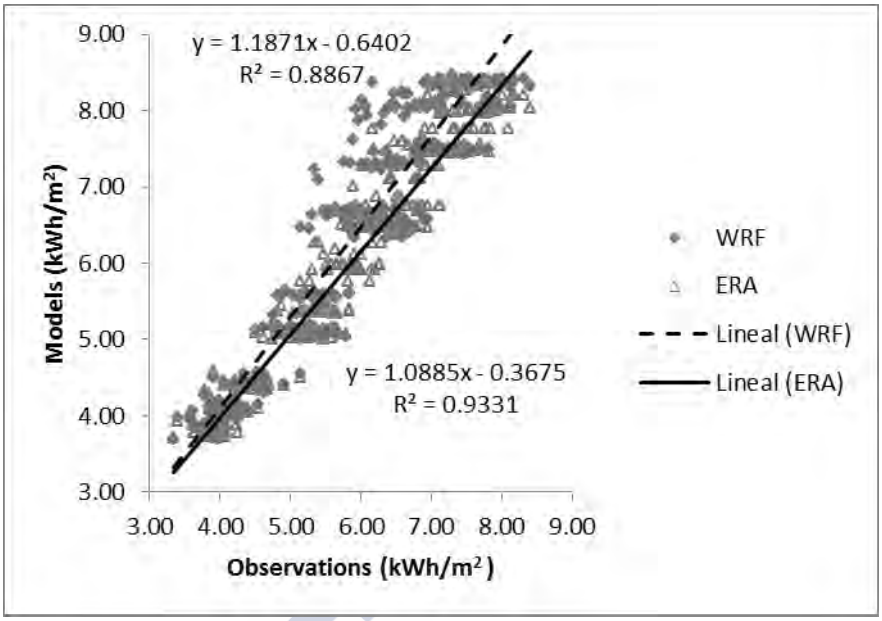

Fig. 9 Correlation plot of monthly GHI of Observation vs Models (WRF and ERA-Interim).

The observed effect could be related to the monsoon and hurricane season that covers the same time period (May – November). During the monsoon season (May – July) thunderstorms are formed due to a "desert heat low" that is formed in the Sonora desert, which pulls moisture into the region that contributes to their formation. Additionally during the hurricane season (May – November) many tropical storms strike the region, which could greatly impact the monthly GHI.

The observations clearly show that there is less radiation than estimated from the WRF model and it could be related that the model doesn't solve correctly this kind of storms with the cumulus parametrization chosen (New Kain-Fritsch) as shown by Gilliland and Rowe [36]. A possible evidence of this is shown in Fig. 10, the rRMSE doesn't increase proportionally with radiation; the green triangles are the rRMSE on the Monsoon/Hurricane season and it's evident that the greatest errors occur on that time.

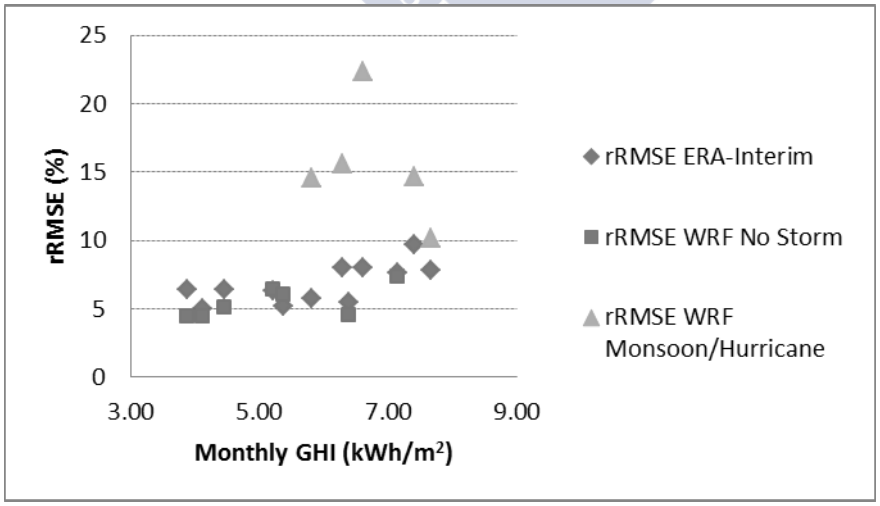

Fig. 10 Monthly rRMSE for ERA-Interim, WRF monsoon season and WRF No storm season.

Additionally, the monsoon system it's a phenomenon that occurs on a larger scale than the one

selected on the initial boundary conditions. Possibly, boundary conditions aren't including clouds, which have to be entirely formed within the boundary domain. This lack of information on monsoon clouds could result in an underestimation of cloud cover over the region of study. However the ERA-Interim, being a global analysis system, takes in consideration this kind of systems that develop outside of the area selected in the WRF model.

4. Conclusions

In this research a downscaling of the south of Sonora Mexico region was performed in order to obtain a highly temporal resolution solar potential assessment as well as a validation between the output and observations.

The graphical results processed from the WRF output indicate that the horizontal resolution for this example could be sufficient, in other words a higher resolution is not necessary for this region due to the homogeneity of the outputs and not drastic topographical changes. In general terms, the model represents the GHI of the region with a higher temporal resolution (10 min vs 12 hours).

Overall the results for the WRF present less accuracy, related to the weather stations, in annual terms. However in non-storm season WRF has better results than ERA-Interim outputs. Since the annual rRMSE values are low (average 9.91%) we conclude that the model has relatively good accuracy and could be an alternative to study the solar resource on regions where climate conditions are similar to the studied region; especially if high temporal resolution (10 min) is necessary.

The overestimation of the WRF model on the spring-summer period is related to the storm solving problem of the initial configuration. In order to improve GHI accuracy during this season, it is necessary to carry out a sensitivity study on the different cumulus and radiation parametrizations that the WRF model uses. Moreover, it is necessary to do a further research in different regions and climate conditions so as to compare the effects observed during the present study with the results in such conditions.

5. Acknowledgments

The first author was supported by a doctoral grant from the Science and Technology Council of Mexico (Consejo Nacional de Ciencia y Tecnología, CONACYT). We would like to thank the PIEAES and INIFAP for providing the surface solar radiation data. The authors also want to acknowledge the support provided by CESGA. In this study solar radiation records of the ECMWF reanalysis datasets ERA-Interim [10] were used.

6. References

[1] López-Agüera A, Domingues-Azevedo J, Rodríguez-Cabo I, Rey-Rey D, Gándara-Villadoniga V, Vieites-Montes E, et al. Ecoaldeas or Self-Sustainable Communities and renewable energy solutions (SSC). First approach Ecuador and Mexico. In: Pérez-Donsión M, editor. Renew. ENERGY POWER Qual. J., Santiago de Compostela: 2012, p. 487–94.

[2] Hammer A, Heinemann D, Hoyer C, Kuhlemann R, Lorenz E, Müller R, et al. Solar energy assessment using remote sensing technologies. Remote Sens Environ 2003;86:423–32.

doi:10.1016/S0034-4257(03)00083-X.

[3] Lorenz E, Hurka J, Heinemann D, Beyer HG. Irradiance Forecasting for the Power Prediction of Grid-Connected Photovoltaic Systems. IEEE J Sel Top Appl Earth Obs Remote Sens 2009;2:2–10. doi:10.1109/JSTARS.2009.2020300.

[4] Lorenz E, Remund J, Müller SC, Traunmüller W, Steinmaurer G, Pozo D, et al. BENCHMARKING OF DIFFERENT APPROACHES TO FORECAST SOLAR IRRADIANCE. 24th Eur. Photovolt. Sol. energy Conf., Hamburg, Germany: 2009, p. 25–34.

[5] Prabha T, Hoogenboom G. Evaluation of solar irradiance at the surface—inferences from in situ and satellite observations and a mesoscale model. Theor Appl Climatol 2010;102:455–69. doi:10.1007/s00704-010-0329-0.

[6] Perez R, Kivalov S, Schlemmer J, Hemker K, Renné D, Hoff TE. Validation of short and medium term operational solar radiation forecasts in the US. Sol Energy 2010;84:2161–72. doi:10.1016/j.solener.2010.08.014.

[7] Angela K, Taddeo S, James M. Predicting Global Solar Radiation Using an Artificial Neural Network Single-Parameter Model. Adv Artif Neural Syst 2011;2011:1–7. doi:10.1155/2011/751908.

[8] Mathiesen P, Kleissl J. Evaluation of numerical weather prediction for intra-day solar forecasting in the continental United States. Sol Energy 2011;85:967–77. doi:10.1016/j.solener.2011.02.013.

[9] Peralta-Jaramillo J. Modelamiento Computacional del Recurso Solar y Eólico para aplicación de Sistemas de Energía Renovable. Universidad de Santiago de Compostela, 2015.

[10] Dee DP, Uppala SM, Simmons a. J, Berrisford P, Poli P, Kobayashi S, et al. The ERA-Interim reanalysis: configuration and performance of the data assimilation system. Q J R Meteorol Soc 2011;137:553–97. doi:10.1002/qj.828.

[11] Ortega A, Escobar R, Colle S, de Abreu SL. The state of solar energy resource assessment in Chile. Renew Energy 2010;35:2514–24. doi:10.1016/j.renene.2010.03.022.

[12] Lara-Fanego V, Ruiz-Arias JA, Pozo-Vázquez D, Santos-Alamillos FJ, Tovar-Pescador J. Evaluation of the WRF model solar irradiance forecasts in Andalusia (southern Spain). Sol Energy 2012;86:2200–17. doi:10.1016/j.solener.2011.02.014.

[13] Zamora RJ, Dutton EG, Trainer M, McKeen S a., Wilczak JM, Hou Y-T. The Accuracy of Solar Irradiance Calculations Used in Mesoscale Numerical Weather Prediction. Mon Weather Rev 2005;133:783–92. doi:10.1175/MWR2886.1.

[14] Almanza R, López S. Radiación solar global en la República mexicana mediante datos de insolación. Ser Del Inst Ing 1975.

[15] Almanza-Salgado R, Estrada-Cajigal-Ramírez V, Barrientos-Avila. J. Actualización de los mapas de irradiación global solar en la Republica Mexicana. Ser Del Inst Ing 1992.

[16] Galindo-Estrada I, Cifuentes-Nava G. Radiación Solar Global en la República Mexicana: Valores Horarios Medios. Ciudad de México: 1996.

[17] Garatuza-Payán J, Pinker RT, Shuttleworth WJ, Watts CJ. Solar radiation and evapotranspiration in northern Mexico estimated from remotely sensed measurements of cloudiness. Hydrol Sci J 2001;46:465–78. doi:10.1080/02626660109492839.

[18] Valdes M, Riveros-Rosas D, Bonifaz R. Solarimetric Network for Solar Radiation Assessment in Mexico. SolarPACES 2012, Marrakech: 2012.

[19] Valdes-barrón M, Riveros-rosas D, Arancibia-bulnes C a, Bonifaz R. The solar Resource Assessment in Mexico : State of the Art. Energy Procedia 2014;57:1299–308. doi:10.1016/j.egypro.2014.10.120.

[20] GTZ. Nichos de mercado para sistemas FV en conexión a red en méxico. Eschborn: 2009.

[21] INEGI. Sitio del INEGI en Internet. Mapa digital de México. Online 2014. http://gaia.inegi.org.mx/mdm6/ (accessed January 1, 2014).

[22] PIEAES. Red Agrometeorológica del Sur de Sonora. Online 2014. http://pieaes.dyndns.org (accessed June 15, 2014).

[23] INIFAP. Red de estaciones del INIFAP. Onlilne 2014. http://clima.inifap.gob.mx/redinifap/ (accessed June 15, 2014).

[24] Lhendup T, Lhundup S. Comparison of methodologies for generating a typical meteorological year (TMY). Energy Sustain Dev 2007;11:5–10. doi:10.1016/S0973-0826(08)60571-2.

[25] Janjai S, Deeyai P. Comparison of methods for generating typical meteorological year using meteorological data from a tropical environment. Appl Energy 2009;86:528–37. doi:10.1016/j.apenergy.2008.08.008.

[26] Chan ALS, Chow TT, Fong SKF, Lin JZ. Generation of a typical meteorological year for Hong Kong. Energy Convers Manag 2006;47:87–96. doi:10.1016/j.enconman.2005.02.010.

[27] Davies JA, McKay DC, Luciani G, Abdel-Wahab M. Validation of Models for Estimating Solar Radiation on Horizontal Surfaces: Final Report. 1988.

[28] Djemaa AB, Delorme C. A comparison between one year of daily global irradiation from ground-based measurements versus METEOSAT images from seven locations in Tunisia. Sol Energy 1992;48:325–33. doi:10.1016/0038-092X(92)90061-E.

[29] Supit I, van Kappel RR. A simple method to estimate global radiation. Sol Energy 1998;63:147–60. doi:10.1016/S0038-092X(98)00068-1.

[30] Schillings C, Meyer R, Mannstein H. Validation of a method for deriving high resolution direct normal irradiance from satellite data and application for the Arabian Peninsula. Sol Energy 2004;76:485–97. doi:10.1016/j.solener.2003.07.037.

[31] Skamarock WC, Klemp JB, Dudhia J, Gill DO, Barker DM, Duda MG, et al. A Description of the Advanced Research WRF Version 3. Boulder: 2008. doi:10.5065/D68S4MVH.

[32] Mlawer EJ, Taubman SJ, Clough S a. RRTM : A Rapid Radiative Transfer Model. In: ANDERSON GP, PICAED RH, CHETWYND JH, editors. Proc. 18th Annu. Conf. Atmos. Transm. Model., Bedford, MA: Phillips Laboratory; 1995, p. 150–7.

[33] Dudhia J. Numerical Study of Convection Observed during the Winter Monsoon

Experiment Using a Mesoscale Two-Dimensional Model. J Atmos Sci 1989;46:3077–107. doi:10.1175/1520-0469(1989)046<3077:NSOCOD>2.0.CO;2.

[34] Kain JS. The Kain–Fritsch Convective Parameterization: An Update. J Appl Meteorol 2004;43:170–81. doi:10.1175/1520-0450(2004)043<0170:TKCPAU>2.0.CO;2.

[35] Sosa-Tinoco I, Peralta-Jaramillo J, Otero-Casal C. WRF GHI Mexico daily. Santiago de Compostela: 2015. doi:10.5281/zenodo.16994.

[36] Gilliland EK, Rowe CM. A comparison of cumulus parameterization schemes in the WRF model. Proc. 87th AMS Annu. Meet. 21th Conf. Hydrol., San Antonio, Texas: 2007. doi:10.3402/tellusa.v25i5.9701.

Appendix 3

USC
UNIVERSIDADE
DE SANTIAGO
DE COMPOSTELA

Day	Month	Year	Day	Month	Year	Day	Month	Year
1	3	2005	1	7	1996	1	12	1995
2	3	2010	2	7	1999	2	12	2000
3	3	1996	3	7	2005	3	12	1982
4	3	1996	4	7	1992	4	12	1989
5	3	2008	5	7	2010	5	12	1991
6	3	1988	6	7	2005	6	12	2005
7	3	1990	7	7	2010	7	12	2005
8	3	1983	8	7	2006	8	12	2005
9	3	1987	9	7	2009	9	12	1999
10	3	1987	10	7	1999	10	12	2000
11	3	1991	11	7	2007	11	12	2010
12	3	2010	12	7	1983	12	12	1997
13	3	1981	13	7	2006	13	12	1989
14	3	1983	14	7	2009	14	12	2010
15	3	1987	15	7	1992	15	12	2002
16	3	2004	16	7	2009	16	12	2003
17	3	2007	17	7	1991	17	12	1986
18	3	1986	18	7	2004	18	12	1994
19	3	2002	19	7	2004	19	12	2003
20	3	1996	20	7	1996	20	12	2009
21	3	2004	21	7	1995	21	12	2009
22	3	1985	22	7	1996	22	12	2010
23	3	1988	23	7	2003	23	12	1981
24	3	1981	24	7	2010	24	12	2011
25	3	1981	25	7	1999	25	12	2010
26	3	1981	26	7	1985	26	12	1983
27	3	1981	27	7	1988	27	12	1995
28	3	1981	28	7	2008	28	12	1989
29	3	2000	29	7	2003	29	12	1987
30	3	1998	30	7	2008	30	12	1995
31	3	2001	31	7	2003	31	12	1995

USC
UNIVERSIDADE
DE SANTIAGO
DE COMPOSTELA

Appendix 4

USC
UNIVERSIDADE
DE SANTIAGO
DE COMPOSTELA

STP280 - 24/Vd

SUNTECH

Solar powering a green future™

280 Watt
MÓDULO SOLAR POLICRISTALINO

Presentación

Alta eficiencia de conversión
(hasta el 14,4 %), gracias a una superior tecnología de célula y a una mejor tecnología de fabricación

Tolerancia positiva
Tolerancia positiva garantizada desde el 0~5 % que asegura la fiabilidad de la potencia de salida

Suntech's TruPower™
El proceso Suntech's TruPower™ neutraliza el efecto LID (degradación inducida por luz) inicial

Excelente rendimiento con luz débil
Excelente rendimiento en entornos con poca luz (mañanas, tardes y días nublados)

Elevada resistencia al viento y a las cargas de nieve
El modulo entero ha sido certificado para soportar elevadas cargas de viento (2.400 Pascal) y cargas de nieve (5.400 Pascal) *

Proceso de clasificación por Intensidad de Suntech
Todos los módulos de Suntech están clasificados y empaquetados por amperaje, maximizando la salida de sistema al reducir las pérdidas por desajustes hasta un 2%

Certifications and standards:
IEC 61215, IEC 61730, conformity to CE

Confíe en Suntech para un rendimiento fiable a largo plazo

- Fabricante líder mundial de módulos fotovoltaicos de silicio cristalino
- Capacidad de fabricación inigualable y tecnología de clase mundial
- Riguroso control de calidad que cumple los estándares internacionales más elevados: ISO 9001: 2008 y ISO 14001: 2004

Garantía líder en la industria

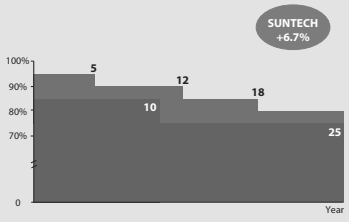

- Garantiza un 6,7% más potencia que el estándar del mercado para 25 años
- Garantía transferible de 25 años de potencia de salida: 5 años/95%, 12 años/90%, 18 años/85%, 25 años/80% **
- Basado en la potencia nominal
- 5 años de garantía para el material y su mano de obra de fabricación

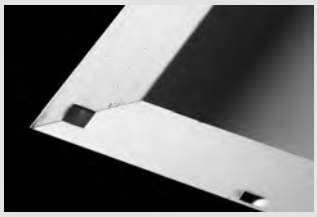

El diseño exclusivo de los orificios de drenaje y la construcción rígida impiden que el marco se deforme o se rompa debido a las heladas y otras fuerzas.

La caja de conexiones clase IP67 mejora la estabilidad del rendimiento del módulo. Los conectores de alto rendimiento proporcionan una interconexión de baja resistencia para asegurar la plena utilización de la potencia de salida del módulo.

* Consulte el manual de instalación de módulos estándar de Suntech para más detalles.
** Consulte la garantía de producto de Suntech para más detalles.

STP280 - 24/Vd

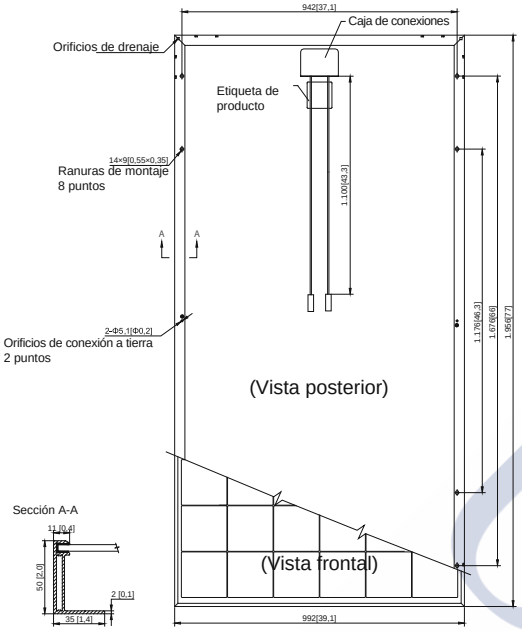

Nota: mm [pulgadas]

Curva de Intensidad-Tensión y Potencia-Tensión (280-24)

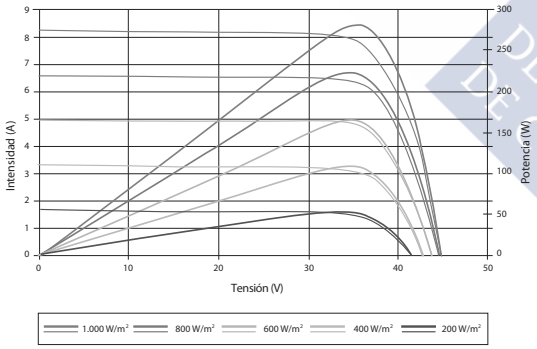

Excelente rendimiento bajo condiciones de luz débil: Con una intensidad de radiación de 200 W/m² (AM 1,5, 25 °C), se alcanza el 95,5 % o más de la eficiencia bajo condiciones de prueba STC (1000 W/m²)

Características de temperatura

Temperatura Nominal de Operación de Célula (**NOCT**)	45±2°C
Coeficiente de temperatura de Pmax	-0,44 %/°C
Coeficiente de temperatura de Voc	-0,33 %/°C
Coeficiente de temperatura de Isc	0,055 %/°C

Características eléctricas

STC	**STP280-24/Vd**
Tensión óptima de operación (Vmp)	35,2 V
Corriente óptima de operación (Imp)	7,95 A
Tensión en circuito abierto (Voc)	44,8 V
Corriente de cortocircuito (Isc)	8,33 A
Máxima potencia STC (Pmax)	280 W
Eficiencia del módulo	14,4%
Temperatura de operación	-40 °C hasta +85 °C
Tensión máxima de sistema	1.000 V DC (IEC) / 600 V DC (UL)
Corriente máxima por fusible en serie	20 A
Tolerancia de potencia	0/+5 %

STC: Irradiancia 1000 W/m², temperatura del módulo 25 °C, AM=1,5
Tolerancia de medición de potencia: ± 3%

NOCT	**STP280-24/Vd**
Potencia máxima (W)	204 W
Tensión de potencia máxima (V)	32,0 V
Corriente de potencia máxima (A)	6,39 A
Tensión en circuito abierto (Voc)	40.8 V
Corriente de cortocircuito (Isc)	6,74 A

NOCT: Irradiancia 800 W/m², temperatura ambiental 20 °C, velocidad del viento 1 m/s
Tolerancia de medición de potencia: ± 3%

Características mecánicas

Célula solar	Policristalina 156 × 156 mm (6 pulgadas)
Número de células	72 (6 × 12)
Dimensiones	1.956 × 992 × 50 mm (77,0 × 39,1 × 2,0 pulgadas)
Peso	27,0 kg (59,5 lbs.)
Vidrio frontal	Vidrio templado de 4,0 mm (0,16 pulgadas)
Marco	Aleación de aluminio anodizado
Caja de conexiones	Clase IP67
Cables de salida	TUV (2Pfg1169:2007), UL 4703, UL 44
	4,0 mm² (0,006 pulgadas²), longitudes simétricas (-) 1100 mm (43,3 pulgadas) y (+) 1100 mm (43,3 pulgadas)
Conectores	Conectores de cierre enrollados RADOX® SOLAR integrados

Configuración de embalaje

Contenedor	**Contenedor estándar de 20' (GP)**	**Contenedor estándar de 40' (GP)**	**Contenedor High Cube de 40'(HC)**
Unidades por palet	21	21	21
Palets por contenedor	6	12	24
Unidades por contenedor	126	252	504

Campo de información para el distribuidor

Las especificaciones están sujetas a cambios sin previo aviso

Appendix 5

USC
UNIVERSIDADE
DE SANTIAGO
DE COMPOSTELA

Silicio FerroSolar
Grupo ■ FerroAtlántica

MODULO FV SILICIO FERROSOLAR

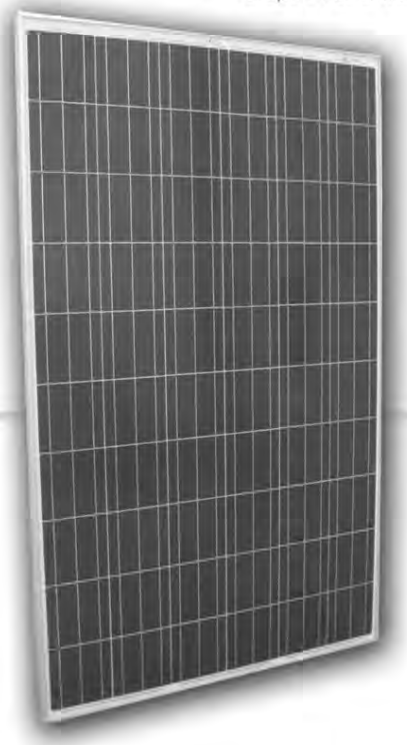

Todo ello con la **GARANTÍA DE FERROATLANTICA.**
NOS ADAPTAMOS A SUS NECESIDADES.

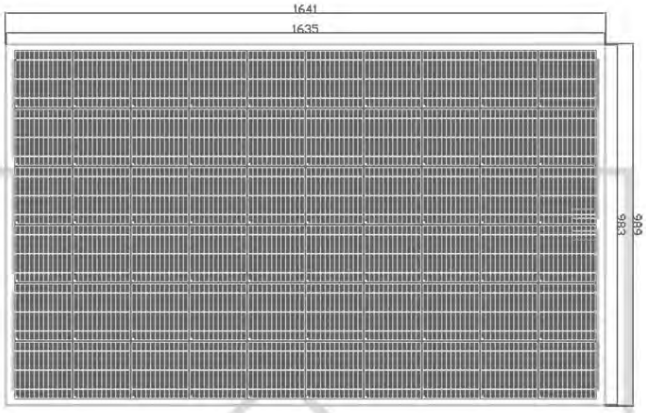

Modelo	Dimensiones (mm)	Pmpp(W)	Vmpp(V)	Impp(A)	Voc(V)	Isc(A)
SFS-200	1641x989x46	200	28,85	6,93	36,15	7,55
SFS-205	1641x989x46	205	29,04	7,06	36,30	7,67
SFS-210	1641x989x46	210	29,22	7,19	36,48	7,80
SFS-215	1641x989x46	215	29,38	7,32	36,63	7,94
SFS-220	1641x989x46	220	29,55	7,45	36,84	8,05
SFS-225	1641x989x46	225	29,85	7,54	37,08	8,11
SFS-230	1641x989x46	230	30,12	7,64	37,32	8,18
SFS-235	1641x989x46	235	30,47	7,71	37,62	8,23
SFS-240	1641x989x46	240	30,84	7,78	37,98	8,28

Otros valores:

- **Peso (kg):** 23,5
- **Nº Células:** 60
- **Tolerancia en la potencia del módulo**: 0% / +3%.
- **Caja de conexiones**: Tyco, IP 65.
- **Diodos de protección:** 3 diodos Schottky SL1515A

Condiciones de operación:

- **Temp. de operación:** -40 ºC a + 85 ºC.
- **Tensión máxima del sistema**: 1.000 V.
- **Carga max de viento**: 2.400 Pa (130 km/h).
- **Carga máx de nieve**: 5.400 Pa (550 kg/m2).
- **Resistencia al impacto**: Impacto de granizo de 25 mm de diámetro a 23 m/s.

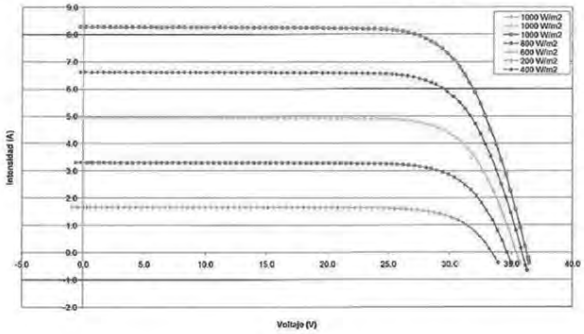

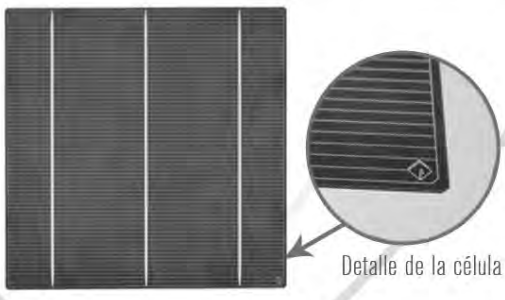

Detalle de la célula

Los módulos fotovoltaicos poseen la certificación TUV de Intercert. Están formados por 60 células solares de silicio multicristalino conectadas en serie. Silicio Ferrosolar ofrece una gama amplia de módulos solares fotovoltaicos para todo tipo de instalaciones, dependiendo de las necesidades de nuestro cliente. Al ser fabricantes de módulos, diseñamos diferentes tamaños especiales cuando la instalación lo requiera, tanto en medidas de anchos y largo como de voltaje. Éstos han sido diseñados según los estándares de calidad más exigentes. Se caracterizan por su gran eficiencia, por su robusta construcción mecánica e impermeabilidad para condiciones climatológicas normales.

TÜV InterCert

Células solares realizadas con substratos de silicio purificado por la vía metalúrgica.

USC
UNIVERSIDADE
DE SANTIAGO
DE COMPOSTELA

Appendix 6

USC
UNIVERSIDADE
DE SANTIAGO
DE COMPOSTELA

1. INTRODUCCIÓN Y RECOMENDACIÓN GENERAL

ISOFOTON,S.A. empresa española pionera y líder en el sector fotovoltaico es fabricante de células y módulos desde su fundación en 1981. Debido a una larga experiencia, utilización de materiales de primera calidad y exhaustivos controles de calidad, los módulos fotovoltaicos fabricados por ISOFOTON,S.A. presentan una vida útil por encima de los 20 años con un funcionamiento óptimo desde el primer al último día.

Lea atentamente todas las instrucciones del presente documento antes de instalar, conectar o manipular el módulo fotovoltaico. Las recomendaciones dadas para un módulo fotovoltaico se pueden hacer extensivas para más de uno.

ISOFOTON,S.A. no asume responsabilidad alguna en caso de pérdida, rotura, deterioro o coste adicional debido a la mala manipulación del producto por personal ajeno a esta empresa.

2. DATOS TÉCNICOS

Los módulos fotovoltaicos fabricados por ISOFOTON,S.A. utilizan células pseudocuadradas de silicio monocristalino de alta eficiencia para transformar la energía de la radiación solar en energía eléctrica de corriente continua.

El circuito de células se lamina utilizando E.V.A. (acetato de etilen-vinilo) como encapsulante en un conjunto formado por un vidrio templado en su cara frontal y un polímero plástico (TEDLAR) en la cara posterior que proporciona resistencia a los agentes ambientales y aislamiento eléctrico.

El laminado se encaja en una estructura de aluminio anodizado. Las cajas de terminales con proteccion IP-65, están hechas a partir de plásticos resistentes a temperaturas elevadas y contienen los terminales, las bornas de conexión y los diodos de protección (diodos de by-pass).

El marco dispone de varios agujeros para la fijación del módulo a la estructura soporte y su puesta a tierra en caso de ser necesario.

En la Figura 1 se muestra esquemáticamente la sección de un módulo fotovoltaico.

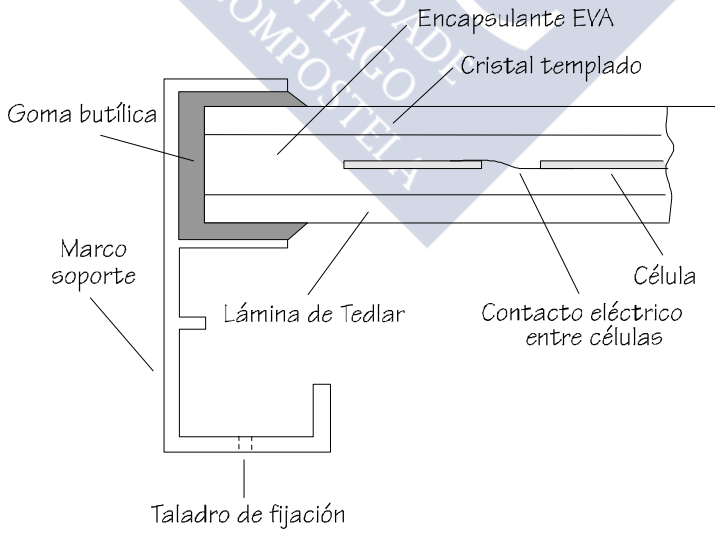

Figura 1.- Sección de un módulo fotovoltaico

En las siguientes tablas se muestran las características técnicas físicas y eléctricas, respectivamente, más relevantes de cada modelo de módulos fotovoltaicos.

FÍSICAS	***MÓDULO I-47***	***MÓDULO I-50/I-53/I-55***	***MÓDULO I-94***	***MÓDULO I-100/I-106/I-110***	***MÓDULO I-159/I-165***
Altura	1219 mm	1302 mm	1206 mm	1310 mm	1310 mm
Ancho	328 mm	338 mm	652 mm	652 mm	969 mm
Espesor	34 mm	34 mm	34 mm	34 mm	40 mm
Peso	5,5 kg	5,7 kg	10 kg	11 kg	17 kg
Células en serie · paralelo	33	36	33·2	36·2	36·3
TONC ($800W/m^2$; 1,5MA; 20ºC)	47ºC	47ºC	47ºC	47ºC	47ºC

Tabla 1.- Características físicas de los módulos fotovoltaicos ISOFOTON.

ELÉCTRICAS	***MÓDULO I-47***	***MÓDULO I-50/I-53 I-55***	***MÓDULO I-94***	***MÓDULO I-100/I-106 I-110***	***MÓDULO I-159/I-165***
Potencia pico (P_{max})	47W	50/53/55W	94W	100/106/110W	159/165W
Corriente de cortocircuito (I_{sc})	3,27A	3,27 / 3,27 3,38 A	6,54A	6,54 / 6,54 6,76 A	9,81/10,14A
Tensión de circuito abierto (V_{oc})	19,8V	21,6V	19,8V	21,6V	21,6V
Corriente de máxima potencia (I_{max})	2,94A	2,87 / 3,05 3,16 A	5,88A	5,74 / 6,10 6,32 A	9,14/9,48A
Tensión de máxima potencia (V_{max})	16V	17,4V	16V	17,4V	17,4V

Tabla 2.- Características eléctricas de los módulos fotovoltaicos ISOFOTON (12V).

ELÉCTRICAS	MÓDULO I-94/24	MÓDULO I-100/24	MÓDULO I-106/24	MÓDULO I-110/24
Potencia pico (P_{max})	94W	100W	106W	110W
Corriente de cortocircuito (I_{sc})	3,27A	3,27A	3,27A	3,38A
Tensión de circuito abierto (V_{oc})	39,6V	43,2V	43,2V	43,2V
Corriente de máxima potencia (I_{max})	2,94A	2,87A	3,05A	3,16 A
Tensión de máxima potencia (V_{max})	32V	34,8V	34,8V	34,8V

Tabla 3.- Características eléctricas de los módulos fotovoltaicos ISOFOTON (24V).

Estos valores son los que se obtienen en las condiciones estándares de medida que se corresponden con una irradiancia de 1000 W/m^2, espectro de 1,5 M.A. y una temperatura de la célula de 25ºC.

Ahora bien, las condiciones de trabajo reales de los módulos una vez instalados pueden ser muy diferentes a las del laboratorio, por lo que conviene conocer las variaciones que pueden producirse, a fin de efectuar las pertinentes correcciones en los cálculos.

Por otra parte, mientras la corriente generada por un módulo fotovoltaico es proporcional a la intensidad de la radiación solar, la tensión varía con la temperatura de las células. En las figuras siguientes se representa ambos efectos.

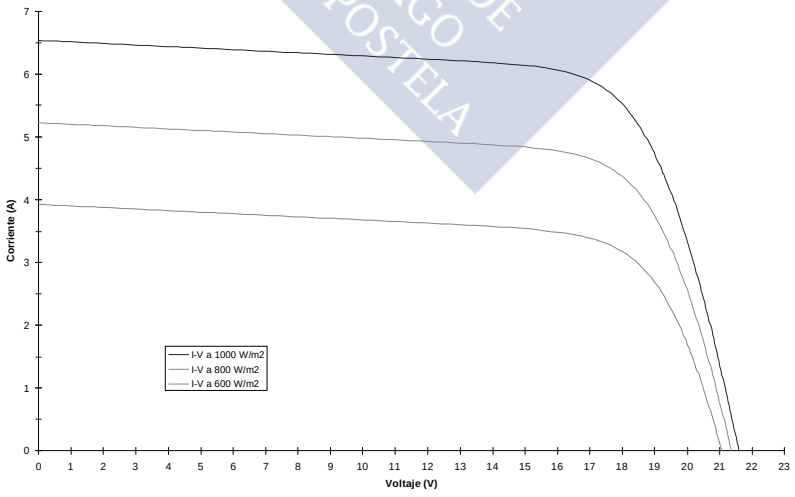

Figura 2.- Variación de curva I-V en función de la irradiancia solar incidente a temperatura de célula constante.

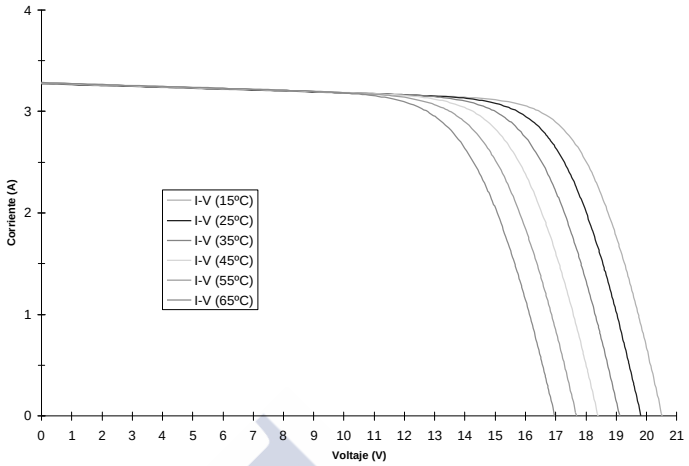

Figura 3.- Variación de curva I-V en función de la temperatura de las células a radiación incidente constante.

La variación con la temperatura de las magnitudes eléctricas de los módulos, es la siguiente:

- El voltaje disminuye a razón de 2,22 mV/ºC por cada célula en serie que contenga el módulo y cada grado que supere los 25º C.
- La corriente aumenta a razón de 17?A/cm^2.ºC de área de células en paralelo y cada grado que supere los 25º C.

Hay que tener en cuenta que la temperatura de la célula a que nos hemos estado refiriendo no coincide con la temperatura ambiente debido a que la célula, se calienta al incidir la luz del sol.

El incremento de temperatura de la célula respecto a la temperatura del aire depende de las características de la misma y de las de construcción del propio módulo.

En función de la radiación incidente, la temperatura y la carga que esté alimentando, un módulo fotovoltaico podrá trabajar a distintos valores de corriente y tensión.

En la Figura 4 se representa esquemáticamente una curva característica I-V de un módulo fotovoltaico junto con la curva de la potencia generada y dos puntos de trabajo diferentes, A y B.

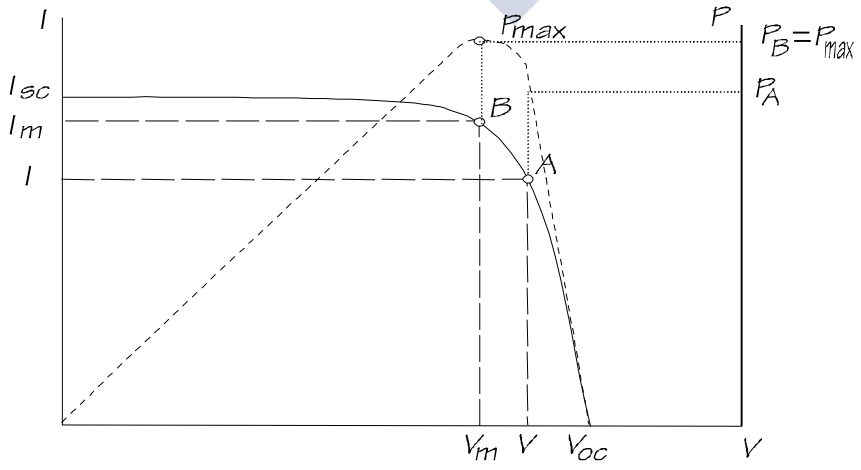

Figura 4.- Curva característica I-V y curva de potencia generada.

Se puede observar que cuanto más cerca hagamos trabajar al módulo fotovoltaico de la tensión de máxima potencia, mayor será la potencia que obtendremos de él.

En resumen, en función de la radiación solar, la temperatura de las células (que dependerá a su vez de la temperatura ambiente, humedad, velocidad del viento, etc.) y de los equipos a los que esté conectado, el módulo fotovoltaico generará una determinada corriente a una determinada tensión de trabajo, cuyo producto marcará la potencia generada por el módulo.

En el Capítulo 12 se encuentran las curvas características I-V para cada modelo en función de la irradiancia incidente y la temperatura de célula.

3. DIODOS DE PROTECCIÓN

El sombreado de alguna célula puede provocar un voltaje inverso en ella. Esta célula consumiría por tanto potencia generada por las demás en serie con ella produciéndose un calentamiento indeseado de la célula sombreada.

Este efecto, llamado de punto caliente, será tanto mayor cuanto mayor sea la radiación incidente sobre el resto de células y menor la que reciba esta célula debido a la sombra. En un caso extremo la célula podría llegar a romperse por sobrecalentamiento.

El uso de diodos de protección o by-pass reduce el riesgo de calentamiento de las células sombreadas, limitando la corriente que pueda circular por ellas y evitando de este modo la rotura de las mismas.

Todos los módulos con un número de células igual o superior a 33 en serie fabricados por ISOFOTON,S.A., se suministran con diodos de protección que se encuentran situados en las cajas de conexión tal y como se puede apreciar en los esquemas de las mismas incluidos en el capítulo siguiente.

En los módulos con menor número de células en serie no se hacen necesarios los diodos de by-pass, pues el efecto de punto caliente no llega al nivel de riesgo de rotura de las células.

4. CAJAS DE CONEXIÓN

Las cajas de conexión de los módulos están situadas en la parte posterior de los mismos. Como se ha señalado anteriormente, estas son cajas estancas preparadas para intemperie con un IP-65, siempre y cuando se respete la estanqueidad en los pasacables o prensaestopas al hacer pasar los cables a través de ellos.

En cada módulo existe bien una sola caja de conexiones para ambos terminales o bien una caja para el terminal positivo y otra para el negativo. Deberá respetarse la polaridad en las conexiones para el buen funcionamiento de los módulos.

Las cajas de conexión son similares en los módulos con igual tensión nominal. En las Figuras 5 y 6 se muestran los esquemas de las cajas de conexión para módulos de tensión nominal 12V y 24V respectivamente.

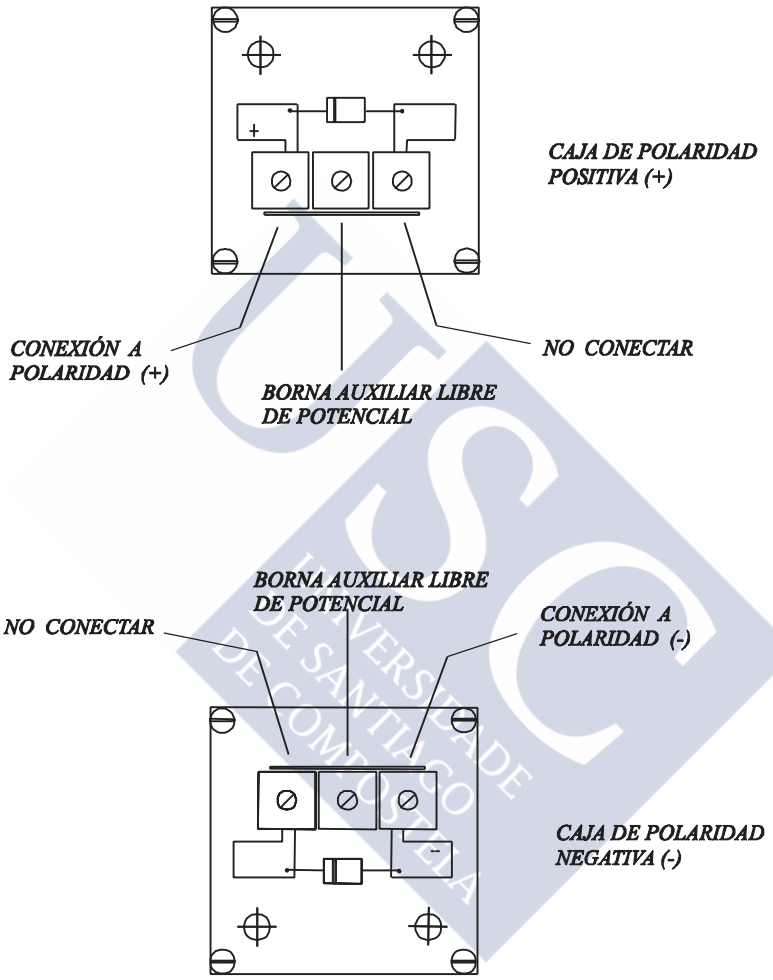

Figura 5.- Cajas de conexión para módulos de 12 V

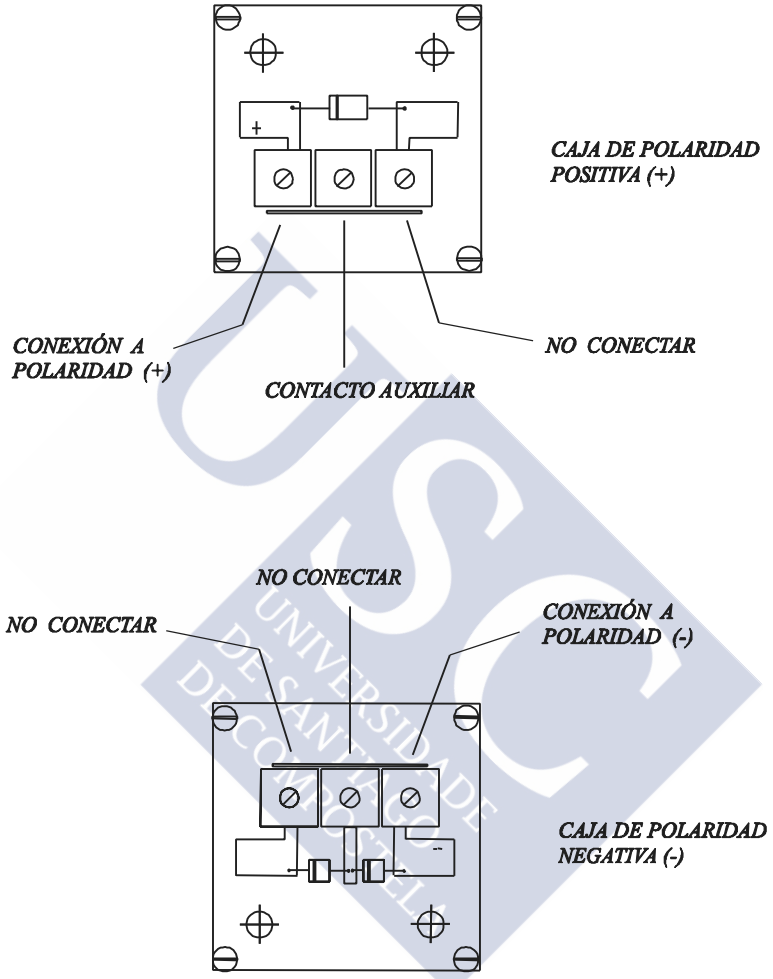

Figura 6.- Cajas de conexión para módulos de 24 V

MÓDULO I-47

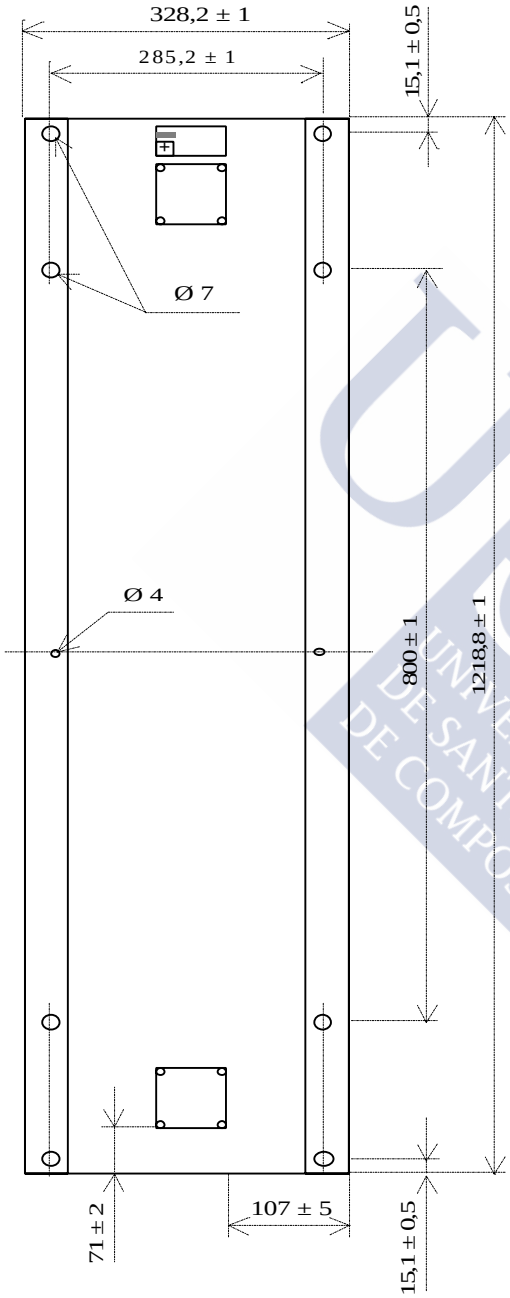

Vista posterior

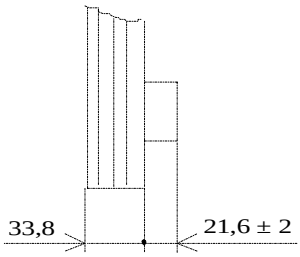

Detalle de perfil

MÓDULO I-50, I-53, I-55

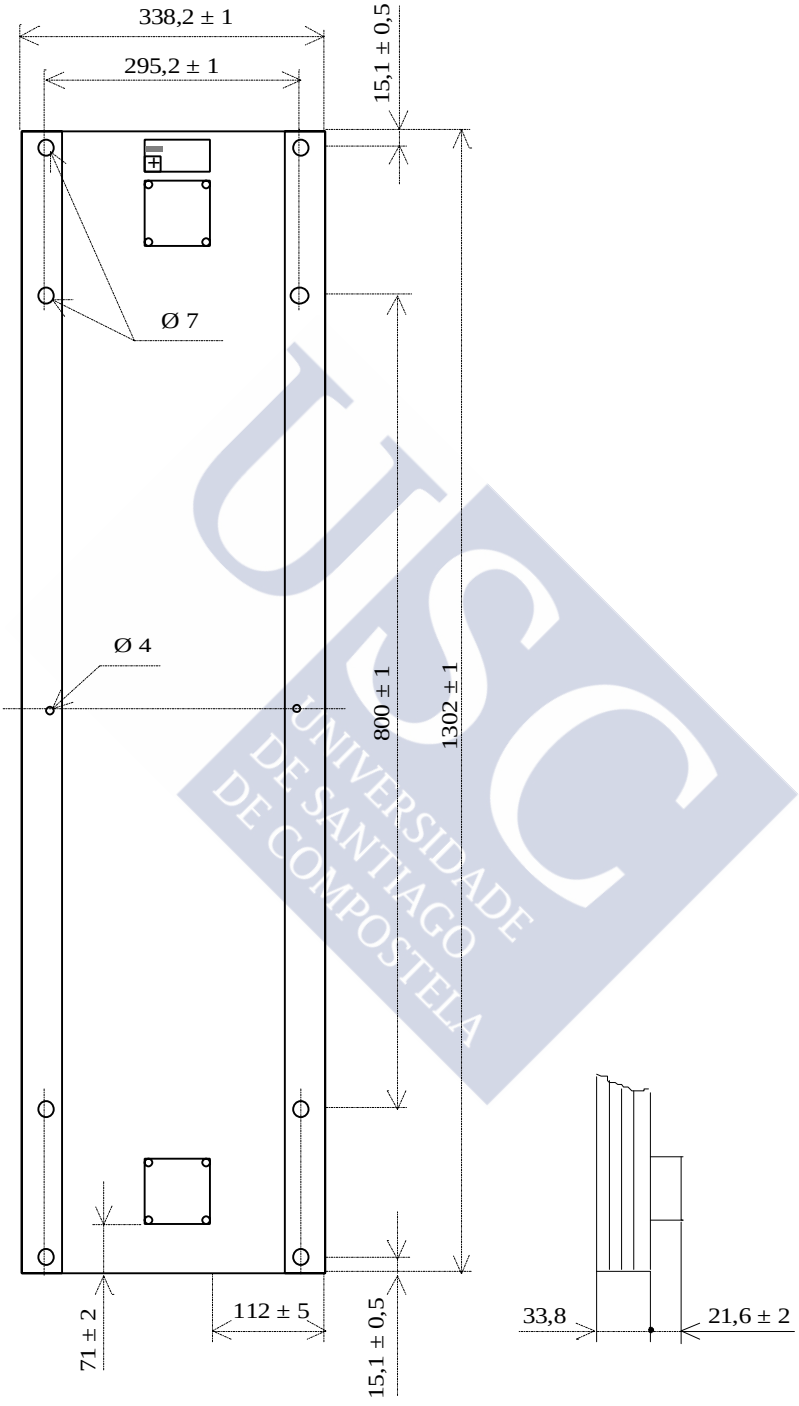

VISTA POSTERIOR

DETALLE VISTA PERFIL

USC
UNIVERSIDADE
DE SANTIAGO
DE COMPOSTELA

Appendix 7

USC
UNIVERSIDADE
DE SANTIAGO
DE COMPOSTELA

Tailor-made modules

Thanks to their esthetic design and their flexibility in size, form and output CIS modules are extremely suitable for the tailor-made integration in products of everyday life. Due to the special manufacturing procedure the technical properties can be adjusted to the desired system solution already in the process of production.

DIENEC-KARPRINZEN 05/07/1/SIP

Technical data	
Module qualities	
Basic material	CIS on float glass
Connecting possibilities	Contact strips or connecting cables

Dimensions and weight	
min. dimension (mm)	120 x 120
standard dimension (mm)	600 x 1,200
max. dimension (mm)	2,400 x 2,600 (Special fabrications on request)
standard thickness of module (mm)	6.5
min. thickness of module (mm)	5.5 (Special fabrications on request)
Weight (g)	length (mm) x width (mm) x depth (mm) x 0,0025

Data of the individual cell		
Open-circuit voltage U_{oc}	V	0.65
Voltage at max. performance U_{max}	V	0.50
Short-circuit current I_{sc}	mA/cm²	26
Current at max. performance I_{max}	mA/cm²	23

What does the path from the idea to the product that is really driven by solar energy look like?

As manufacturer of innovative photovoltaic modules we search the contact with creative product designers. So if you could imagine having your product driven by photovoltaics or if you are interested in an alternative to the traditional silicone technology we should get in touch! **Just call us or get in contact with us over our website!**

WÜRTH SOLAR

Würth Solar GmbH & Co. KG
Alfred-Leikam-Straße 25
D-74523 Schwäbisch Hall
Tel. +49 (0) 791 946 00 -0
Fax +49 (0) 791 946 00 -119
wuerth.solar@we-online.de
www.wuerth-solar.com

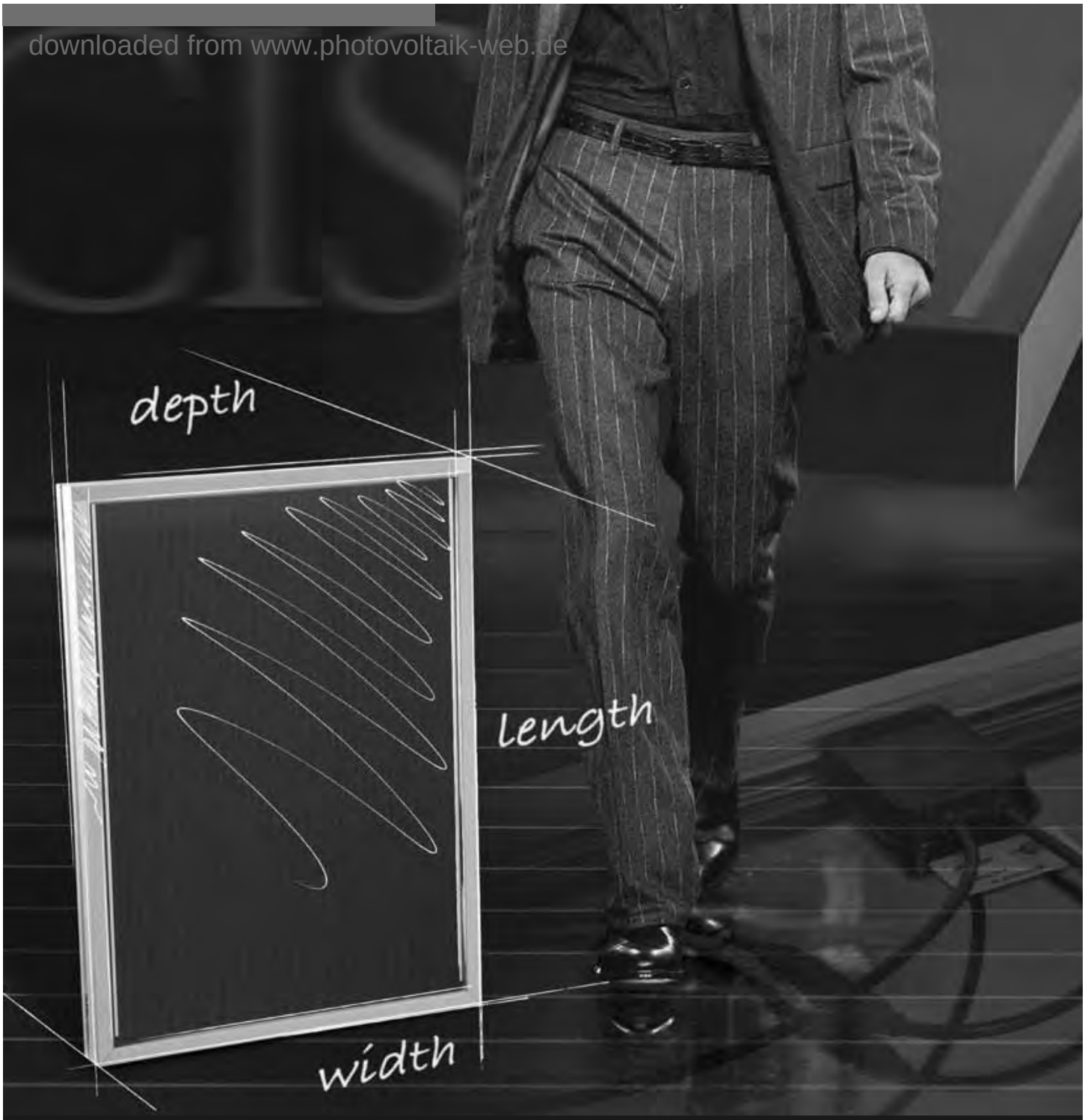

The Haute Couture of Photovoltaics

CIS Solar Modules

Technical Data Sheet

WÜRTH SOLAR

CIS-Photovoltaic Modules

The CIS modules of Würth Solar consist of multilayered CIS (copper-indium-diselenide) solar cells that are connected in series. They absorb a wide spectrum of light energy and ensure maximum energy generation also under unfavorable weather conditions. Thanks to the great reliability and the long life of our CIS solar modules they are suitable for almost all fields of application and sizes of solar energy systems.

The CIS solar modules are offered as standard and customer-specific versions. They distinguish themselves by their homogeneous black module surface and thus meet the highest requirements on esthetics and product design.

General technical data:

Thermal parameters		
NOCT [1]	°C	47 ± 3
Temperature coefficient of short circuit curren	%/°C	0.05
Temperature coefficient of open-circuit voltage	%/°C	-0.29
Temperature coefficient of nominal output	%/°C	-0.36

Limiting values		
Maximum module temperature	°C	-40 ... +85
Surface pressure	N/m²	2,400
Maximum torsion	°	1.2

Intensity -and temperature-dependent behavior

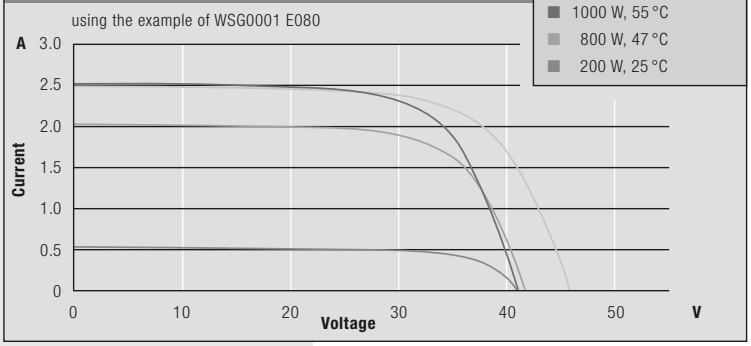

Technical data

	WSK0001	WSK0039	WSK0019	WSK0020
Nominal output (W)	5.5	12.0	23.0	35.0
Voltage MPP (V)	12.0	12.0	12.0	12.0
Current in MPP (A)	16.5	16.5	16.5	16.5
Strom im MPP (I_{mpp}) in A	0.33	0.73	1.40	2.12
Open-circuit voltage (V)	22.0	22.0	22.0	22.0
Short circuit current (A)	0.35	0.78	1.50	2.29
Open-circuit voltage (V) at -10 °C	24.3	24.3	24.3	24.3
MPP voltage (V) at +70 °C	13.8	13.8	13.8	13.8
Change of voltage per °C (%)	-0.29	-0.29	-0.29	-0.29
Change of power per °C (%)	-0.36	-0.36	-0.36	-0.36
Dimensions in mm (H x B x T)[2]	205 x 305 x 31	405 x 305 x 31	405 x 605 x 31	605 x 605 x 31
Weight (kg)	1.3	2.4	4.5	6.5
Connecting variant (see below)	①	①	①	①

The electrical data apply to standard test conditions (STC): 1,000 W/m², AM 1.5, 25 °C

[1] Normal operating temperature of cells in case of irradiation: I = 800 W/m²
Environmental temperature: T_U = 20°C
Wind velocity: V_W = 1 m/s

Frame Variants
• Frame made of anticorrosive aluminum, anodized black (standard)
• Frameless module (on request)

Due to permanent optimization of our modules changes to the data indicated in the technical data sheet are possible all times. Therefore please use the most current data sheets, which you may find under **www.wuerth-solar.com** or contact our sales representatives.

Modules in **standard version**

CIS modules of Würth Solar are delivered in glass/glass compound with or without frame. The front glass used is extremely translucent and protects the module even against toughest environmental conditions.

The standard modules are submitted to laboratory tests for a wide spectrum of operating conditions and are produced according to strict guidelines of quality. The customer can get a test certificate for each type of module.

It will be a pleasure for us to provide you with further information on request			
WSK0021	**WSG0036 E075**	**WSG0025 E080**	**WSG0035 E075**
55.0	75.0	80.0	75.0
12.0	24.0	120.0	12.0
16.5	35.0	120.0	16.5
3.33	2.15	0.67	4.42
22.0	44.5	160.0	22.0
3.56	2.36	0.72	5.01
24.3	49.0	177.0	23.5
13.8	29.3	101.0	14.2
-0.29	-0.29	-0.29	-0.29
-0.36	-0.36	-0.36	-0.36
605 x 905 x 35	605 x 1,205 x 35	605 x 1,205 x 35	605 x 1,205 x 35
9.7	12.7	12.7	12.7
③	②	②	③

Connection variants

① 2 connecting buttons with cable socket

Dimension: 30 x 50 x 12 mm (W x L x D)

② Socket (Bez. PV-JB / K-2 / N4SOL)
Male plug (Bez. PV-KST4, PV-KBT4)

Dimension: 55 x 91 x 13 mm (W x L x D)

③ Socket

Dimension: 100 x 158 x 35 mm (W x L x D)